


# Modelling the effect of different carbonate weathering rates on Earth system resilience



Submitted by Daneen Cowling to the University of Exeter as a thesis for the degree of *MSc by Research in Geography*, May 2020.

This *thesis* is available for Library use on the understanding that it is copyright material and that no quotation from the thesis may be published without proper acknowledgement.

I certify that all material in this thesis which is not my own work has been identified and that any material that has previously been submitted and approved for the award of a degree by this or any other University has been acknowledged.

Signature: 

## Abstract

Carbonate weathering is an important feedback to regulate the carbon cycle and climate of the Earth system. Focus of the behaviour of this feedback has been on geological scales. Little attention has been given to the responses of this feedback to shorter-scale Earth system perturbations, especially how different uplifted masses of carbonate have influenced this strength. Hence, using the Earth system model cGENIE, this study will explore the carbon and climate responses to different carbonate weathering rates, and how these rates produce different resilience to a range past and future carbon perturbations. These experiments have shown a considerable carbon and climate influence from higher carbonate weathering rates. This is especially evident in response to perturbations, where higher carbonate weathering rates show considerable resilience contribution to the system, notably in the longer-term recovery period. This has therefore exposed an important role of carbonate weathering on a previously underappreciated temporal scale. Further, this study has also demonstrated carbonate weathering does have an important control on resilience and recovery direction, hence is an important variable to refine for future impacts and rate of recovery.

# Contents

Abstract .....	2
List of Figures.....	5
List of Tables.....	7
List of Equations .....	8
List of Acronyms and Chemical Species .....	9
Acknowledgements.....	11
1. Introduction .....	12
1.1 Carbonate Weathering and the Global Carbon Cycle.....	12
1.1.1 Background .....	12
1.1.2 Oceanic Carbon Cycle .....	14
1.2 Weathering Influences on the Carbon Cycle.....	17
1.2.1 Geology .....	17
1.2.2 Ocean dynamics.....	19
1.2.3 Ice Sheet Coverage.....	21
1.2.4 Biological influence.....	23
1.3 Climate, Carbon and Earth System Resilience Changes.....	24
1.3.1 Introduction.....	24
1.3.2 Deep Time Carbon and Climate Disasters .....	24
1.3.3 Past Resilience.....	27
1.4 The Significance of Chalk .....	29
1.4.1 Timing of Uplift.....	29
1.4.2 Weatherability of Chalk .....	30
1.4.3 Current Observations .....	31
1.5 Project Rationale .....	36
1.5.1 Originality and Justification .....	36
1.5.2 Aims.....	38
2. Methodology .....	39
2.1 cGENIE.....	39
2.2 Model Simulations.....	41
3. Results .....	46
3.1 Ensemble 1: Sensitivity to CaCO <sub>3</sub> weathering .....	46
3.2 Relational Statistics.....	54
3.3 Ensemble 2: Weathering Strength Against CO <sub>2</sub> Pulse .....	57
3.3.1 RCP6 .....	57
3.3.2 RCP8.5 .....	59
3.3.3 PETM.....	60

3.4 Ensemble 3: Bioturbation Sensitivity Analysis.....	69
3.5 Reducing Weathering Rate from Higher Initial Rate .....	73
4. Discussion.....	78
4.1 Relative Strength of CaCO <sub>3</sub> Weathering .....	78
4.1.1 Controls on Climate .....	78
4.1.2 Controls on Chemistry .....	79
4.1.3 Sedimentary Controls.....	81
4.1.4 Bioturbation Influence.....	84
4.2 CaCO <sub>3</sub> Weathering Response to CO <sub>2</sub> Forcing.....	85
4.2.1 PETM.....	85
4.2.2 Insights Through Time.....	96
4.2.3 Looking to the Future .....	104
4.3 Limitations .....	113
5. Conclusions .....	116
5.1 Summary .....	116
5.2 Future Opportunities .....	118
6. Appendices .....	120
7. Bibliography .....	122

## List of Figures

<b>Figure</b>	<b>Title</b>	<b>Page</b>
1.1	Long Term Carbon Cycle	13
1.2	Variability in Subduction Zones	15
1.3	Carbonate Weathering with Temperature	34
1.4	Chalk Cliff Erosion	35
2.1	SedGEM Schematic	40
2.2	cGENIE Modules	40
3.1	Ocean and Atmospheric Temperature: Open vs Closed	49
3.2	pCO <sub>2</sub> Flux: Open vs Closed	50
3.3	CaCO <sub>3</sub> Sedimentary Responses: Open vs Closed	51
3.4	pH and DIC Responses: Open vs Closed	52
3.5	10W Spin-Ups: Open vs Closed	53
3.6	pH and pCO <sub>2</sub> relationships	55
3.7	CaCO <sub>3</sub> Composition and pCO <sub>2</sub> relationships	56
3.8	RCP6: pCO <sub>2</sub> and Temperature Responses	63
3.9	RCP6: Carbonate Chemistry Responses	64
3.10	RCP8.5: pCO <sub>2</sub> and Temperature Responses	65
3.11	RCP8.5: Carbonate Chemistry Responses	66
3.12	PETM: pCO <sub>2</sub> and Temperature Responses	67
3.13	PETM: Carbonate Chemistry Responses	68
3.14	Bioturbation Influence: pH	70
3.15	Bioturbation Influence: pCO <sub>2</sub>	71
3.16	Bioturbation Influence: CaCO <sub>3</sub> Sediment Composition	72
3.17	Weathering Spin-Up Comparison	75

3.18	High Initial Weathering: Carbon and Climate Response	76
3.19	High Initial Weathering: Carbonate Chemistry Response	77
4.1	PETM pCO <sub>2</sub> Change	86
4.2	CaCO <sub>3</sub> Observations at PETM Onset	90
4.3	PETM CaCO <sub>3</sub> Sediment Content Records	93
4.4	Southern Ocean Currents	95
4.5	Mass Extinctions Through Time	98
4.6	Cenozoic Alkalinity Changes	101
4.7	RCP Ocean Changes	107
6.A	RCP CO <sub>2</sub> Concentrations	120
6.B	Model Configuration Maps	121

## List of Tables

<b>Table Number</b>	<b>Title</b>	<b>Page</b>
1	Weathering Rate Justification	43
2	Scenario Forcing	44
3	Experiment Details	45
4	RCP Response	105

## List of Equations

<b>Equation Number</b>	<b>Equation</b>	<b>Page</b>
1	Silicate Weathering	12
2	Carbonate Weathering	12
3	Ocean Dissolution	16
4	CCD dissolution	16
5	Revelle Factor	80



## List of Acronyms and Chemical Species

<b>Acronym</b>	<b>Description</b>
CCD	Carbonate Compensation Depth
ITCZ	Inter-Tropical Convergence Zone
SL	Sea Level
SLR	Sea Level Rise
CIE	Carbon Isotope Excursion
LGM	Last Glacial Maximum
DIC	Dissolved Inorganic Carbon
Ca	Calcium
CaCO <sub>3</sub>	Calcium carbonate
CO <sub>2</sub>	Carbon dioxide
H <sub>2</sub> O	Water
Si	Silicate
CaSiO <sub>2</sub>	Calcium silicate
HCO <sub>3</sub> <sup>-</sup>	Bicarbonate
SiO <sub>2</sub>	Silicon dioxide
OAE	Ocean Anoxic Event
PETM	Paleocene–Eocene Thermal Maximum
OA	Ocean Acidification
C-cycle	Carbon Cycle
LIP	Large Igneous Province
RCP	Representative Concentration Pathway
pCO <sub>2</sub>	Partial pressure of carbon dioxide

RMSE	Root mean squared error
$R^2$	Coefficient of determination
SE	Standard error
M Value	Line gradient

## Acknowledgements

I would first like to give big thanks to my awesome supervisor, Tim Lenton.

Continuing the support from my dissertation, the encouragement and enthusiasm you have provided has been unwavering. You have consistently made me overcome any doubt I had and been a great person to share ideas with and get excited about my research. The opportunities you have exposed me to are beyond what I would have even envisioned to be possible, and for that I am incredibly grateful!

Secondly, I would like to thank Andy Ridgwell. The welcoming support you provided when inviting me out to Riverside to get me up to speed with cGENIE has been invaluable to this project. Your help has been a significant contribution and been a memorable part of this Masters.

Thanks also goes out to Olly. Your experiences help and support have been so influential at getting me to the end of this beast of a project. You've always been there (even at crazy hours throughout the night) for any type of question I would throw at you. You've given me the willpower I needed to dig deep for the motivation I've needed to finish my thesis. To have given the levels of support you have at the same time as finishing your PhD and a global pandemic, proves you're an incredible person, and I'm very grateful!

I would also like to thank my trusty proof-readers; Emily, Ellie and Jess – your help and suggestions have been key to moulding a thesis that actually makes sense!

Thanks also to my dogs; Jess and Charlie, for allowing me to keep smiling throughout!

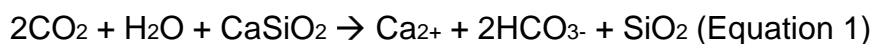
## 1. Introduction

This section will introduce the contextual literature that lay the foundation for this project and review the current discussions and controversies in research, as well as highlighting any knowledge gaps that have informed project motivations and aims.

### 1.1 Carbonate Weathering and the Global Carbon Cycle

#### 1.1.1 Background

The carbon cycle is an integral modulator of Earth system climate and the composition of the atmosphere and oceans (Sarmiento et al., 1998). The long-term carbon cycle is comprised of continual CO<sub>2</sub> inputs from the crust via volcano and mid-ocean ridge outlets, then cycling through the oceans, atmosphere and the terrestrial biosphere where it either remains in sinks or recycled into the crust at subduction zones on geologic timescales (Berner, 2003). Consumption of CO<sub>2</sub> is orchestrated by carbonate and silicate weathering, which have stabilised climate and carbon through Earth's history (Berner, Lasaga and Garrels., 1983; Walker, Hays and Karsting, 1981) (Equation 1 and 2).



Ultimately, Ca and Si weathering act as a sink of carbon within the cycle, consuming CO<sub>2</sub> to be deposited as CaCO<sub>3</sub> sedimentary rocks (Figure 1).

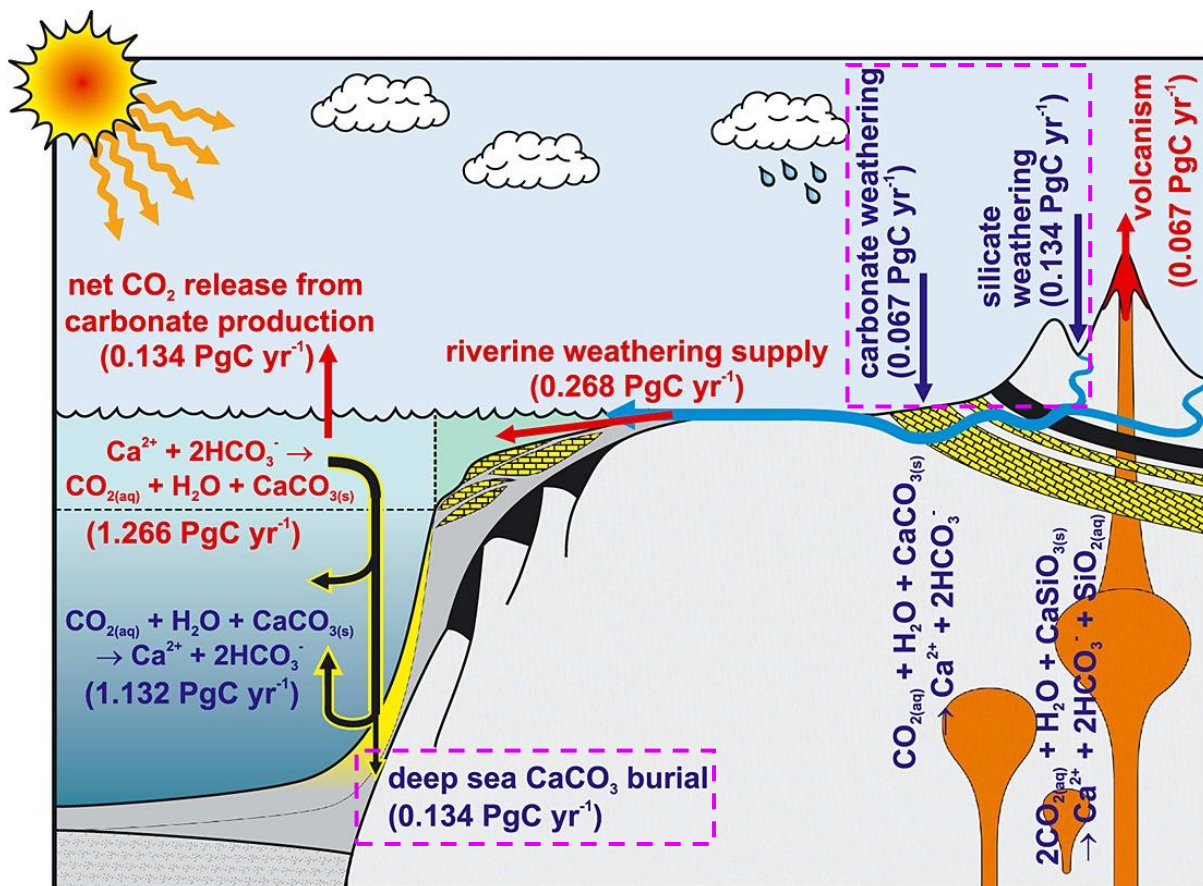


Figure 1.1; Long Term Carbon Cycle.

Diagram shows carbon fluxes, with emphasis on regulatory role of carbonate and silicate weathering and burial (purple dashed boxes). Adapted from (Colbourn, Ridgwell and Lenton, 2015)

On relatively shorter and more geologically recent time scales, the carbon cycle has been significantly influenced by biological controls, which have not only changed CO<sub>2</sub> content through respiration but also by enhancing weathering (Lenton and Watson, 2004; Lenton and Watson, 2011). Short term carbon cycles dynamically transfer carbon between the atmosphere, oceans, terrestrial soils and biology, introducing an organic carbon element to the carbon cycle (Townsend, Vitousek and Holland, 1992; Lenton and Watson, 2011). These changes and short-term perturbations still get regulated and equilibrated by the longer-term processes of rock weathering and sediment burial (Colbourn, Ridgwell and Lenton, 2015). The rates at which these processes operate, and the direction of equilibrium, determines the

Earth's climate (Saltzman, 2017). However, constraints on these variables are relatively uncertain and poorly understood (Caves et al., 2016; Meissner et al., 2012).

### 1.1.2 Oceanic Carbon Cycle

C-cycle contributions are important for ocean biogeochemistry stability by supplying organic and inorganic carbon sediments to sustain life, contribute to a carbonate sediment sink and feed subduction zones to remove accumulated carbon from the system and continue the conveyor of carbon recycling, maintaining a "steady state" in carbonate (Mackenzie and Morse, 1992). However, subduction is also said to increase degassing at the earth's surface, therefore creating an uncertainty around the carbon removal magnitude in deep sea sediments (Mackenzie and Morse, 1992; Berner, 1990). But given that total breadth of subduction and rift zones are variable through time, the scale of influence is complex stasis with erosion (Figure 1.2) (Mills et al., 2018).

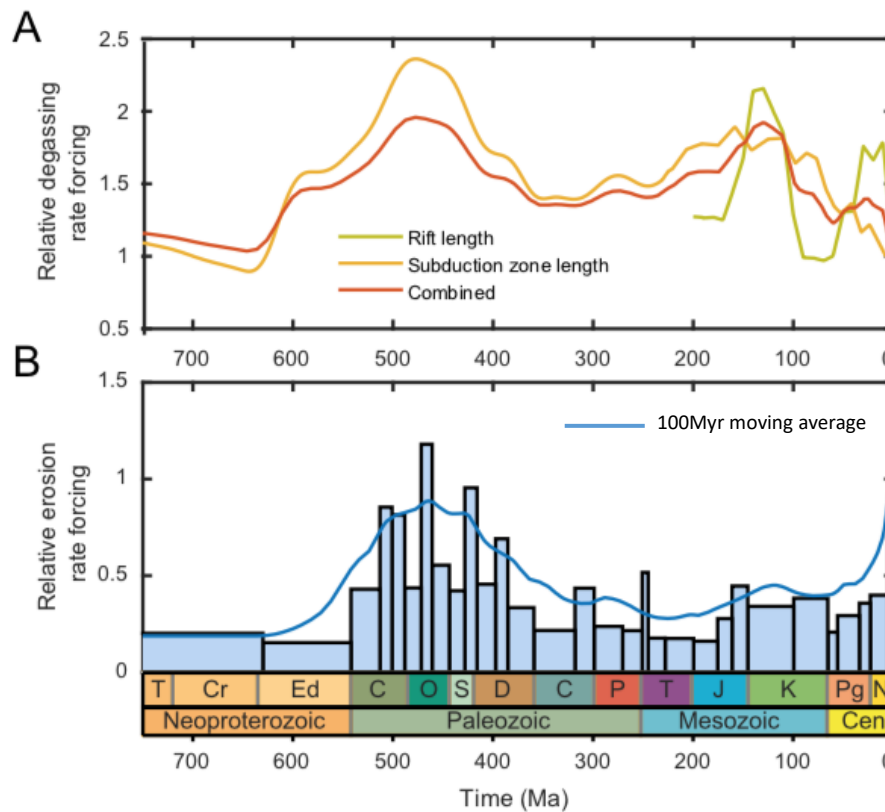
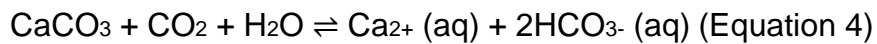
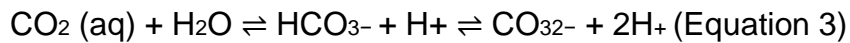


Figure 1.2; Tectonic change over time.

Figure adapted from (Mills et al., 2018) showing degassing rate from rift length reconstructions (A) and erosion rate from sediment accumulation data (B) change over 700Ma.

Increased  $\text{CO}_2$  can increase ocean bicarbonate and  $\text{H}^+$  content and thus ocean acidification (Equation 3). This is counteracted by Si and Ca weathering, and increased dissolution of carbonate sediment on the seafloor, regulated by the Carbonate Compensation Depth (CCD) which dynamically responds to changes in pH and saturation by carbonate dissolution (Equation 4) (Ridgwell and Zeebe, 2005; Kump et al., 2009). Responsivity of the CCD through Earth history is evident by transitions between thick depositions of calcareous skeletons and inorganic matter, to dissolution intervals (Tyrrell, 2007; Kender et al., 2019; Greene et al., 2019). This process is a key feedback in the ocean carbon cycle, maintaining a quasi-steady state (Zeebe and Zachos, 2013).



The oceanic dimensions of the C-cycle reside mostly in coastal ecosystems where there is an instantaneous transfer of gases at the atmosphere interface (Gustafsson, Omstedt and Gustafsson, 2015). Furthermore, shallow seas are densely biologically active, supporting ~30% of primary productivity and creating additional stores and sources of CO<sub>2</sub> through photosynthesis, respiration and decomposition (Andersson and Mackenzie, 2004). A direct interface allows for very responsive feedbacks, but ultimately results in a state that is in disequilibrium on such timescales with relatively rapid turnovers hence influenced by short term changes to atmospheric CO<sub>2</sub>, terrestrial sediment/nutrient delivery, freshwater influx, and seasonality (Smith and Hollibaugh 1993; Sigman and Hain, 2012).

The slow turn-over of oceanic carbon cycle processes exist with short-term, highly responsive processes. These are driven by the biological pump; the carbon sequestration in OM and CaCO<sub>3</sub> by mainly photosynthesis and phytoplankton on 100-year scales and its subsequent sinking and remineralisation at depth (Hain, Sigman and Haug, 2014; Archer, 2003). This accounts for an important carbon sink larger than other bioactive carbon stores (Honjo et al., 2014). However, due to the fragility of biological processes and stressors, the strength and resilience is still poorly constrained (IPCC, 2005; Sabine et al., 2004). Nonetheless, on these scales the control of biological carbon storage and source can impede a long-term weathering signature (Gruber et al., 2009).



Hence, strength and significance of ocean carbon dynamics are relatively uncertain in predictions. This is largely due to the lack of observations of biogeochemical relationships on various scales, lacking in temporal scale for detailed measurements and spatial inaccuracies for geologic records (Fennel et al., 2019; Röthlisberger et al., 2010). Therefore, great bias in models exists depending on which observations of weathering are applied and how empirical relationships are adapted (Colbourn, Ridgwell and Lenton, 2015).

## 1.2 Weathering Influences on the Carbon Cycle

### 1.2.1 Geology

#### *1.2.1.1 Volcanism and LIPs*

As well as a constant background CO<sub>2</sub> emission, volcanism is also a key influence on CO<sub>2</sub> drawdown. This is through weathering of fresh basalt deposits. LIPs spread over large areas globally and are able to contribute to 25-35% of CO<sub>2</sub> Si-weathering consumption (Dessert et al., 2003). In addition to significant surface coverage, basalt allows a rapid rate of chemical weathering by existing for the most of its lifecycle as freshly exposed; vulnerable to external forces (Chen et al., 2020; Ikeda, Tada and Ozaki, 2017).

LIP formations have triggered global cooling via rapid CO<sub>2</sub> removal and consequential reduced greenhouse effect (Enst and Youbi, 2017). Volcanism can therefore initiate a geological scale feedback to keep net change neutral, but in doing so swings Earth's climatic system between different thermostatic and atmospheric

composition states (Ernst, 2014). Habitable conditions on Earth are broadly controlled by weathering that is able to respond and mitigate CO<sub>2</sub> concentration fluctuations (Rushby et al., 2018).

Lithology has an important influence on the C-cycle to determine weathered supply of Si and Ca minerals. Weathering of rocks composed of these materials account for 40% and 60% (respectively) of global CO<sub>2</sub> uptake (Amiotte-Suchet et al., 2003).

#### *1.2.1.2 Continentality and Paleogeography*

Continental mobility influences the distribution and availability of volcanic inputs by opening up ridges and crust recycling at plate margins. This alters CO<sub>2</sub> composition and climate through emission and weathering (Mackenzie and Morse, 1992). Crustal collisions onset periods of uplift and mountain exhumation, which are a dominant and observable source of carbonate and silicate weathering climate regulation; for example, the Neogene exhumation of the Himalayas is hypothesised to have triggered a glacial climate (Zachos et al., 1999). Uplift also influences climate - as the Himalayas are positioned beneath the ITCZ, a relief feedback has strengthened the monsoon and enhanced erosion (Armstrong and Allen, 2010). Erosional climate, steep slopes and high Si and Ca composition have supplied the majority of bulk sediment accumulation rates in SE Asia, contributing greatly to the carbon cycle sink (Berner, 2004; Kender, Yu and Peck, 2014).

Continental arrangement also dictates ice growth and climate through latitudinal placement. Crowley, Hyde and Short (1989) argue that Pangea allowed spatial

climatic contrasts because of latitudinal positioning, permitting ice covered poles. This catalyses erosional forces which create biological and mechanical cryosphere weathering outputs, contributing to shallow marine carbonate production (Walker, Wilkinson and Ivany, 2001). Continental area can also alter the C-cycle by changing amount of exposed weatherable surfaces. Kump (2018) argues that greater continentality reduces the weathering potential, as climate has a reduced influence over land erosion and continental shelf erosive area is reduced. Changes in the shelf area and coastal volume has had greater influences on carbonate production than marine calcifiers diversifying and sea level fluctuations due to changes in rates and volumes of erosion and loci of sediment delivery and accumulation in shallow seas (Walker, Wilkinson and Ivany, 2001). However, large continents with dry interiors can undergo 'megamonsoon' climates as suggested was the case for Pangea (Dubbiel et al., 1991). Relative strength of continental controls over weathering remain controversial (Goddéris et al., 2012).

### 1.2.2 Ocean dynamics

Sea Level (SL) influences weathering by exposure of continental shelf area and fluctuation of the CCD, which effects both shallow sea inflow and biological cycling and deep-sea cycling (Fagherazzi, Howard and Wiberg, 2004; van der Ploeg et al., 2019). Mackenzie and Morse (1992) argue that high SL results in more total fluxes in shallows whereas lower SL means more transportation to deep ocean and potentially a lower rate of cycling (Mackenzie and Morse, 1992). Sabine and Mackenzie (1995) and Berger (1982) also note how a lower SL allows more platform exposed to dissolution, hence increasing an ocean sink.

This was exemplified in the Cretaceous high-stand whereby a sufficient continental area was submerged in a semi-arid area and invited high run off, therefore  $\text{Ca}_{2+}$  inputs were more dominated by a terrestrial weathering system, as opposed to a low sea level state dominating the carbonate supply from slower  $\text{Ca}_{2+}$  supply from organic sources (Mackenzie and Morse, 1992). Opdyke and Wilkinson (1988) also explored how a Cretaceous high SL resulted in a 50% area of epicratonic shelf flooded, a deepened CCD by 1.5km, 3-fold increase in calcite ooze deposition and an 8-fold increase in pelagic limestone from cretaceous rate, in addition to a new evolution of plankton to live in shallow seas (Hays, 2008). This exposes strong communication between coast and shelf and transfer from shallow to deep carbonate accumulation, thus giving a role of influence to sedimentary surface area to predict portioning of carbonate fluxes (shallow or deep sea) and capacity to be source or sink. Future capacity to adjust to SLR is uncertain. A variety of models testing 0.2-0.8m in the next 100 years produce an uncertain behaviour of the inorganic pump, competing influences between OA reducing calcification and increasing dissolution, and an increment in submerged weatherable land reducing Ca and Si input (Tyrrell, 2007).

Carbonate weathering influences the nutrient delivery to surface water, which is where calcification is largely restricted and thus affects the large biological influence over  $\text{CaCO}_3$  (Tyrrell, 2007). The populations of carbonaceous species contribute measurably to the ocean sediment carbonate budget; therefore, any change impacts the carbon cycle (Baumann et al., 2004). Changes to ecosystem behaviour and structure are commonly attributed to an acidification event or a change in delivery of

nutrients from circulatory changes (Honisch et al., 2012; Zeebe and Zachos, 2007), frequently omitting the influence of  $\text{CaCO}_3$  weathering (Cárdenas et al., 2018).

### 1.2.3 Ice Sheet Coverage

Ice dynamics on the Earth's surface have great control over the Ca supply to, and activity within, oceans. The erosive power of glaciers breaks down and mobilises carbonate and silicate bedrock rapidly, flushing directly into the oceans.

Geological records have captured the erosive control ice has had on the global C-cycle. This has been seen for the most extreme events such as snowball earth, where not only did the global coverage of ice halt weathering and influenced the carbon cycle and climate, the exit recession of ice dramatically increased weathering which again had great control on the Earth system (Lenton and Watson, 2011). For glacial-interglacial periods, the highest erosion rate seen between Neogene and present was due to glaciers, which increased Si export and enhanced  $\text{CO}_2$  drawdown, noticeably in the LGM (Mackenzie and Morse, 1992; Hawkings et al., 2018). Glacial weathering coinciding with declining  $\text{CO}_2$  (pre-anthropogenic perturbation) shows it is a dynamic process of carbon capture.

The weathered inputs not only buffer ocean chemistry but can also interact with circulation and upwelling carbon and climate controls (Cape et al., 2019). However, this influence on a geological scale is controversial. Elsworth et al (2017) argue enhanced weathering in the Eocene sufficiently drew down  $\text{CO}_2$  to trigger glaciation but suggest this is a secondary impact of ocean circulation changes. Kender, Yu and

Peck (2014) on the other hand dismiss this control from circulation changes in the mid-Miocene, instead showing CO<sub>2</sub> sequestration and elevated alkalinity was from emergent carbonate and silicate of the Himalayas.

Emerging glacial weathering projects identify high Si discharge from large glacial basins at quantities previously poorly constrained and absent from weathering budgets (Meire et al., 2016) and new accounts of chemical weathering across proglacial meltwaters contributing to a CO<sub>2</sub> sink (St Pierre et al., 2019). Influential spatial scale of erosion and deposition from glacial influence via IRD, sea ice and offshore advection has also been reported (Wadham et al., 2013; Arrigo et al., 2017). Glacial weathering influence has been exemplified in Iceland which has shown a 30% weathering flux increase over 40 years in response to glacial melt (Beaulieu et al., 2012). Similar observations have been made for receding alpine glaciers, which have shown increased preferential weathering of carbonate bedrock, resulting in a CO<sub>2</sub> sink (Anderson et al., 1997; Scribner et al., 2015).

These relationships oppose a common assumption that weathering is temperature dependent (Mills et al., 2018). Although a linear assumption is easy to apply in models, weathering controls can be spatially complex. Therefore, accounting for this complexity could amount to high weathering buffer ability within the carbon cycle through chemical and biological interactions, offering potential resilience on substantial spatial and temporal scales.

#### 1.2.4 Biological influence

As well as being weathering-responsive, biology can also influence weathering. OA threats to carbonate species and coral reefs can change type and distribution of species, hence success of non-calceous species in addition to reduced  $\text{CaCO}_3$  export may weaken the biological pump (Hofman and Schellnhuber, 2009). Some studies have highlighted the carbonate weathering contributions of biology, ranging from a bioerosion balance suppling the coral reef carbonate budget (Perry et al., 2014), to the important flux driven by bottom-dweller bioturbation (Broecker, 2003; Emerson and Hedges, 2008).

Weathering has shown to be sensitive to the type of vegetation that creates temporal and spatial variations of carbon in the soil and water budgets; for example, 20-30% higher carbonate weathering in deciduous than under conifers (Ivory et al., 2014). However, there is controversy about the significance of this weathering influence, with some identifying an opposite relationship (Oeser and Blanckenburg, 2020; D'Antonio, Ibarra and Boyce, 2019). In addition to vegetation, soils can influence weathering through  $\text{pCO}_2$  from respiration altering temperature which has been shown to increase weathering and dissolution (Romero-Mujalli et al., 2019).

Arguably, the most significant influences on weathering have birthed out of Earth climate and carbon catastrophes. The next section will explore such catastrophes and responses in more detail.

## 1.3 Climate, Carbon and Earth System Resilience Changes

### 1.3.1 Introduction

Earth's history has been a succession of temperature and CO<sub>2</sub> fluctuations, which has triggered ocean instabilities and tested resilience of biogeochemical regulatory cycles. Global acidification and anoxia events through time have each exhibited different impacts and recovery mechanisms. Although no past event serves as an analogue for the future (Hönisch et al., 2012), they provide insight into how oceans respond and recover to stresses. Many studies explore various events but have placed different weightings to modelled assumptions on the impacts attributable to ocean resilience (Turner, 2018). Similarly, observations are difficult to filter out geochemical resilience, given the other environmental and ecological changes occurring simultaneously (Ridgwell and Schmidt, 2010). Therefore, to identify sources of resilience one must consider how it would have operated alongside and in response to other environmental changes.

This section will therefore review the past oceanic events from the Permian to Late Pleistocene and whether observations indicate active sources of geochemical resilience.

### 1.3.2 Deep Time Carbon and Climate Disasters

The largest extinction event (Permian-Triassic) wiped out 90% of marine life (Jin et al., 2000). A potential cause are two consecutive flood basalt eruptions (Siberian Traps) that align with timing and explain the CO<sub>2</sub> induced global 16°C warming from a release of 13,000-43,000 PgC in 20-400Kyr (Payne et al., 2010; Sobolev et al.,



2011; Shen et al., 2011). Such heating melted the poles and broke down ocean circulation which resultantly acidified and deoxygenated the ocean (Kump, 2018; Clarkson et al., 2015). Lethal 40°C ocean temperatures along with pH reductions of 0.6-0.7 units lasting for around 10kyrs, led to shallow waters experiencing the greatest losses inhibiting a demise of hypercalcifying taxa and a reef crisis responsible for rugose and tabulate coral extinctions (Clarkson et al., 2015; Kiessling and Simpson, 2010). Large losses, runaway feedbacks and slow recovery is observed from this event, indicative of a lack of resilient mechanisms in place (Foster et al., 2017).

Marine fauna was targeted again in the Triassic-Jurassic extinction event, categorised by a CO<sub>2</sub> increase to more than 7 times modern level and temperatures 3-4°C warmer (Stanley, 2009). Climate change, extra-terrestrial impact and volcanic activity are said to be responsible for land and ocean extinctions, and catastrophically acidified the oceans (Hautmann, Benton and Tomasovych, 2008). Yet, the Cretaceous allowed for a diversification recovery for calcifying marine life, aided by a transition from aragonite to calcite seas (Stanley, Ries and Hardie, 2002). Breakup of Gondwanaland, SLR and a lower saturation ratio of Mg<sup>2+</sup>:Ca<sup>2+</sup> allowed for a Rudist reef, calcareous nanoplankton, diatom and foram expansion (Johnson, 2002). Productive calcification led to the widespread deposits of chalk at 15cm/1000yrs (Stanley, Ries and Hardie, 2005; Stanley, 2009).

Cretaceous success was punctuated with anoxic events (OAE 1a and OAE2) due to a relatively stagnant ocean due to warmer temperatures, weaker mixing and a

continental flooding from SLR, encroaching anoxia into shallow seas consequently leading to widespread shallow and deep-water shale deposits (Danise et al., 2013). Calcareous plankton show 20-30kyr delayed deep-water acidification to OAE1a, followed by a stepwise CO<sub>2</sub> increment and acidification (Erba et al., 2010). Jenkyns (2018) argues these to be due to weathering-induced cooling episodes during a period of high CO<sub>2</sub> and temperature over the 500kyr eruption of the Deccan Traps. An intensified hydrological cycle impacting fresh basalt deposits allowed for CO<sub>2</sub> drawdown and triggered a global cooling, reducing ocean temperatures from 20°C to 9°C (Jenkyns, 2018). Midtkandal et al (2016) suggests other volcanic weathering sources were also responsible for this cooling, including the high Arctic LIP as a contributing factor.

The PETM 10 million years after the end-Cretaceous saw a relatively short but intense high CO<sub>2</sub> and temperature episode causing 30-50% benthic foraminifera loss and significant microbenthic deformity from anoxia and acidification (Zachos et al., 2005; Rodriguez-Tovar et al., 2011). The CCD rose 2km to shallower than 1.5km, reducing CaCO<sub>3</sub> preservation (Honisch et al., 2012; Zachos et al., 2005). Depending on the CO<sub>2</sub> source, models estimate surface pH decline of 0.25-0.45 units and reduction in mean surface ocean aragonite saturation from 3 to 1.5 (Ridegwell and Schmidt, 2010). The consensus suggests the event was triggered by NAVP mass volcanism and penetration into C-rich sediments (Jones et al., 2019). Methane clathrate instability is also argued to contribute additional CO<sub>2</sub> to the perturbation (Gehler, Gingerich and Pack, 2016). Armstrong McKay and Lenton (2018) explore resilient variation at the PETM as a destabilisation in the C-cycle 1.5Myrs before the

event, likely from the NAVP rendering carbon and climate systems vulnerable to tipping points and loss of negative feedback resilience.

### 1.3.3 Past Resilience

As discussed, different perturbations have experienced different scales and rates of climatic and carbon cycle changes, but also revealed inconsistent recovery and resilience. Earth system resilience can be defined as a spectrum of behaviours, but for the purpose of this study, resilience will refer to the carbon cycle recovery to a perturbation. The Earth as a system, encompassing its regulatory feedbacks and inhabitants, has resilience to respond to climatic changes to recover as a new state of relative stability (Lovelock and Margulis, 1974). Questions now arise about whether this resilience has changed over time.

Lenton (2019) identifies changing resilience and recovery post-significant climatic events, suggesting the Earth as a system is evolving to a more resilient state.

Whether the Earth is becoming more resilient due to the types of forcings imposed, availability and strength of feedbacks, or whether it is not changing in resilience at all, remains unknown. However, key components of the climate and carbon system can employ resilience.

The foundation to Earth system resilience is the long-term negative weathering feedback, able to drawdown CO<sub>2</sub>. Weathering feedback strength could have been influenced at different intervals through time depending on whether an appropriate set up of environmental conditions (*explained in Weathering Influences on the*

*Carbon Cycle*). It is difficult to attribute a cause with geological record gaps and environmental changes occurring in tandem with perceived increased weathering resilience strength. Nonetheless, system resilience is important to define and is transferrable to the future if an identified resilience source is still present today (Lenton and Britton, 2006).

Rapid recovery of the PETM is said to have largely been due to enhanced weathering (Chen et al., 2016; Komar and Zeebe, 2011). Dunkley Jones et al (2018) identifies two intervals of PETM recovery is mirrored by an increase of CaCO<sub>3</sub> wt% in sediments, evident also by sedimentation rates increasing to ~6cm ka<sup>-1</sup>, implying large erosion and weathering fluxes. Increased erosion rate is also supported by observations from (Schmitz, Pujalte and Betelu., 2001), argued to be enhanced by changes in hydrological responses and a fall in SL, increasing land-to-slope sediment transfer.

Kender et al (2012) also identify increased erosion and deposition signals in NW Europe, occurring even earlier in the CIE recovery period. They interpret this as an enhanced erosion and runoff sourced from a combination of tectonic uplift, enhanced hydrological cycling and sea level rise. Such environmental conditions marry well to observations elsewhere, contextualising conditions for increased erosion and weathering.

Enhanced weathering driving CO<sub>2</sub> drawdown and cooling is also observable for Eocene warming event recoveries (Elsworth et al., 2017). This coincides with a high

weathering rate that has continued at an increasing trajectory (van der Ploeg et al., 2019). Although small-scale processes are commonly linked to resilience during this time (Sexton et al., 2011), a backdrop of high coastal carbonate weathering could be an underplayed contribution. This is in addition to an increase in the mass of carbonate rock to weather (Mackenzie and Morse, 1992).

## 1.4 The Significance of Chalk

Consistently underappreciated is the observed increase in weathering trend and resilience coexisting with uplift of large chalk bodies. This section will review current discussions on the timing, influence and observation of this uplift, in the context of a possible source of enhanced weathering resilience.

### 1.4.1 Timing of Uplift

Cretaceous chalk was formed by a rain of calcifying organisms to the sea floor. This has produced 'chalk massifs' that have a global coverage as extensive sheer-faced coastal cliffs (Kennedy, Stephenson and Naylor, 2011; Moses and Robinson, 2011).

The date of chalk uplift is poorly constrained, but it is thought that at least for the European continental shelf strata, uplift occurred the same time as the Alpine orogeny in the Tertiary period (66-2.6 Ma) (Dezes, Schmid and Ziegler, 2004). Knox (1996) and Gale and Lovell (2018) refine uplift to be a consequence of the Icelandic plume that further billowed and folded crust. Such folds existing in Northern Europe such as the Weald-Artois anticline, Isle of Wight Monocline and the various folds

along the Jurassic coast have all allowed for the vertical uplift and exposure of 260-500m thick Cretaceous chalk beds (Aldiss, Farrant and Hopson, 2012).

This places chalk uplift around the PETM recovery. Following uplift, SL has followed a dropping trajectory, in addition to increasing glacial and ice sheet sea level influence from dyad polar ice coverage (Wordon, Ruffell and Cornford, 2000; Gasson et al., 2016). This has increased exposure of more carbonate landscapes for erosion and weathering (Gillieson, 2005).

#### 1.4.2 Weatherability of Chalk

The shallow sea origin of chalk means a mostly coastal location of these features, increasing susceptibility to additional erosional and weathering forces. This results in these features being 55% weaker than inland counterparts (Lawrence et al., 2013). Erosive energy from wave, wind and freeze-thaw, which are concentrated where large areas of chalk massifs exist in the Northern Hemisphere, enhance vulnerability imposed on its physical characteristics (van Buchem et al., 2017).

High permeability and porosity, enhanced at a seawater interface by saltwater crystallisation, causes fracture propagation and deeper weathering (Lawrence et al., 2013; Heggheim et al., 2005). Efficient percolation through pores is catalysed by salt intrusion dissolution (Lawrence et al., 2013; Cardell et al., 2003). Upper unsaturated zones of chalk are also susceptible to rainfall intensive weathering (Ireson et al., 2009; Robinson and Jerwood, 1987). The corrosive chemical composition of chalk also creates an avenue for weathering by  $\text{H}_2\text{CO}_3$ , in addition to fine grained matrix

enhancing weatherable surface area (Duperret et al., 2005; Mumallah, 1998). This is especially a risk in northern latitude seas as the dissolution of CO<sub>2</sub> is greater, thus a lower pH of the seawater (Prentice et al., 2001). Enhanced by the sensitivity to perturbation, increasing response of weathering to increased atmospheric CO<sub>2</sub> (Gaillardet et al., 2019).

Soft sedimentary composition of wave-cut platforms also appeals to burrows and other littoral zone species, resulting in down-wasting bioerosion (Naylor and Viles, 2002). Respiration also creates corrosive environments, enhancing chemical weathering in porewaters (Andersson, 2015).

#### 1.4.3 Current Observations

Although these processes make continental shelf sediments biogeochemically active (Thompson et al., 2017), identifying a current geochemical signal from coastal weathering is complex. Field observations alone lack accuracy due to high mixing and various tidal and biological cycles (McGrath et al., 2016; Andersson, Bates and Mackenzie, 2007). More accurate measurements such as those taken on ships are also redundant for coastal studies, as shallows restrict ship access (Kiditis et al., 2012; McGrath et al., 2016; Duarte et al., 2013; Kapsenberg et al., 2017; Bauer et al., 2013). Although mostly used for biological response (Blondeau-Patissier et al., 2014), carbonate weathering signatures have also been observable using remote sensing methods (Shutler et al., 2019). However, as it is in its infancy, this method used to measure ocean chemistry is controversial in its accuracy (Aurin and Dierssen, 2012).

Therefore, chalk weathering and dissolution investigations are mostly limited to lab experiments, at the expense of capturing environmental influences (Ireson et al., 2009). Lab dissolution rates of  $7.7 \times 10^{-4} \text{ mol m}^{-2} \text{ s}^{-1}$  have been observed but carry bias of a controlled environment (Peng et al., 2016). Field measurements in controlled environments can add to lab experiments with insight of some external influence. Observations from chalk aquifers show dissolution rates to range from  $3 \times 10^{-6} - 6 \times 10^{-5} \text{ mol m}^{-2} \text{ s}^{-1}$  (Bourdon et al., 2009). These rates are comparable to those observed in deep sea sediment environments, inclusive of 30% biogenic carbonate, producing bulk dissolution rates of  $4 \times 10^{-7} - 2 \times 10^{-6} \text{ yr}^{-1}$  (units of g/g/yr) (Maher, DePalo and Lin, 2004).

Few field studies have been undertaken to account for a biological influence, however due to accessibility of field stations and priority of research, such carbonate weathering rates are biased to tropical carbonate environments (Kwiatowski et al., 2016; Kline et al., 2015; Price et al., 2012; Yates et al., 2007). Although studies provide detailed carbonate chemistry data, reefs differ in type, rate and volume of  $\text{Ca}^{2+}$  produced, and exist in relatively lower energy systems than coastal carbonate weathering sites. Weathering tends to instead come from biological pressures for example bleaching events, as opposed to physical weathering (Wizemann et al., 2018; Perry et al., 2014). Hence, extrapolations from reef environments likely apply underestimations and geographical bias of carbonate weathering and dissolution used in a variety of models, especially given the limited temporal range of data



(Cummings et al., 2011; Morse, Andersson and Mackenzie, 2006; Andersson et al., 2003, 2005).

Some studies exploring discharge from rivers commonly make assumptions that homogenise lithology influences (Clargo et al., 2015; Krumins et al., 2013). Variable coastal erosion, weathering, bioturbation and human influence have also been frequently omitted, contributing to the underestimations of rate and volume of  $\text{CaCO}_3$  supply (Emerson and Hedges, 2006). Some studies that have prioritised lithology show limestone is able to weather 10 times faster than granitic lithology (Meybeck, 1986). (Gaillardet et al., 2019) review carbonate run-off observations and relationship with temperature, exposing a peak for temperate climates (Figure 1.4).

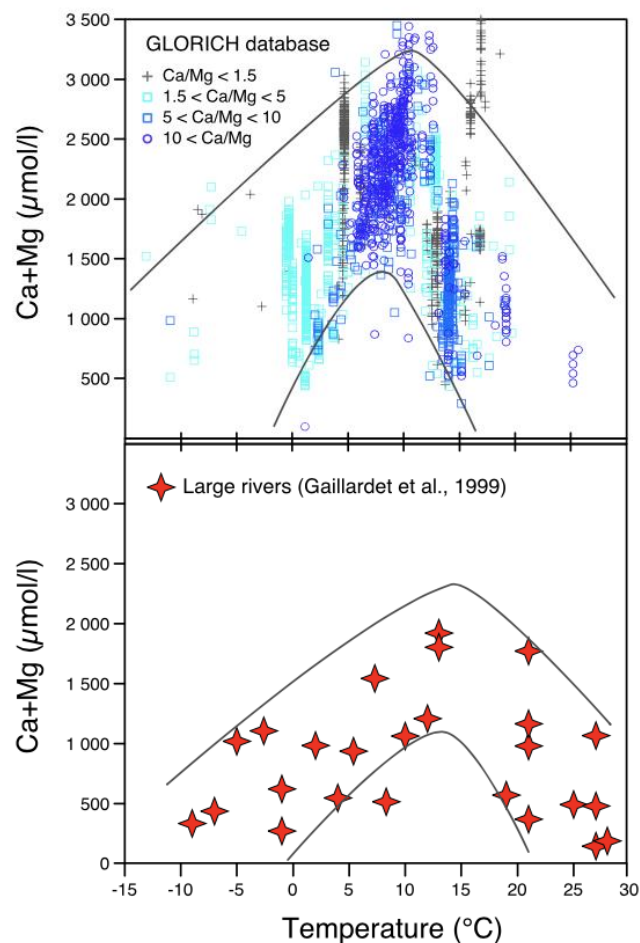


Figure 1.3; Carbonate Weathering with Temperature

*CaCO<sub>3</sub> weathering intensity relationship with latitudinal temperature ranges, using GLORICH database and Large River data from (Gaillardet et al., 1999). Figure adapted from (Gaillardet et al., 2019).*

In the interest of coastal protection, there is collected measurements of coastal erosion, including those at carbonate sites. Measurements have been taken to quantify bioerosion, general retreat and event scale erosion loss at carbonate coasts across NW Europe (Figure 1.4). Unlike other studies, measurements at coasts have revealed active background rates of bioerosion capable of removing 40% of rock surface (Moore and Shedd, 1977), the role of acid rain able to dissolve 2.79% of surface (Mulec and Prelovsek, 2015), and the role of freeze-thaw weathering influencing loss of ~5% of surface (Robinson and Jerwood, 1987; Letortu et al.,

2019). While average volume loss of  $>50000\text{m}^3$  occurs from an erosion events (in Northern Europe), demonstrating a scale of erosion/weathering incomparable to studies aforementioned (Bowman and Take, 2014). These measurements are still sparse and difficult to relate to weathering, omitting detail of the transformation of eroded cliff.

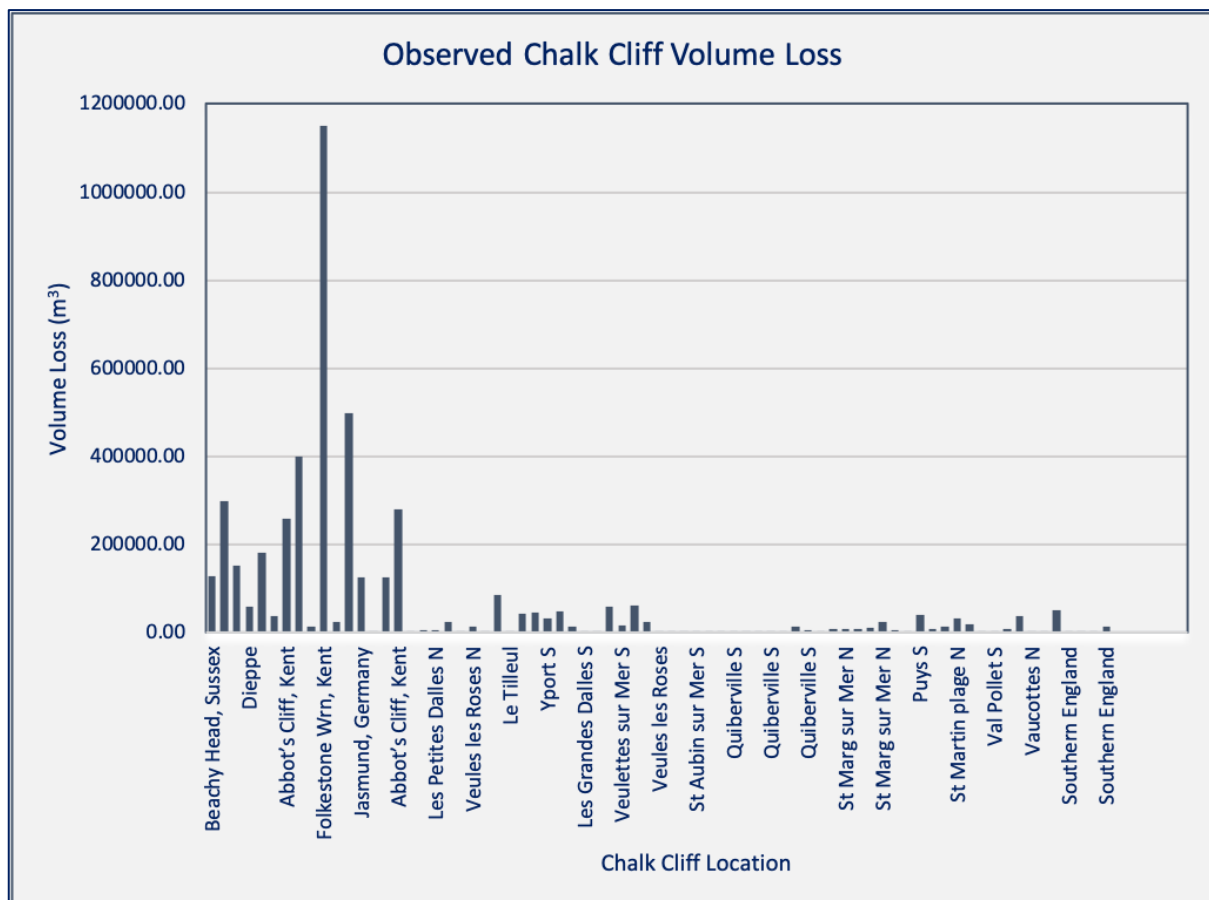


Figure 1.4; Chalk Cliff Erosion

Figure shows various observation from NW Europe chalk cliffs and their captured volume loss from erosion events (1943-2012). Data sourced from (Bowen and Take, 2014).

Observations have also been sought in geoenvironmental efforts, hypothesising addition to crushed carbonate to alkalise the ocean (Bach et al., 2019; Renforth and

Henderson, 2017; Taylor et al., 2015). Although geoengineering proposals are countered by spatial scale, global commitment and sustainability limitations (Feng et al., 2016), there has been a drive to experiment with CaO and olivine weathering (Paquay and Zeeb, 2013; Montserrat et al., 2017). Although methods are still controversial, it has heightened importance of carbonate weathering observations and understanding given its potential (Lenton and Vaughan, 2009).

Resultantly, there are deficiencies in global coastal carbonate weathering data (Duarte et al., 2013; McGrath et al., 2016). Although there is an argument that ocean-wide data is more valuable for understanding OA response importance (Caldeira and Wickett, 2003; Mackenzie, Ver and Lerman, 2000), it is increasingly apparent that the responses are especially variable for coasts, currently not captured in climate models (McGrath et al., 2016; Bauer et al., 2013). Variability in coastal weathering, which is currently represented as a constant global variable, could mean important influences are not quantified (Baldry, Mountford and Greenwood, 2017; Andersson, Mackenzie and Lerman, 2005).

## 1.5 Project Rationale

### 1.5.1 Originality and Justification

This project seeks to shed light on uncertainties from lack of observations and relational understanding that limits much of the application of carbonate weathering in past and future resilient studies. This is motivated from initial research for a novel undergraduate dissertation, exploring field and modelled carbonate coastal chemistries for alternate geologies. Upscaling to investigate carbonate coastal

geology influence on regional-global scales has only been implied to have biogeochemical influence, but such a study has not been done (to author's knowledge). Few studies give carbonate geology significance, in addition to a relative absence of literature exploring the response of this process to geological and anthropogenic pressures (Zeng, Liu and Kaufmann, 2019). This project will therefore be unique in the way it will pair geochemical signature with coastal geology and explore ways it will influence carbon and climate system resilience.

This research is important not only to understand the controls of recovery from past dramatic Earth system changes, but also to help inform what will be controlling the resilience for the future and if in any way this can be influenced. This has potential to refine timescales of recovery which help inform policies, preparedness and contribute to geoengineering feasibility insight (Legge et al., 2020). Slow processes need to be integrated into climate sensitivity analysis for there to be relevance to current climate policy (Royer, 2016). This is especially key for an expected increase of 50-500ppm CO<sub>2</sub> by end of century, thus imperative to increase understanding of deep-time changes and currently poorly resolved feedbacks, as they provide the only way to observe the complete Earth system responses to these changes (Hayhoe et al., 2017; Royer, 2016).

Rapidity of changes in response to anthropogenic forcing's have already triggered ocean ecological deterioration and chemical imbalances and compromised many regulatory feedbacks as they advance tipping points (Lenton et al., 2019). However, a common omission in assessment of Earth system responses is the dynamism of

coastal erosion and weathering (Cozannet et al., 2019), specifically of chalk coastlines and exposed land masses. As well as seeing dramatic chemical changes, significant carbonate uplift has occurred in geologically recent time (Gale and Lovell, 2018). This resource of weatherable  $\text{CaCO}_3$  rock in addition to enhanced weathering processes with climate change may provide an additional resilience to the carbon cycle and the ocean ecosystem. Previous studies have alluded to the erosion inputs from coasts having a role at geochemically stabilising the carbon balance in the oceans but have yet to explicitly capture the role of carbonate coasts, their rates of influence and the strength of stabilisation.

This study will therefore assess the relative role of the carbonate coasts as a carbon system stabiliser, and how significant its influence was in the past and how significant it will be in the future at amplifying system resilience to future changes in climate and carbon cycle dynamics.

### 1.5.2 Aims

- Test the sensitivity of the Earth System to a range of carbonate weathering rates
- Explore the relative geochemical weathering influence along with other cooperating influences during past climate event, namely the PETM
- Examine the differences in environmental settings between present and past events, and evaluate whether current settings allow for future additional resilience

## 2. Methodology

This chapter will elaborate on the tools used for analysis, and how the model analysis was designed.

### 2.1 cGENIE

cGENIE is a Fortran-based carbon cycle Grid Enabled Integrated Earth system model of Intermediate Complexity (EMIC). The model has the capacity to simulate complexities of the Earth system by modelling different components in isolation or together e.g. oceans, atmosphere, sediments etc., coupling 2D and 3D zonal atmospheres and oceans to account for biogeochemical cycles of elements and isotopes (Ridgwell et al., 2007). The model also has an additional deep-sea sediment module (SEDGEM) accounting for carbonate burial and preservation. This module represents carbon cycling in sediments which regulate the saturation,  $\text{CaCO}_3$  dissolution and aerobic respiration and can produce sediment cores of burial and compositions (Figure 2.1). This module has been refined and extensively explained by (Ridgwell and Hargreaves, 2007; Ridgwell, 2007). The model also incorporates a RokGeM module to support carbon cycling and terrestrial rock weathering. Fluxes of alkalinity and DIC are routed to coastal oceans as a result of silicate and carbonate rock weathering (Greene et al., 2019). Weathering in the model is commonly applied as a function of temperature (Colbourn et al., 2013). Schematic of modules shown below (Figure 2.2).

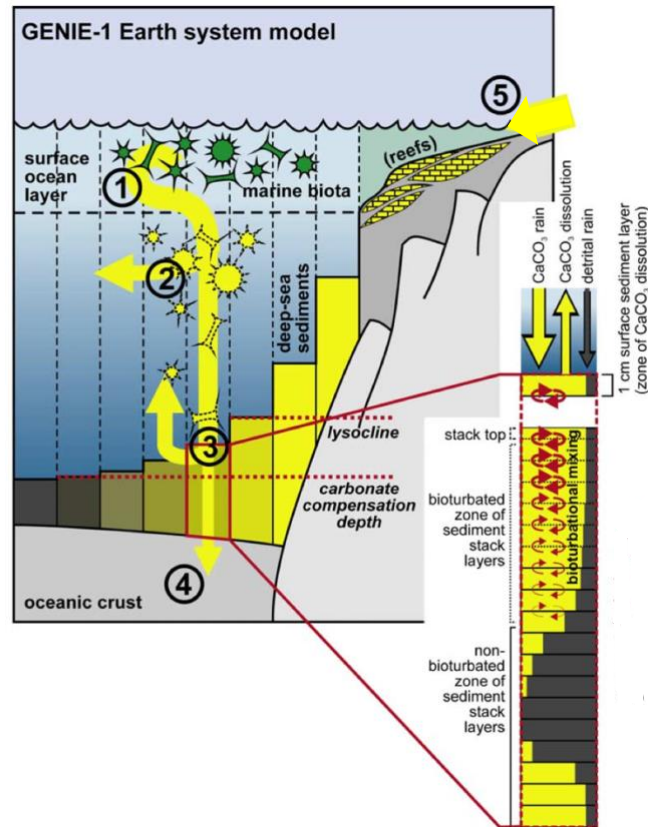


Figure 2.1; SedGEM Schematic

Diagram of the sediment module configuration and carbonate cycling relationship. Comprises of (1) Plankton calcification and surface ocean export (2) Biogenic  $\text{CaCO}_3$  dissolution in water column (3) Surface sediment  $\text{CaCO}_3$  dissolution (4) Sediment burial of accumulated and preserved  $\text{CaCO}_3$  (5) Terrestrially weathered solute supply to ocean. Also highlighted is calculation of surface layer  $\text{CaCO}_3$  accumulation/dissolution and bioturbation mixing layers. Adapted from (Ridgwell 2007).

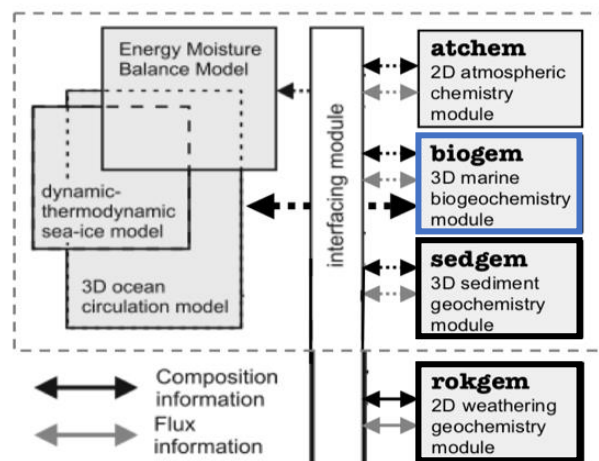


Figure 2.2; cGENIE Modules

Diagram showing the various modules in cGENIE. Highlighted bold are RokGem and SEDGEM discussed in this section. Highlighted blue is Biogem which has predominantly been used for outputs of marine biogeochemistry results. Adapted from (Colbourn et al., 2013)



Embedded in the model is an array of possible paleogeography and bathymetry configurations, added over successive development. Each configuration comes with pre-defined conditions of the specific scenario/world being modelled. This project uses a new configuration of a 'FAKE' world, by where there is a continental configuration of averaged relief across a 18x18 grid. The ocean depths are averaged to correct volume, then border either side by linear landmass. This configuration allows for different depths of continental shelf.

## 2.2 Model Simulations

Experiments were undertaken to explore the sensitivity and influence of enhanced Carbonate weathering for different scenarios. Following similar methods to Hargreaves and Ridgwell (2007), an initial 50kyr spin-up was run under a "closed" system to force the ocean-atmosphere carbon cycle to a prescribed CO<sub>2</sub> (pre-industrial: 278 ppm). A global-averaged weathering rate of  $10 \times 10^{12}$  mol Ca<sub>2+</sub> yr<sup>-1</sup> was used to track predicted responses and equilibrium of carbonate chemistry, without a CO<sub>2</sub>/climate response. A second 50kyr spin-up of an "open" system was also run, with climate and CO<sub>2</sub> now able to respond to changes induced by set weathering rate ( $10 \times 10^{12}$  mol Ca<sub>2+</sub> yr<sup>-1</sup>). Unlike similar open study systems (Greene et al., 2019; Archer et al., 2009; Colbourn, Ridgwell and Lenton, 2013), carbonate weathering is not temperature-dependent and is instead forced to produce a temperature response. Equilibrium and fixed CO<sub>2</sub> content then decided a closed system spin-up would be most appropriate to run following simulations from.

Next, 20kyr ensembles from the closed-system spin-up used different weathering rates for open and closed systems, to identify how the spun-up equilibrium state differs with varying regulatory  $\text{CaCO}_3$  weathering. The weathering rates applied were changed to 2, 5, 15 and 20, in addition to the default global average value of 10 ( $\times 10^{12} \text{ mol Ca}_{2+} \text{ yr}^{-1}$ ). Set weathering rates were used to represent a range of environmental conditions (Table 1), instead of applying a rate diagnosed from burial flux (Greene et al., 2019).

Table 1; Weathering Rate Justification

Table showing the weathering rates used in this analysis (shaded blue) and where these have been refined from similar values in the literature (shaded grey).

Weathering rate applied ( $\times 10^{12}$ mol $\text{Ca}_{2+}$ $\text{yr}^{-1}$ )	Justification
<b>2</b>	20% of average rate, to represent exceptionally low weathering environment and capture lower extremes for relativity.
<b>5</b>	50% of average to represent reasonable low weathering environment.
<b>10</b>	Average global rate used in cGENIE (Ridgwell, 2007).
<b>15</b>	Used to represent reasonably high weathering environment, striking a median of rates discussed below.
<b>20</b>	Double average rate to represent upper limit extreme of a high weathering environment, assuming previous high estimates underestimations.
<b>12</b>	Rate from (Morse and Mackenzie, 1990), also used in LOSCAR model (Zeebe, 2012).
<b>12</b>	LGM weathering rates (Simmons, Myask and Matthews, 2016).
<b>24</b>	Carbonate weathering from average carbon fluxes (Shields and Mills, 2017)

A PETM style  $\text{CO}_2$  pulse was applied using similar event characteristics to Erba et al., (2010) and Panchuk, Ridgwell and Kump (2008).  $\text{CO}_2$  forcing was changed and scaled to force a 45000PgC pulse for 10,000 years of the simulation. Further  $\text{CO}_2$  pulse experiments were adapted from IPCC RCP6 and RCP8.5 scenarios, using data from Meinhausen et al (2011) (Figure 6.A), which was scaled to a rate applicable to force in the model (Table 2). Ensembles for timescales of pulse and amount of  $\text{CO}_2$  released were adapted from other cGENIE experiments assessing

carbon cycle responses (Ridgwell, 2007; Ridgwell and Hargreaves, 2007; Greene et al., 2019).

*Table 2; Scenario Forcing*

*Table showing the carbon forcing, duration and full run duration.*

<b>Scenario Name</b>	<b>Forcing (PgC)</b>	<b>Forcing Duration (years)</b>	<b>Simulation Duration (years)</b>
RCP 6	1000	1000	20,000
RCP 8.5	4500	1000	20,000
PETM	45000	10,000	80,000

Additional experiments were also undertaken to test relative strength of weathering rates against other enhancing features. Bioturbation was switched on to assess the effect on carbonate chemistry and sediments similar to experiments by Panchuk, Ridgwell and Kump (2008). Sensitivity runs were also started from a new 50kyr equilibrium spin-up using an open simulation using  $20 \times 10^{12}$  mol  $\text{CaCO}_3$   $\text{yr}^{-1}$  weathering rate. With this, the impact of a higher starting  $\text{CaCO}_3$  composition (wt%) could be assessed on systems with different weathering states. Additional 20kyr runs were undertaken using the higher weathering 50kyr spin up, apply all 5 weathering rates. All model runs are outlined in (Table 3).

Table 3; Experiment Details

Table shows the included features of all model runs undertaken for this analysis. 50kyr spin ups were used to set up a new stabilised starting environment, then tested for weathering rate sensitivity for 20kyrs. Table also shows what weathering rates were tested for a range of perturbation experiments and sensitivity analysis. Instances when the forcing had to be changed is also noted. Total number of runs for type of experiment are shown in final column.

Experiment name	System		Weathering Rate (x 10 <sup>12</sup> )					Perturbation Changes		Total
	Open	Closed	2	5	10	15	20	Forcing Change	CO <sub>2</sub> Forcing	
50kyr spin ups	✓	✓			✓		✓			4
20kyr sensitivity	✓	✓	✓	✓	✓	✓	✓			10
Bioturbation On	✓	✓	✓	✓	✓	✓	✓			10
20kyr RCP 6	✓		✓	✓	✓	✓	✓	✓	✓	5
20kyr RCP 8.5	✓		✓	✓	✓	✓	✓	✓	✓	5
80kyr PETM	✓		✓	✓	✓	✓	✓	✓	✓	5
20kyr High Initial CaCO <sub>3</sub>	✓		✓	✓	✓	✓	✓			5
All										44

All graphed outputs were taken from the BIOGEM module. Graphs were plotted and analysed in Matlab. SedGEM outputs were saved as netCDF files. The data was analysed and displayed using Panoply (<https://www.giss.nasa.gov/tools/panoply/>), against the sedimentary topography of the configuration (Figure 6.B). Simple statistics (average, ranges, medians) were calculated in Microsoft Excel and Matlab. Linear regression statistics were obtained and presented from Matlab for several variable combinations. From this, outputs of significance, error and regression were also obtained. Reference to weathering rate will be communicated as '2W', '5W', '10W', 15W and '20W'.

## 3. Results

### 3.1 Ensemble 1: Sensitivity to CaCO<sub>3</sub> weathering

#### Temperature (Figure 3.1)

Clear temperature variation exists between different weathering rates for an open system, ranging by 2.4°C. The lowest weathering rate (2W) increases by 1.4°C over the 20000 years, the highest weathering rate (20W) decreases by -0.9 °C. 15W shows a tight temperature range to 10W; 0.16°C less than 10W but 0.92°C more than 20W by the end of the simulation. Ocean temperature mirrors these weathering temperature trends. Ocean temperature is smaller than atmospheric (1.7°C).

Maximum temperatures in the ocean are 3.6°C higher than atmospheric. For a closed system, the temperature range is limited as induced by the model to maintain a constant pCO<sub>2</sub>. No distinct trend is visible for each weathering rate. Temperatures fluctuate around an average 11.7°C (atm) and 15.8°C (ocean).

#### pCO<sub>2</sub> (Figure 3.2)

Atmospheric pCO<sub>2</sub> reflects the same trends as temperature change for weathering rates, ranging by  $1.6 \times 10^{-4}$  (atm). 10W and 15W follow a tight, relatively stable trend around  $2.8 \times 10^{-4}$  (atm) while 5W and 2W increase by 20% and 32.4% respectively, and 20W decreases by 20.6%. For sea-to-air pCO<sub>2</sub> flux, 2W-10W follow a decreasing trend from starting values ranging between  $1.15 \times 10^{12}$  to  $2.66 \times 10^{12}$ . 15W and 20W have an increasing trajectory, from  $3.25 \times 10^{10}$  and  $-7.21 \times 10^{11}$  respectively. 15W has a concave trend, increasing at a relatively stable average rate of  $-4.93 \times 10^7$  yr<sup>-1</sup>. 20W increases by 142% during the first 10000 years, followed by a remaining average rate of  $1.9 \times 10^7$  yr<sup>-1</sup>. All weathering rates except 15W finish the

20kyr on a flux  $\sim 0$ . 15W finishes at  $-1$  ( $\text{mol yr}^{-1}$ ), a change of  $9.86 \times 10^{11}$  across 20kyr. The maximum change of  $1.98 \times 10^{12}$  was for 2W, while the minimum was for 20W at  $6 \times 10^{11}$ . For a closed system, flux values range between  $6$  -  $-6$ , with all weathering rates equally split in flux response that follows a trend to 0 flux, highest fluxes are observed for the lowest weathering rates. Small instances of variability are notable for the last 10,000 years of the simulation for 2W and 5W, values ranging by  $1.98 \times 10^{12}$  and  $1.07 \times 10^{12}$  respectively.

### **Carbonate Sediments (Figure 3.3)**

Mean  $\text{CaCO}_3$  composition ranges 37.8% more for an open than closed system. Both systems demonstrate lowest wt% for lowest weathering rate. An end value difference of 9.07wt% exists between 5W-10W in an open system, while the difference is only 5.06wt% between 10W-15W. The difference between 15W-20W is 35% higher than this. Only 20W and 15W increase in  $\text{CaCO}_3$  composition for a closed system. Ocean to  $\text{CaCO}_3$  sediment fluxes 20kyr fluxes range by  $4.01 \times 10^{12}$   $\text{mol yr}^{-1}$  for an open system and  $1.33 \times 10^{12}$   $\text{mol yr}^{-1}$  for a closed. The most range is shown by 2W, also shown by 20W which ranges by  $3.87 \times 10^{11}$  in ocean-sediment  $\text{CaCO}_3$  flux peaks.

### **Ocean Chemistry (Figure 3.4)**

For an open system, pH ranges between 7.9 and 8.1 which is 90% greater than the range for a closed system. Both open and closed follow the same order of weathering rate trends, however for an open system 15W and 10W are closer in pH relative to 5W and 20W, whereas a closed system shows weathering trends spread by equal magnitude across the range of pH. For an open system, 20W increases by

0.096 pH, demonstrating similar to the inverse trends for 2 and 5 (-0.145 and -0.091 respectively). For both systems, 15W and 20W are the only trends exhibiting an increase. 15W and 20W are also the only to increase for DIC, with all rates demonstrating a variable stepped profile, whereas 10W is relatively stable. For an open system, 15W and 20W overlap in trends, initially 15W is higher than values for 20W, but for the latter 10,000 years 20W continues an increasing trajectory finishing the 20000 years with a DIC 0.9% higher than 15W. This differs to a closed system, where 15W is a median between 20W and 10W trends. A closed system also has a 76.4% larger range.

### **50kyr Comparison (Figure 3.5)**

For mean  $\text{CaCO}_3$  composition changes, a closed system stabilises earlier and less dramatically than an open system. A closed system decreases by  $-5.34 \times 10^{-4}$  yr from 4ky after initial faster decrease of  $-7.47 \times 10^{-3}$  yr<sup>-1</sup>, whereas for an open system the rate from 4kyr is 0.6% higher. Both finish simulation at equilibrium states 15.7 wt% (open) and 21.3 wt% (closed).  $\text{pCO}_2$  increases throughout simulation, except for a -1.33% decrease from 20 years to 105 years. The increase rate of  $4.78 \times 10^{-9}$  yr<sup>-1</sup>, finishes the simulation with a  $\text{pCO}_2$  58% higher than the forced  $2.78 \times 10^{-4}$  concentration in a closed simulation. Atmospheric temperature stabilises relatively quickly for an open system, equilibrating at 14°C at year 27000. By the end of simulation, temperature is 20.25% higher than a closed system. Open system temperature decreases by 2.9°C between years 120-900, then increases to its stable state.



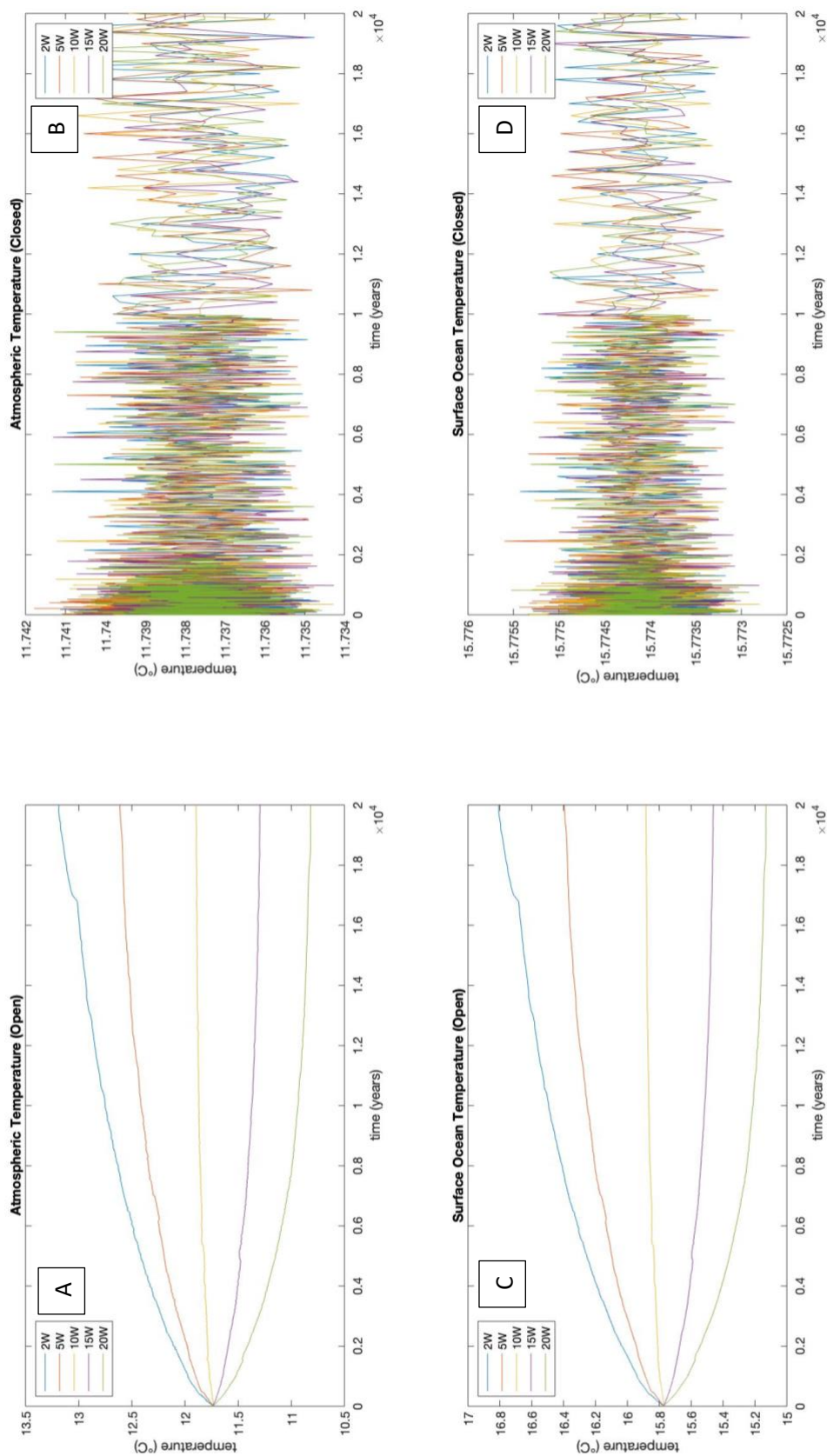


Figure 3.1; Ocean and Atmospheric Temperature: Open vs Closed

Figure shows both ocean and atmosphere temperature responses to different weathering rates under open and closed systems. (A) Atmosphere response, open (B) Atmosphere response, closed (C) Ocean response, open (D) Ocean response, closed.

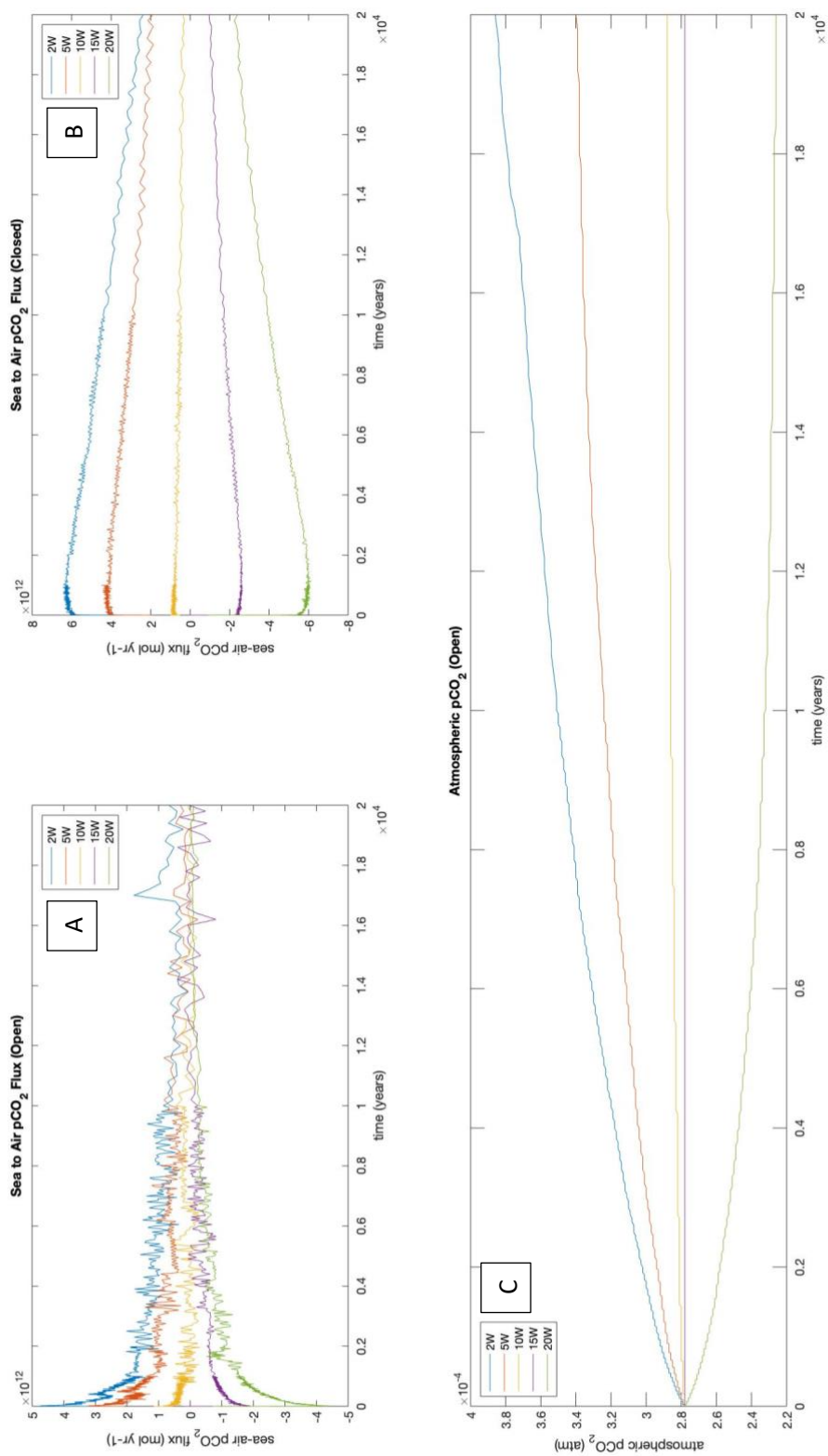


Figure 3.2;  $p\text{CO}_2$  Flux: Open vs Closed

(A) shows the sea-to-air transfer flux of  $p\text{CO}_2$  response for different weathering rates (B) Shows the same for a closed system which demonstrates where  $\text{CO}_2$  flux needs to be to maintain constant atmospheric  $\text{CO}_2$  (C) shows the atmospheric  $p\text{CO}_2$  response for different weathering states in an open system.

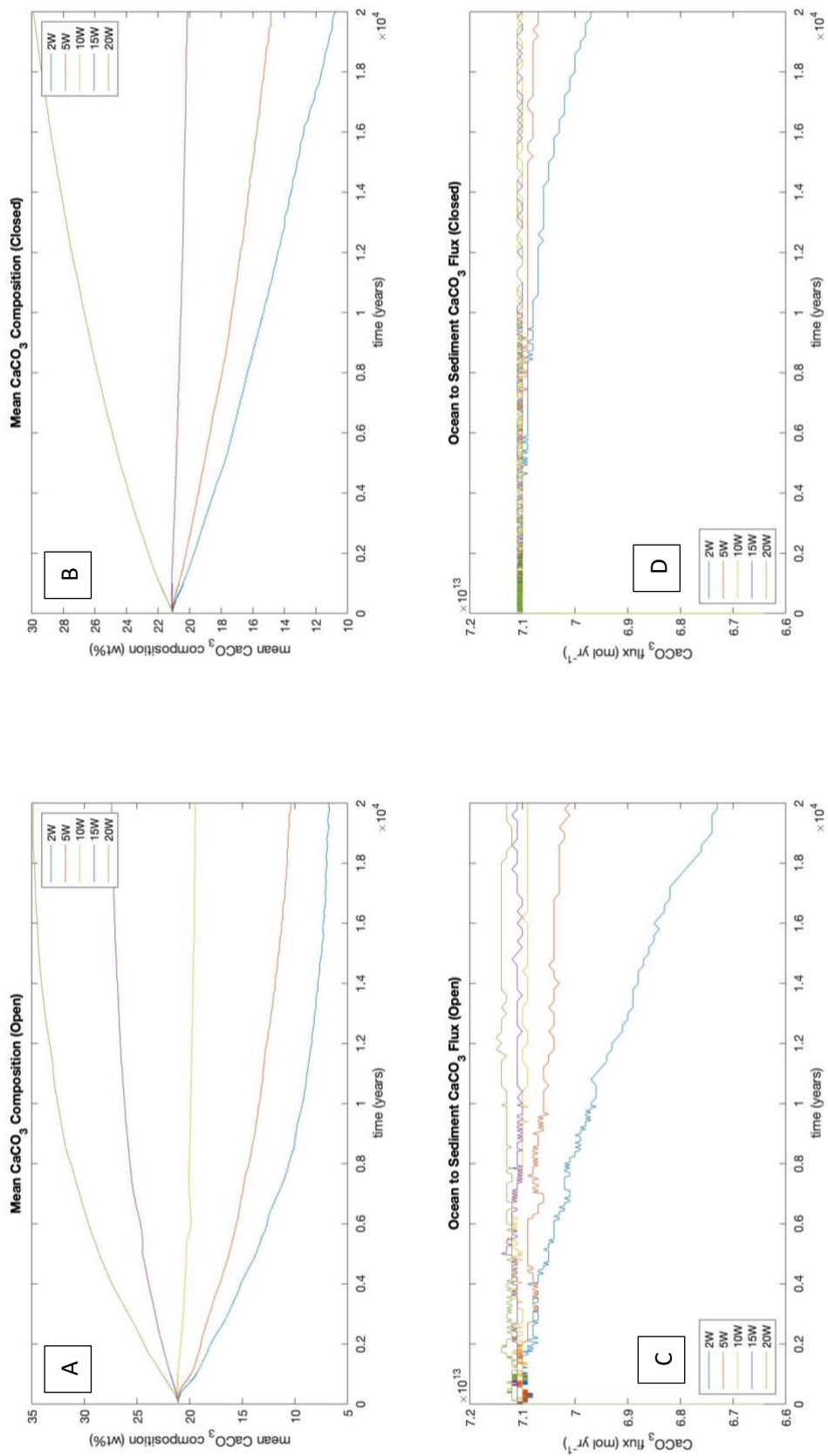


Figure 3.3;  $\text{CaCO}_3$  Sedimentary Responses: Open vs Closed

(A) and (B) show the mean  $\text{CaCO}_3$  sedimentary composition responses to open and closed systems respectively, with applied range of weathering rates. (C) and (D) show the ocean-to-sediment  $\text{CaCO}_3$  flux response for same weathering rates, for open and closed systems respectively.

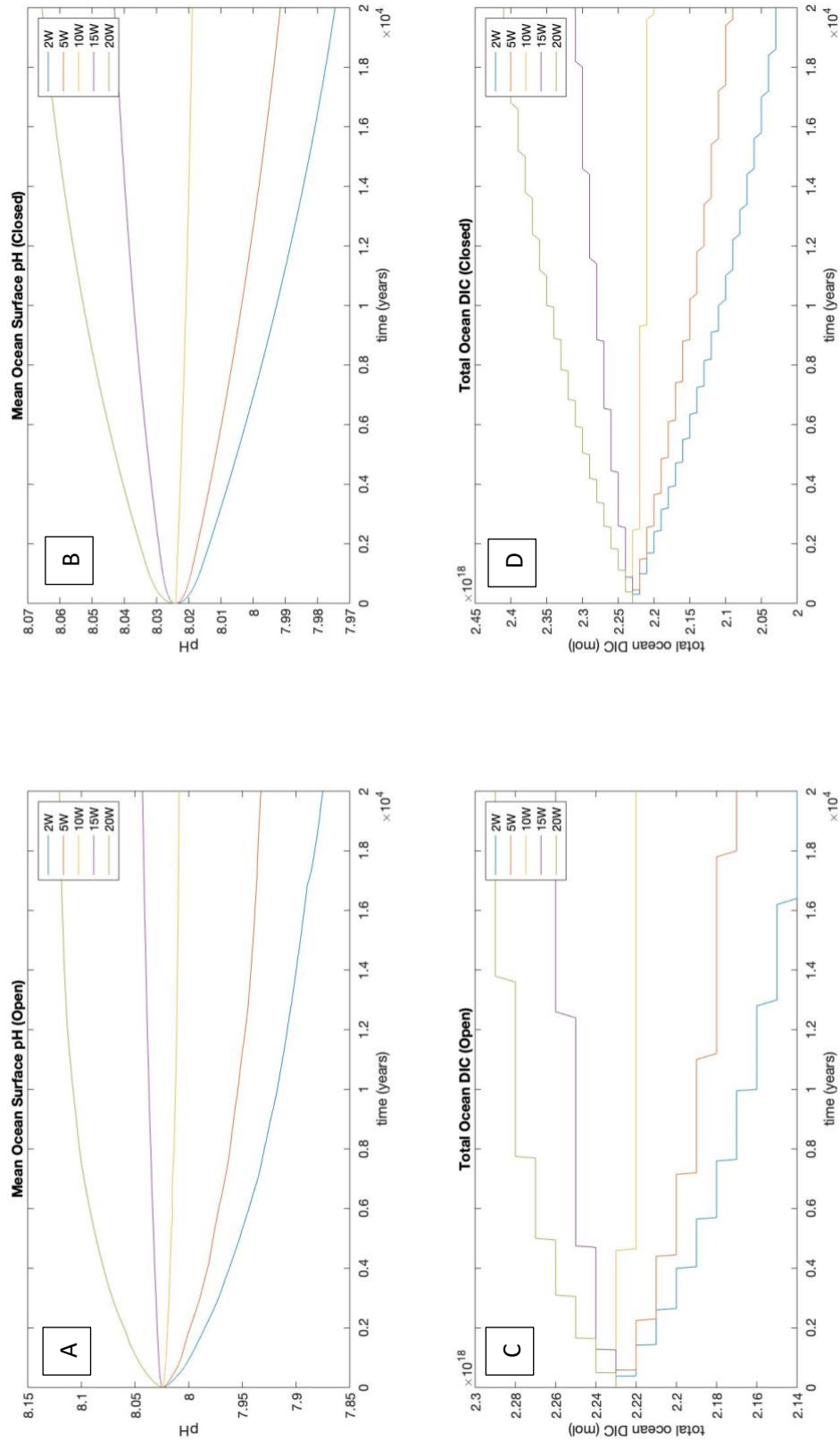


Figure 3.4; pH and DIC Responses: Open vs Closed

Figure shows pH and DIC responses to range of weathering rates under open and closed systems. (A) and (B) show pH responses under open and closed systems respectively. (C) and (D) show DIC responses to open and closed systems respectively.

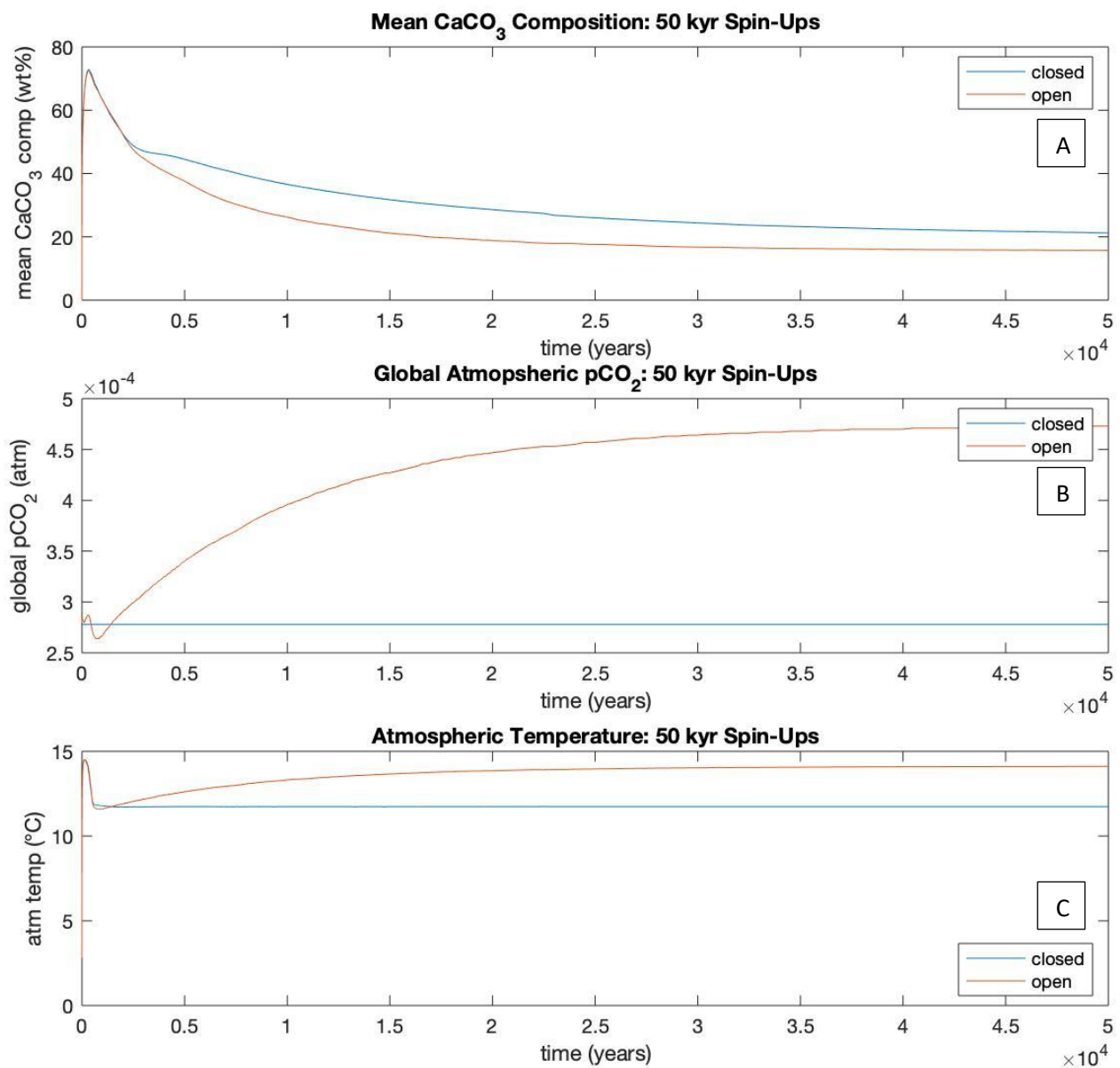


Figure 3.5; 10W Spin-Ups: Open vs Closed

Figure shows a comparison of the carbonate and climate states after 50kyr spin ups with 10W, for both open and closed systems. (A) shows the response of CaCO<sub>3</sub> sedimentary composition (B) Atmospheric pCO<sub>2</sub> (C) Atmospheric Temperature.

### 3.2 Relational Statistics

(Figure 3.6) shows regressions for the relationships between pH and pCO<sub>2</sub> which all show very high (0.991-0.999) R<sub>2</sub> values, the lowest for 10W. RMSE decreases with increasing weathering rate to 15W, ranging from 0.00174 (2W) to 0.000537 (15W), then increases for 20W to 0.000838. M value decreases as weathering rate increases, decreasing by -389.9 from 2W to 20W.

Regressions for the CaCO<sub>3</sub> to pCO<sub>2</sub> relationships (Figure 3.7) also show high R<sub>2</sub> values, again lowest for 10W at 0.932. These R<sub>2</sub> values are on average 0.02 lower than those for the R<sub>2</sub> for pH and pCO<sub>2</sub>. Aside from the minimum at 10W, R<sub>2</sub> decreases with increasing weathering rate, ranging from 0.988 (2W) to 0.978 (20W). SE increases with increasing weathering rate, while RMSE reaches its highest values for the lowest (2W) and highest (20W) weathering rates; 0.523 and 0.681, respectively.

All relationships tested were of significance <0.05 p value.

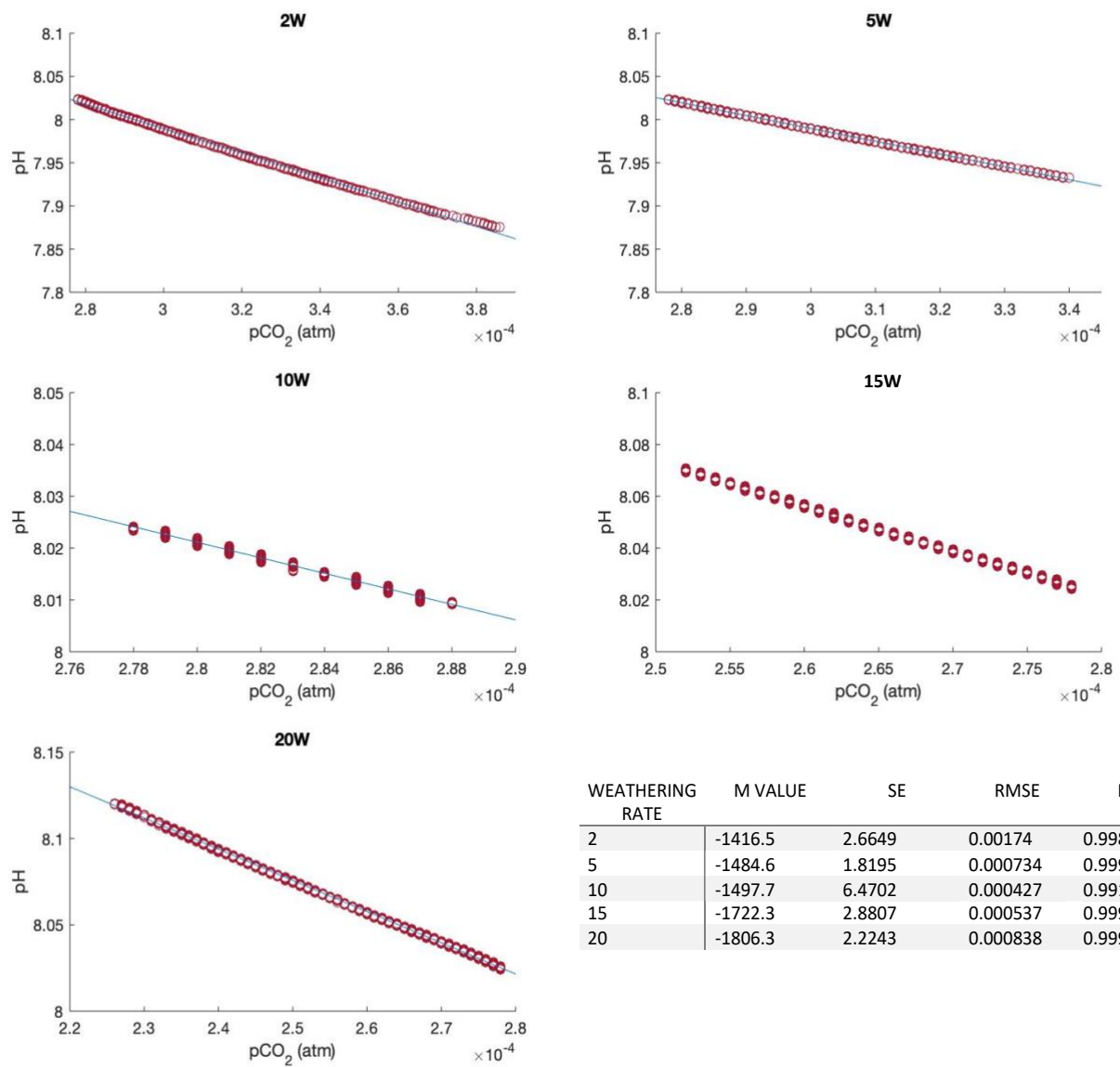


Figure 3.6; pH and  $p\text{CO}_2$  relationships

Figure shows the regression relationships between pH and  $p\text{CO}_2$  and how this varies with weathering rate. Points are plotted along ordinary least squares regression line. Table details additional statistical outputs.

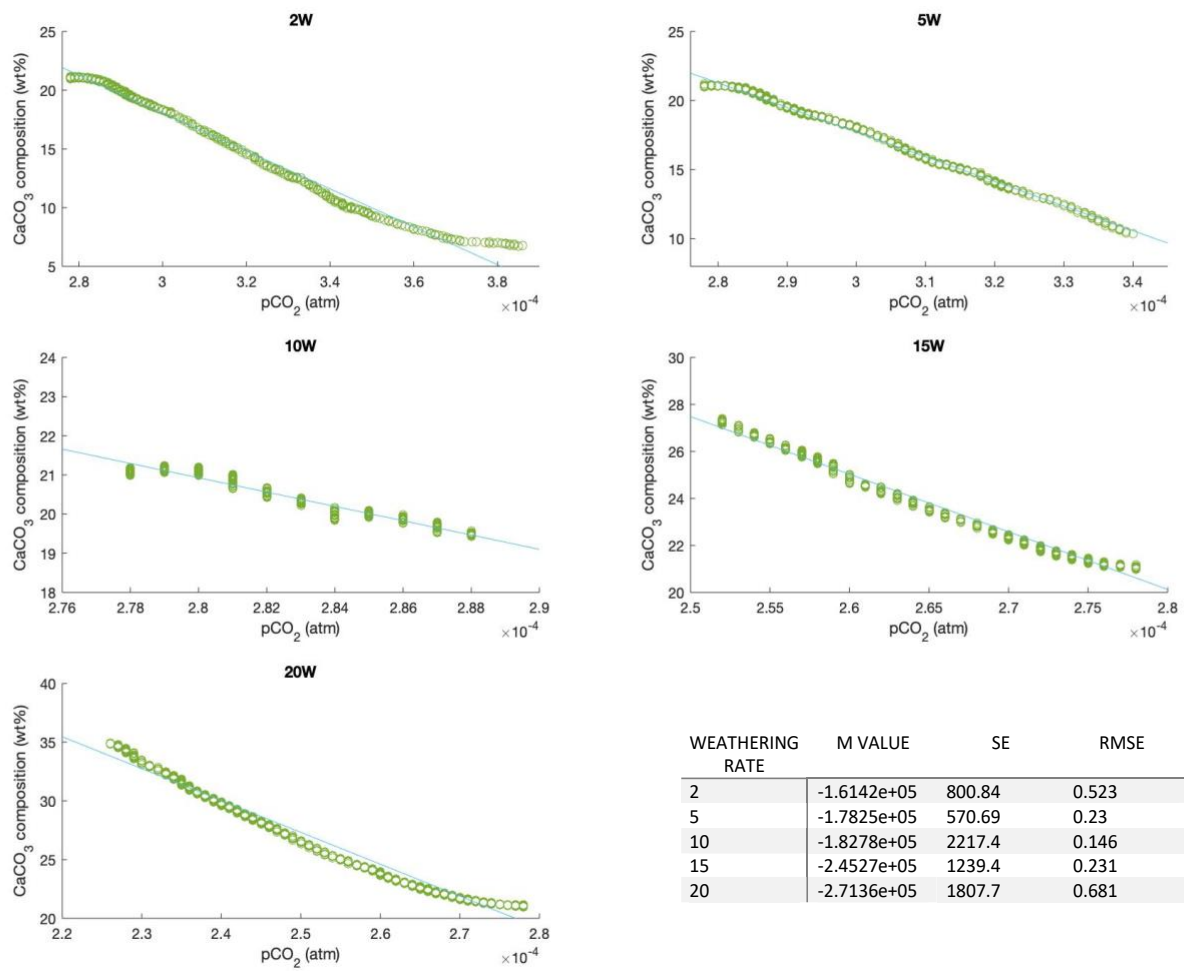


Figure 3.7;  $\text{CaCO}_3$  Composition and  $\text{pCO}_2$  relationships

Figure shows the regression relationships between  $\text{CaCO}_3$  sediment composition and  $\text{pCO}_2$  and how this varies with weathering rate. Points are plotted along ordinary least squares regression line. Table details additional statistical outputs.



### 3.3 Ensemble 2: Weathering Strength Against CO<sub>2</sub> Pulse

#### 3.3.1 RCP6

##### **pCO<sub>2</sub> and Temperature Response (Figure 3.8)**

Clear differences exist for the pCO<sub>2</sub> response across all weathering rates, shown by an end-simulation range between  $\sim 5 \times 10^{-4}$  atm -  $\sim 2.6 \times 10^{-4}$  atm. During the first 4kyr after pulse end, all decrease by rates ranging from  $-2.02 \times 10^{-8}$  yr<sup>-1</sup> (atm) (2W) to  $-3.63 \times 10^{-8}$  yr<sup>-1</sup> (atm) (20W). From 4kyr 2W starts an increase trajectory at a rate of  $2.65 \times 10^{-9}$  (atm) yr<sup>-1</sup>, while all other rates continue to decrease. 20W decreases at the fastest rate of  $-1.12 \times 10^{-8}$  (atm) yr<sup>-1</sup>. pCO<sub>2</sub> finishes on higher concentrations than ensemble 1 for lower weathering rates but relatively similar for higher rates.

Sea to Air pCO<sub>2</sub> flux decreases at an average rate range of  $-4.27 \times 10^{10}$  mol yr<sup>-2</sup> (2W) to  $4.63 \times 10^{10}$  mol yr<sup>-2</sup> (20W) during the event. Post-event recovery to no-net-flux staggers between weathering rates, achieved at years 3500 for 2W, then 19000 for 20W. Relative to ensemble 1, lower fluxes are present across all weathering rates for RCP6 forcing.

Temperature decreases immediately across all weathering rates after event end, decreasing at a rate range of  $-1.86 \times 10^{-4}$  °C (2W) –  $4.11 \times 10^{-4}$  °C (20W) for 3.5kyr. Post this, 2W increases to an end simulation maximum of 14.32 °C. 10-20W decrease to a final temperature range of 12.76°C – 11.56°C respectively, while 5w remains relatively stable at a T of  $\sim 13$ °C. Compared to ensemble 1, temperatures are on average 1.4 °C higher.

##### **Sediment and Carbonate Chemistry Response (Figure 3.9)**

CaCO<sub>3</sub> decreases by a range of 42% (2W) to 32% (20W) over the 1kyr event. From year ~2000 10W, 15W and 20W increase by 7.7 wt%, 14.8 wt% and 21.4 wt% respectively across the remainder of the run. 20W and 15W end with compositions 18.3% and 56.7%, higher than starting composition, respectively. 2W and 5W decrease, similar to that without a forcing. Overall, trends are more positive but cover less of a range than ensemble 1.

Ocean to sediment CaCO<sub>3</sub> fluxes demonstrate a stepped decrease during event, resulting in minimums ranging from  $6.28 \times 10^{13}$  mol yr<sup>-1</sup> (2W) to  $6.72 \times 10^{13}$  mol yr<sup>-1</sup> (20W). After the event all increase to maximum at year ~3000. 20W does so first but has a maximum value 0.03% less than 15W and 10W. All rates but 2W finish at a flux of  $\sim 7 \times 10^{13}$  (mol yr<sup>-1</sup>), while 2W decreases throughout the remainder of the 20kyr finishing at a flux of  $6.64 \times 10^{13}$  (mol yr<sup>-1</sup>).

pH trends increase from event end at rate ranges of  $4.03 \times 10^{-6}$  pH yr<sup>-1</sup> (5W) to  $1.36 \times 10^{-5}$  pH yr<sup>-1</sup> (20W), while 2W decreases from 3000 years. After 20000 years 2W pH is only 0.24% more than event minimum pH (7.78). 15W and 20W surpass starting pH, 20W reaching a maximum of 8.08 by end of 20kyr, a 0.75% increase. Event minimums range from 7.78 (2W) to 7.83 (20W).

DIC trends for 10W, 15W and 20W all continue to increase immediately after event end. 5W follows a stable trend while 2W decreases by -1.09%. During event, all increase by a rate range of  $3.22 \times 10^{16}$  mol (2W) to  $5.64 \times 10^{16}$  mol (20W). By year 20000, all DIC trends are higher than starting DIC, most for 20W which is 8.9% higher than it's starting DIC.

### 3.3.2 RCP8.5

#### **pCO<sub>2</sub> and Temperature Response (Figure 3.10)**

By the end of event, pCO<sub>2</sub> increased by an average of 514% across all weathering rates. Descent after event happens the fastest for the highest weathering rate at  $-5.95 \times 10^{-8}$  atm yr<sup>-1</sup>. pCO<sub>2</sub> ranges by  $6.32 \times 10^{-4}$  atm at 20000 years. Unlike the RCP6 experiment, no weathering rate achieves a return to start pCO<sub>2</sub>, with the lowest pCO<sub>2</sub> (20W) still  $2.59 \times 10^{-4}$  atm higher than starting pCO<sub>2</sub>. pCO<sub>2</sub> reaches a peak 3.2 times higher than that for RCP6.

Sea to air pCO<sub>2</sub> flux decreases to a minimum of ranging from  $-1.28 \times 10^{14}$  mol yr<sup>-1</sup> (2W) to  $-1.39 \times 10^{14}$  mol yr<sup>-1</sup> (20W). This occurs mid-way through event (500 years), after which there is an increase until end of event. From a flux of  $\sim -1.20 \times 10^{14}$  mol yr<sup>-1</sup> there is an increase to values around 0 during a 4000-year duration. 15W and 20W remain the lowest by end of simulation at  $-3.10 \times 10^{12}$  mol yr<sup>-1</sup> and  $-2.56 \times 10^{12}$  mol yr<sup>-1</sup> respectively, while 2W fluctuates around 0 by  $2.56 \times 10^{12}$  mol yr<sup>-1</sup>. Reaching 0 flux takes 1000 years longer than RCP6.

No weathering rate returns to starting temperature by end of simulation. Peak temperature occurring at end of event reaches 19.6°C (2W). All rates decrease after event end, however 2W stabilises from 5000 years at 18°C. 20W decreases by 4.6°C from event peak, to 14.7°C. Relative to RCP6, temperatures finish on average 3.6°C higher for RCP8.5.

#### **Sediment and Carbonate Chemistry Response (Figure 3.11)**

CaCO<sub>3</sub> composition decreases to  $\sim 3$  wt% for all weathering rates by end of event, an average 80% decrease over 1000 years. Post event composition continues to

decrease for 800 years, to minimums ranging from 0.92 wt% (2W) to 2.1 wt% (20W). Composition remains relatively stable for all rates until 10000 years, and 20W dramatically increases by  $1.3 \times 10^{-2}$  wt% yr<sup>-1</sup> until end simulation, finishing at composition 17.4wt%. 15W follows a similar increase 2500 years later finishing at 9.1wt%. CaCO<sub>3</sub> composition is unable to return to original levels and is on average 60% less than final RCP6 values.

Ocean to sediment CaCO<sub>3</sub> flux returns to, and exceeds, starting values for 20W and 15W. End-event minimums range from  $2.64 \times 10^{13}$  mol yr<sup>-1</sup> (2W) to  $2.95 \times 10^{13}$  mol yr<sup>-1</sup> (20W), and are then followed by relatively rapid increase in the 5000 years after event end ranging in rates of  $3.76 \times 10^9$  yr<sup>-2</sup> (2W) to  $7.29 \times 10^9$  yr<sup>-2</sup> (20W). Post this, 2W stabilises at  $4.24 \times 10^{13}$  mol yr<sup>-1</sup>, while all other fluxes increase. Ranges of ocean-sediment CaCO<sub>3</sub> are on average greater by  $3.75 \times 10^{13}$  mol yr<sup>-1</sup> greater than for RCP6.

pH and DIC follow a similar trend to ocean-sediment CaCO<sub>3</sub> flux, also demonstrating a post-event 5000-year faster increase, followed by a large ranging increase for all but results for 2W. pH decreases by an average 8.38%. By event end no trends return to original pH. 20W achieves a pH after 20000 years, 2.5% lower than that for RCP6. DIC however increases through pre- to post-event, increasing by an average rate of  $1.31 \times 10^{14}$  mol yr<sup>-1</sup> during event, to a maximum rate (20W) of  $2.47 \times 10^{13}$  yr<sup>-1</sup> post-event.

### 3.3.3 PETM

#### **pCO<sub>2</sub> and Temperature Response (Figure 3.12)**

During the 10,000-year event, increases in pCO<sub>2</sub> for different weathering rates diverge to an end event range of 3.69x10<sup>-4</sup> atm. For the remaining 70kyr, 2W remains relatively stable at 1.2x10<sup>-3</sup> atm, while other weathering rates decrease in pCO<sub>2</sub>. 20W decreases at a rate of -6.44x10<sup>-9</sup> atm yr<sup>-1</sup>. By 40kyr pCO<sub>2</sub> for 20W and 15W stabilises at 4.54x10<sup>-4</sup> atm 5.05x10<sup>-4</sup> atm respectively.

Similar trends are produced for temperature change; maximum temperature at the end of event range from 18.3°C (2W) to 16.9°C (20W). Post event, 20W decreases to stabilise from 40kyr at 13.9°C. 2W instead decreases only by 0.4°C over 1000 years, then increases again to 18.5°C.

Sea-to-air pCO<sub>2</sub> flux decreases during the 10kyr event, ranging from -1.76x10<sup>13</sup> mol yr<sup>-1</sup> (2W average) to -2.43x10<sup>13</sup> mol yr<sup>-1</sup> (20W average). Post event, all rates increase to 0, met first by 2W at 11200 years to 34000 years for 10W. 5W-20W stabilise and fluctuate around 0 for the remaining duration, while 2W increases to a peak of 2.57x10<sup>13</sup> mol yr<sup>-1</sup> at 12000 years, before decreasing again 1000 years later to 0.

### **Sediment and Carbonate Chemistry Response (Figure 3.13)**

CaCO<sub>3</sub> decreases during event at a rate range of -1.91x10<sup>-3</sup> wt% yr<sup>-1</sup> (2W) to -1.68x10<sup>-3</sup> wt% yr<sup>-1</sup> (20W). A minimum CaCO<sub>3</sub> composition of 2.07 wt% is reached at event end by 2W. Post event CaCO<sub>3</sub> rapidly increases for rates 20W-10W, however there is a lag before the sharp gradient for weathering rates 15W and 10W. 20W increases by 1.07x10<sup>-3</sup> wt% yr<sup>-1</sup> for 22000, which continues until simulation end at a rate of 5.33x10<sup>-5</sup> wt% yr<sup>-1</sup>. 20W and 15W both finish on compositions 45.2% and 3.4% higher than starting composition, respectively. Of all outputs for PETM in

displayed figures,  $\text{CaCO}_3$  is the only trend whereby 5W is unable to increase to values closer to 10W than 2W.

End event ocean to sediment  $\text{CaCO}_3$  flux decreases to a range from  $6.06 \times 10^{13}$  mol  $\text{yr}^{-1}$  (20W) to  $3.76 \times 10^{13}$  mol  $\text{yr}^{-1}$  (2W). Post event, 20W increases the fastest at a rate of  $1.61 \times 10^9$  mol  $\text{yr}^{-2}$  for 8000 years after event, before stabilising at a flux of  $7.36 \times 10^{13}$  mol  $\text{yr}^{-1}$  from 48000 years. 2W increases at the slowest rate of  $6.39 \times 10^7$  mol  $\text{yr}^{-2}$  after event. Maximum flux of  $7.53 \times 10^{13}$  mol  $\text{yr}^{-1}$  is reached at year 22000 by 20W. Rates 20W, 15W and 10W all achieve fluxes higher than starting flux.

During event, pH decreases by a range of -0.56 pH (2W) to -0.38 pH (20W). 20W increases by 0.32 pH from event minimum. No rate is able to return to starting pH. DIC increases relatively rapidly during event. Post event, 2W reduces in its rate of increase by 97%, while 20W maintains high rates until stabilising from 40kyr.

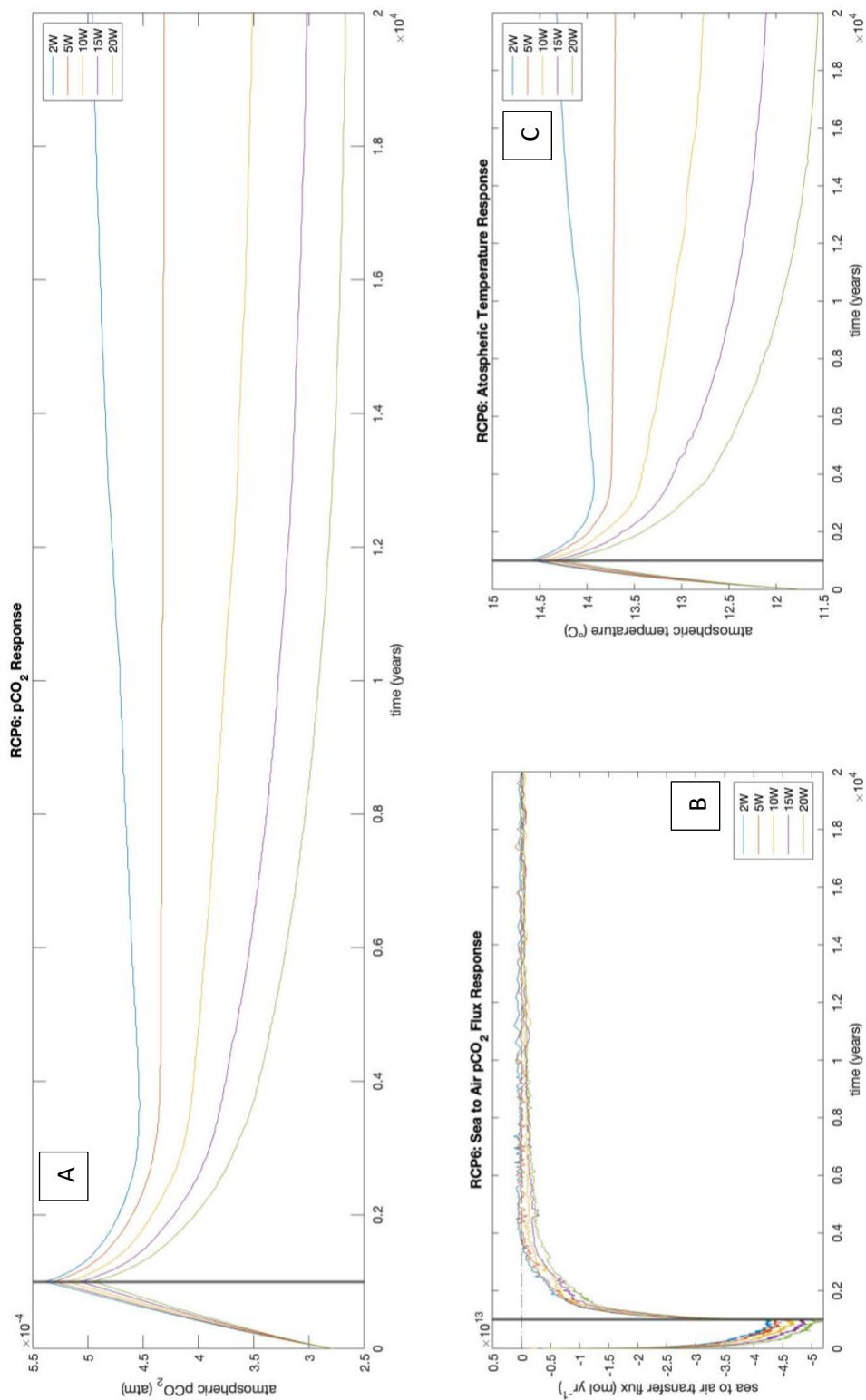


Figure 3.8; RCP6: pCO<sub>2</sub> and Temperature Responses

(A) shows the pCO<sub>2</sub> response to an RCP6 forcing under various weathering rates (B) shows the same for sea-to-air pCO<sub>2</sub> flux (C) is the atmospheric temperature response. Bold vertical line on graphs at year 1000 to represent forcing end. (B) dotted line partitions ocean sink/source.

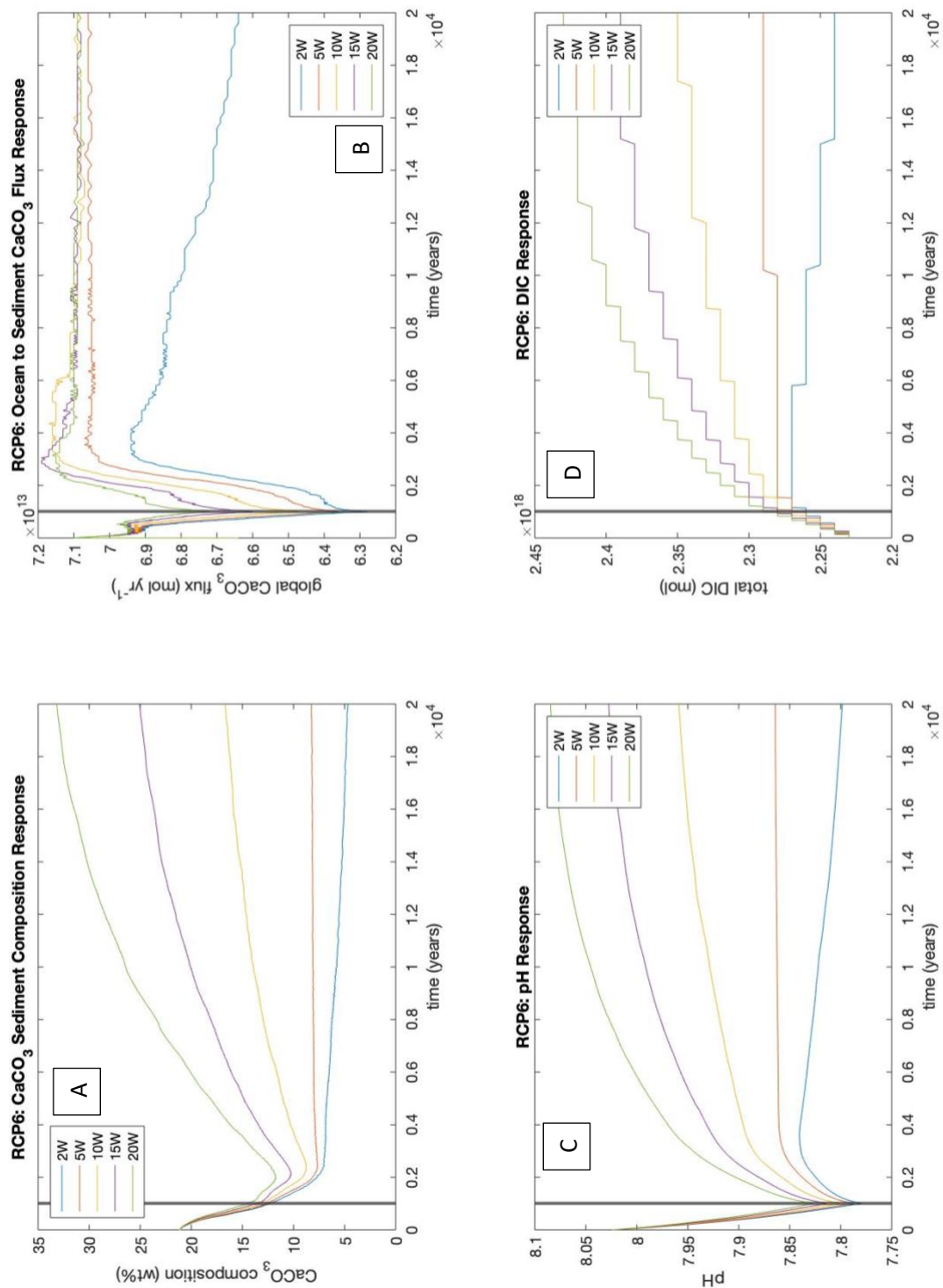


Figure 3.9; RCP6: Carbonate Chemistry Responses

(A) Shows the sediment carbonate composition response to RCP6 forcing under different weathering rates (B) Ocean to sediment CaCO<sub>3</sub> flux (C) pH response and (D) DIC response. Bold line at year 1000 represents end of forcing event.



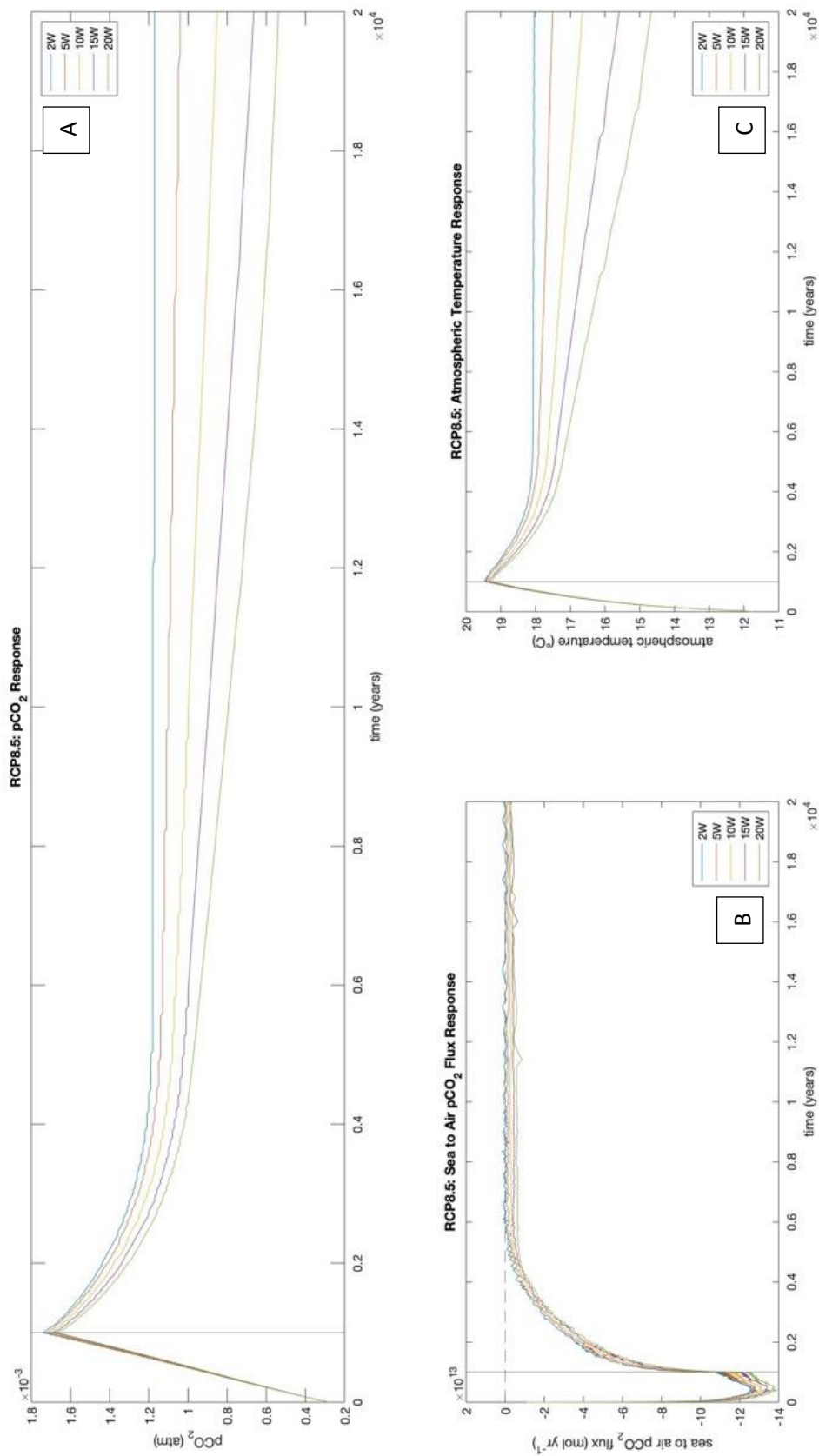


Figure 3.10; RCP8.5: pCO<sub>2</sub> and Temperature Responses

(A) shows the pCO<sub>2</sub> response to an RCP8.5 forcing under various weathering rates (B) shows the same for sea-to-air pCO<sub>2</sub> flux (C) is the atmospheric temperature response. Bold vertical line on graphs at year 10000 to represent forcing end. (B) dotted line partitions ocean sink/source.

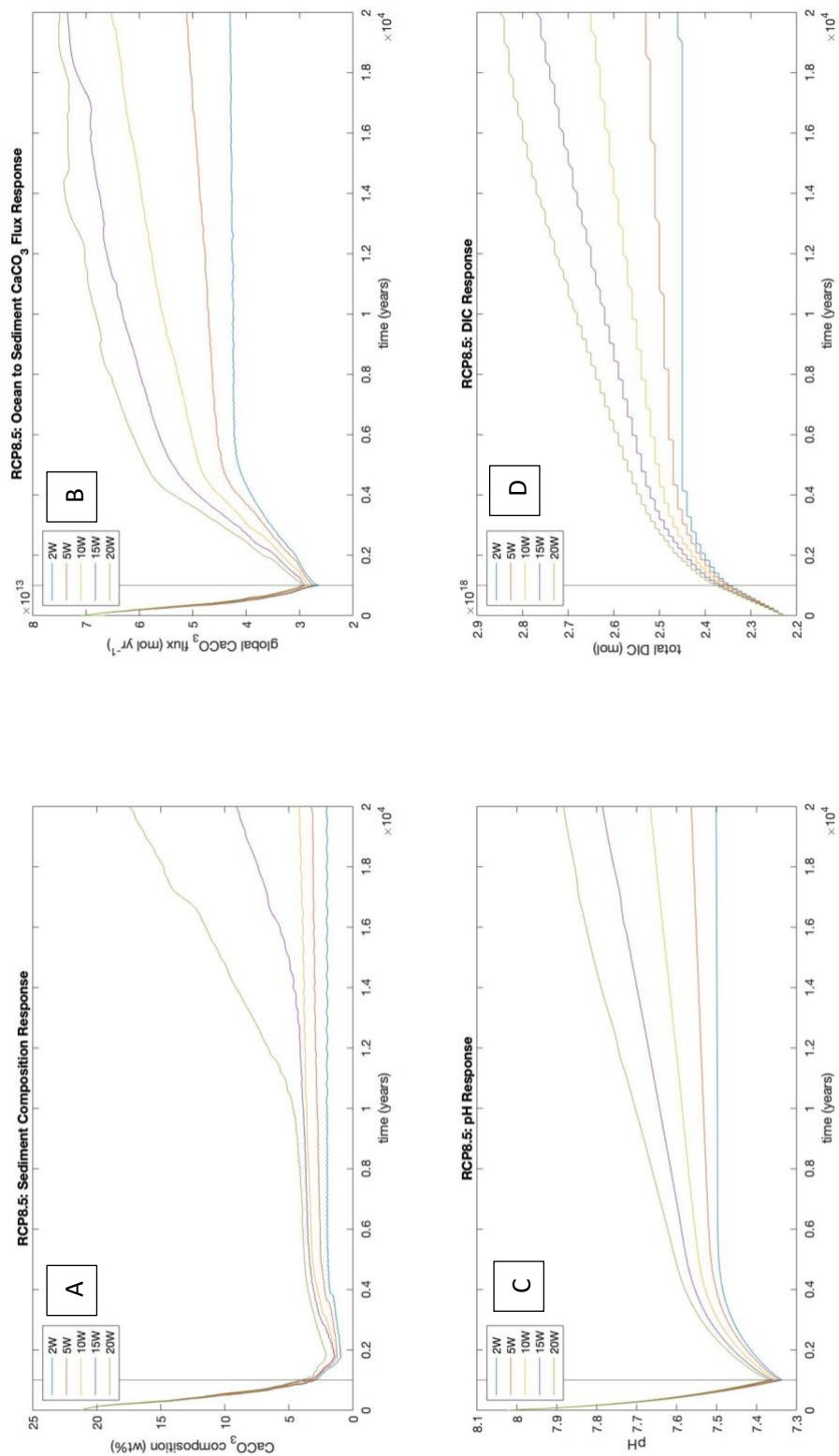


Figure 3.11; RCP8.5: Carbonate Chemistry Responses

(A) Shows the sediment carbonate composition response to RCP8.5 forcing under different weathering rates (B) Ocean to sediment CaCO<sub>3</sub> flux (C) pH response and (D) DIC response. Bold line at year 10000 represents end of forcing event.

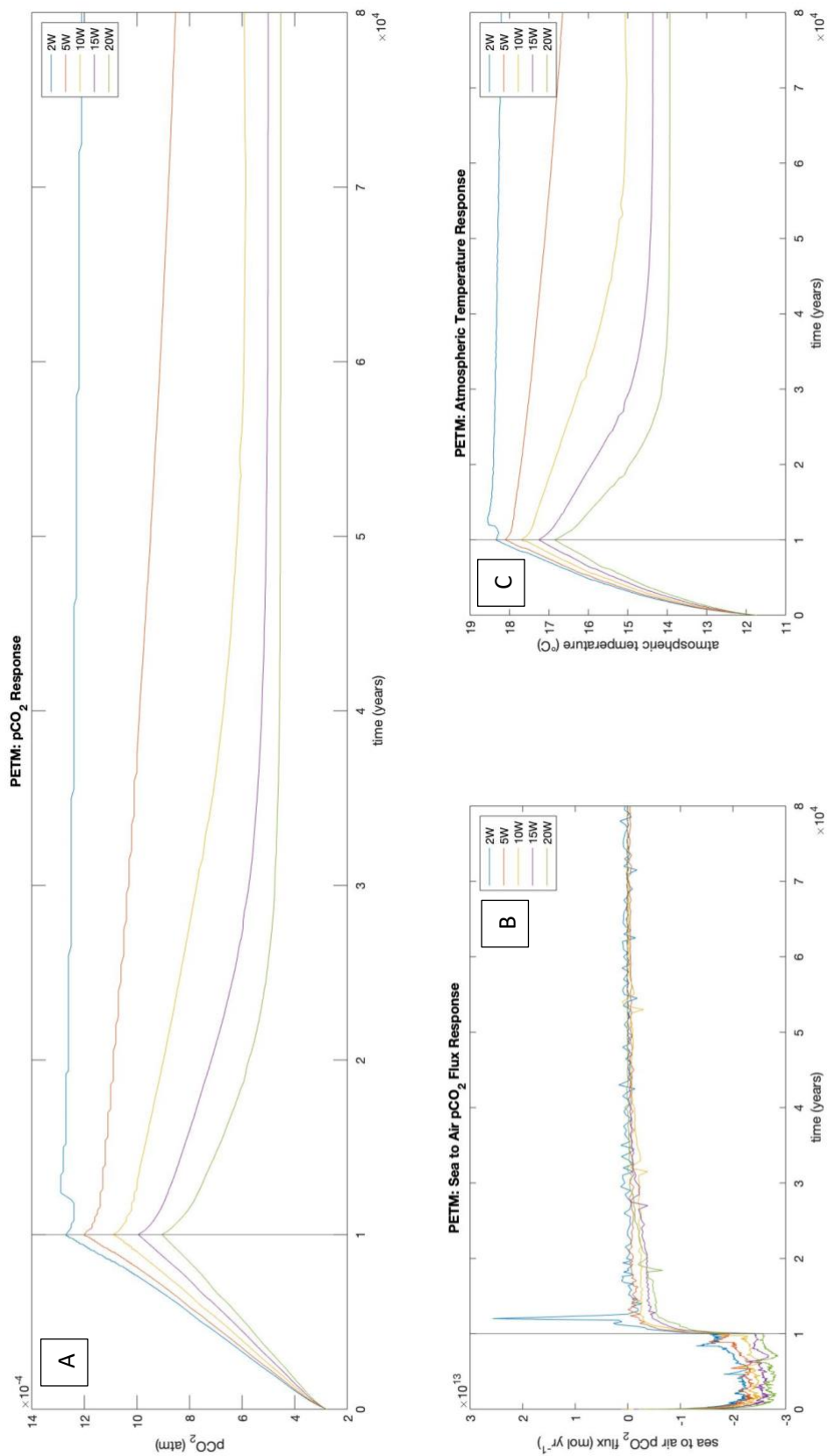


Figure 3.12; PETM: pCO<sub>2</sub> and Temperature Responses

(A) shows the pCO<sub>2</sub> response to a PETM forcing under various weathering rates (B) shows the same for sea-to-air pCO<sub>2</sub> flux (C) is the atmospheric temperature response. Bold vertical line on graphs at year 10000 to represent forcing end.

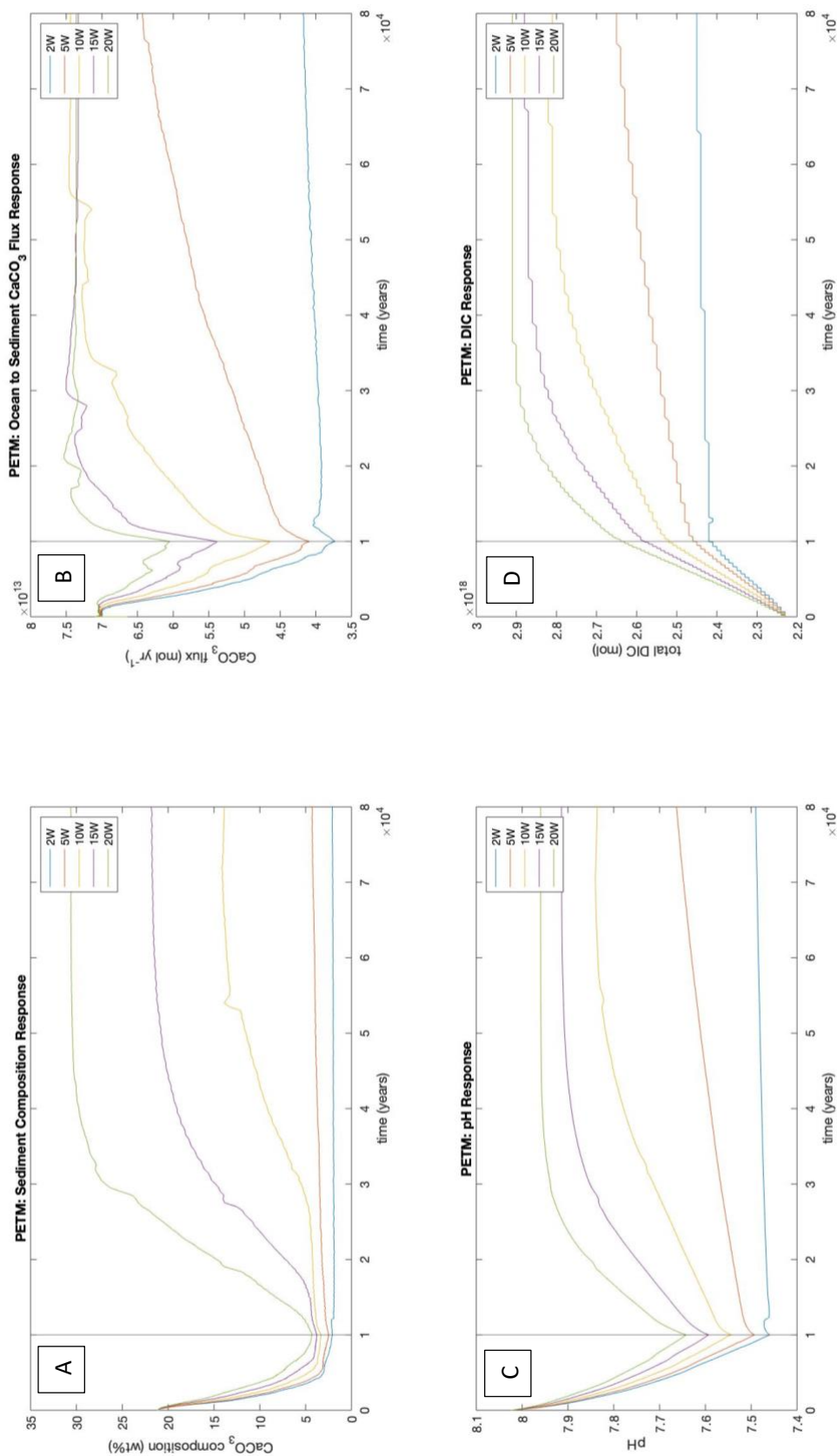


Figure 3.13; PETM: Carbonate Chemistry Responses

(A) Shows the sediment carbonate composition response to a PETM forcing under different weathering rates (B) Ocean to sediment  $\text{CaCO}_3$  flux (C) pH response and (D) DIC response. Bold line at year 10000 represents end of PETM event forcing.

### 3.4 Ensemble 3: Bioturbation Sensitivity Analysis

Bioturbation on average causes increases for lower weathering rates (2W, 5W, 10W) and decreases for higher weathering rates (15W, 20W). The highest difference from bioturbation is apparent for  $\text{CaCO}_3$  composition, which it differs most for 2W (20% higher with bioturbation) (Figure 3.16). Bioturbation only causes a positive difference for  $\text{pCO}_2$  for 20W, while for other weathering rates bioturbation creates a negative difference (Figure 3.15). Bioturbation reduces pH reduction most for 2W, while for 15W and 20W, pH is lower with bioturbation on (Figure 3.14).

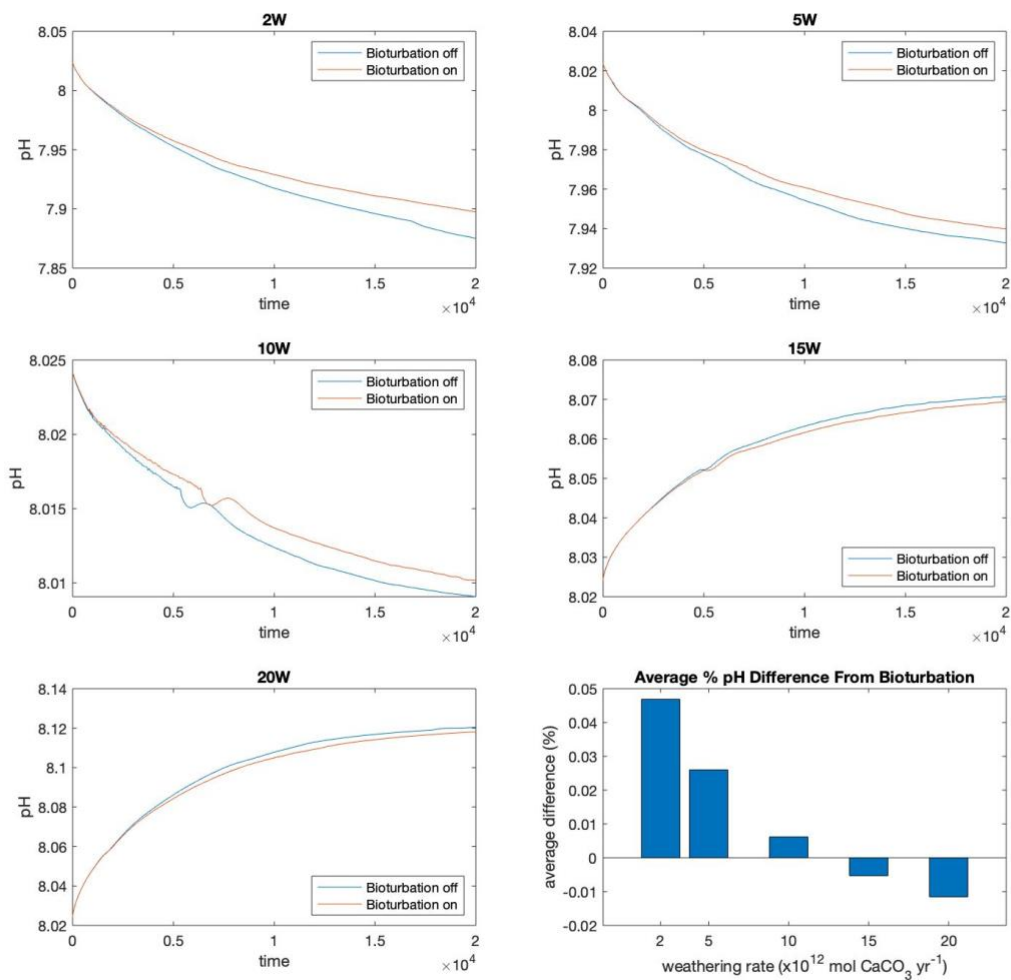


Figure 3.14; Bioturbation Influence: pH

Figure shows how pH varies with the addition of bioturbation processes. Shown to have a greater positive influence for lowest weathering and vice versa.

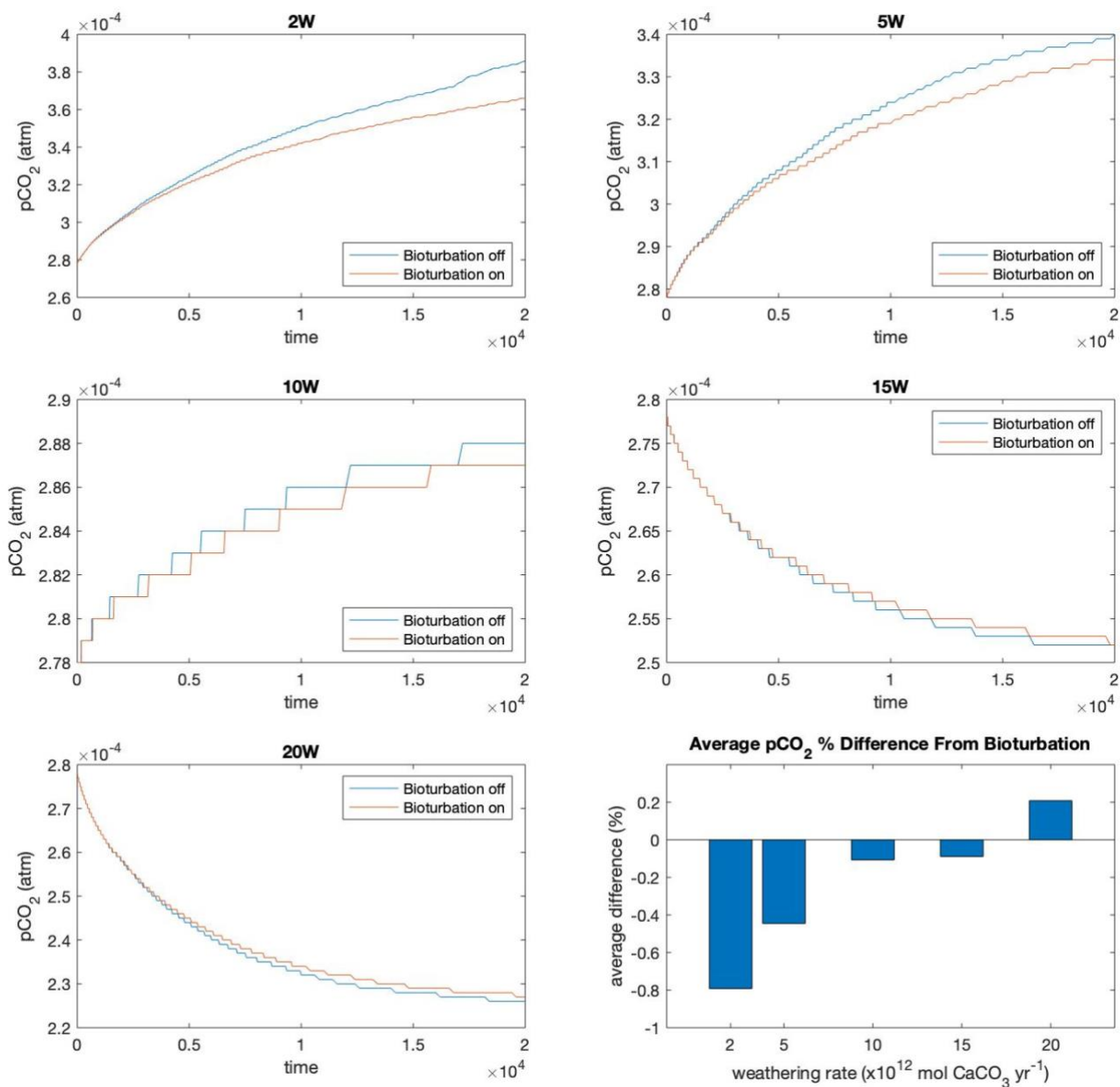


Figure 3.15; Bioturbation Influence:  $pCO_2$

Figure shows how  $pCO_2$  varies with the addition of bioturbation processes. Shown to have a greater positive influence for highest weathering and vice versa.

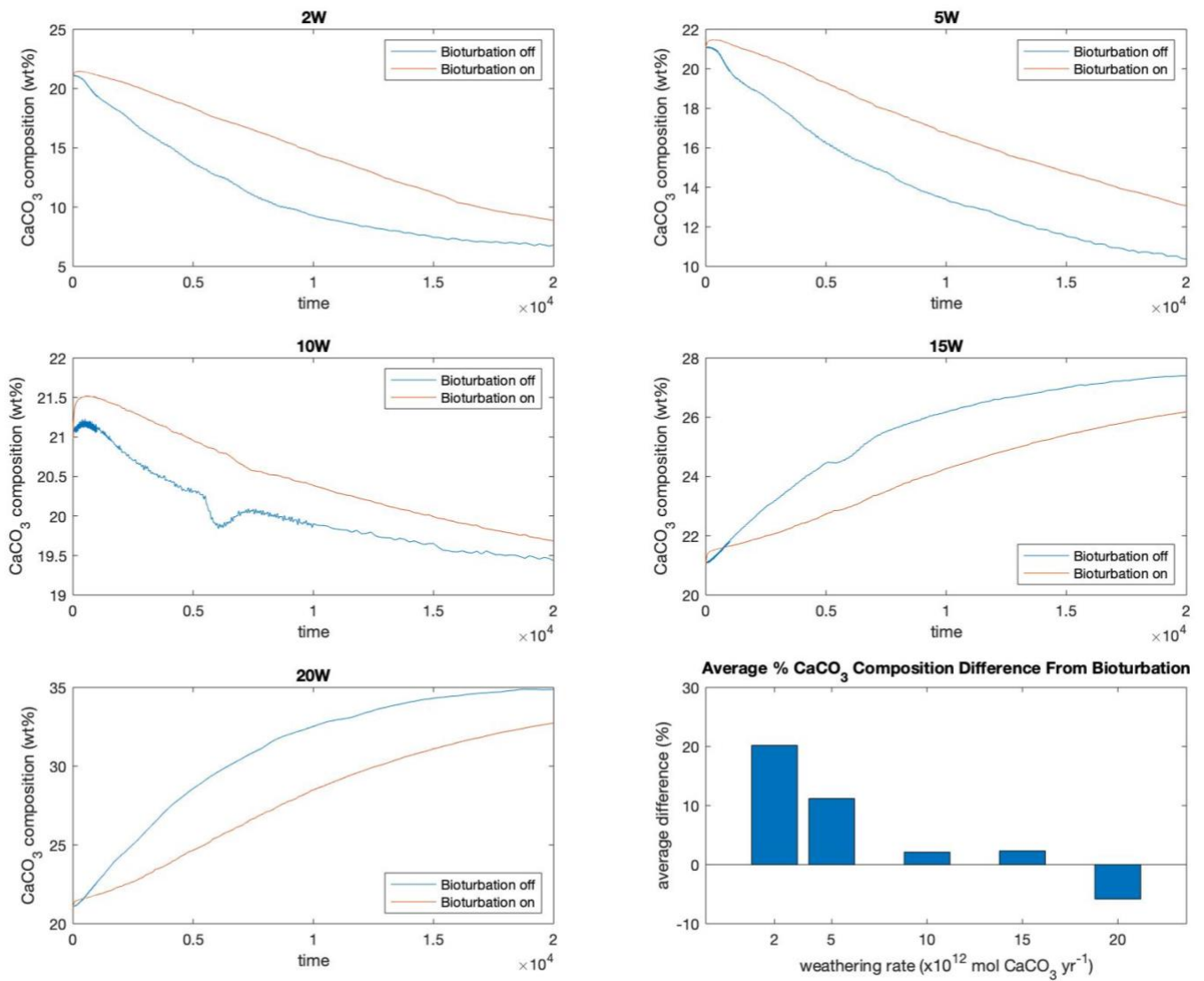


Figure 3.16; Bioturbation Influence:  $\text{CaCO}_3$  Sediment Composition

Figure shows how  $\text{CaCO}_3$  composition varies with the addition of bioturbation processes. Shown to have a greater positive influence for lowest weathering and vice versa.



### 3.5 Reducing Weathering Rate from Higher Initial Rate

(Figure 3.17) shows a 20W 50kyr spin-up stabilises at a  $\text{CaCO}_3$  composition of 32.75 wt%, 54% higher than the equilibrated composition of 10W.  $\text{pCO}_2$  finishes 50kyr at a concentration -26% for 20W relative to 10W, at  $3.5 \times 10^{-4}$  (atm). 20W equilibrium is reached by year 27000. Temperature stabilises at  $12.75^\circ\text{C}$ , reaching equilibrium by year 9000. 20W differs by  $-1.36^\circ\text{C}$  relative to 10W.

Applying this spin up to 20kyr experiments with other weathering rates shows 20W continuing the equilibrated values from spin up, with other weathering rates deviating (Figure 3.18). 2W increased by 68.6% relative to 20W by end of 20kyr, at  $5.94 \times 10^{-4}$  atm. Trends of order by weathering rate follow for sea to air  $\text{pCO}_2$ . 10W has the largest negative values, with a of minimum  $-9.45 \times 10^{11}$  mol  $\text{yr}^{-1}$ . By end of 20kyr, range between weathering rates is  $8 \times 10^{11}$  -  $-2.6 \times 10^{11}$  mol  $\text{yr}^{-1}$  (2W and 20W respectively). Temperature from 20W remains at  $12.75^\circ\text{C}$ .

(Figure 3.19) shows a high starting  $\text{CaCO}_3$  composition of 32.75 wt%, which all weathering rates decrease from. 2W decreases the most at a rate of  $1.3 \times 10^{-3}$   $\text{yr}^{-1}$ , but still finishes the 20kyr on a composition 2% higher than that for a lower weathering in (Figure 3.3). Ocean to sediment  $\text{CaCO}_3$  flux increases for all weathering rates, the most by 10W peaking at  $7.31 \times 10^{13}$  mol  $\text{yr}^{-1}$ . 2W decreases at year 10,000, transitioning from an increase trend peaking at  $7.23 \times 10^{13}$  mol  $\text{yr}^{-1}$  to a decrease by  $2.3 \times 10^{12}$  mol  $\text{yr}^{-1}$  for the remaining 10,000 years. 15W changes the least, stabilising at a flux  $7.2 \times 10^{13}$  mol  $\text{yr}^{-1}$ ,  $8 \times 10^{12}$  mol  $\text{yr}^{-1}$  higher than 20W. The range of pH for higher weathering is 7.7792 – 8.0252 (2W and 20W respectively).

DIC mirrors the magnitude of trends, with a range of  $2.69 \times 10^{18}$  mol –  $2.51 \times 10^{18}$  mol (20W and 2W respectively).

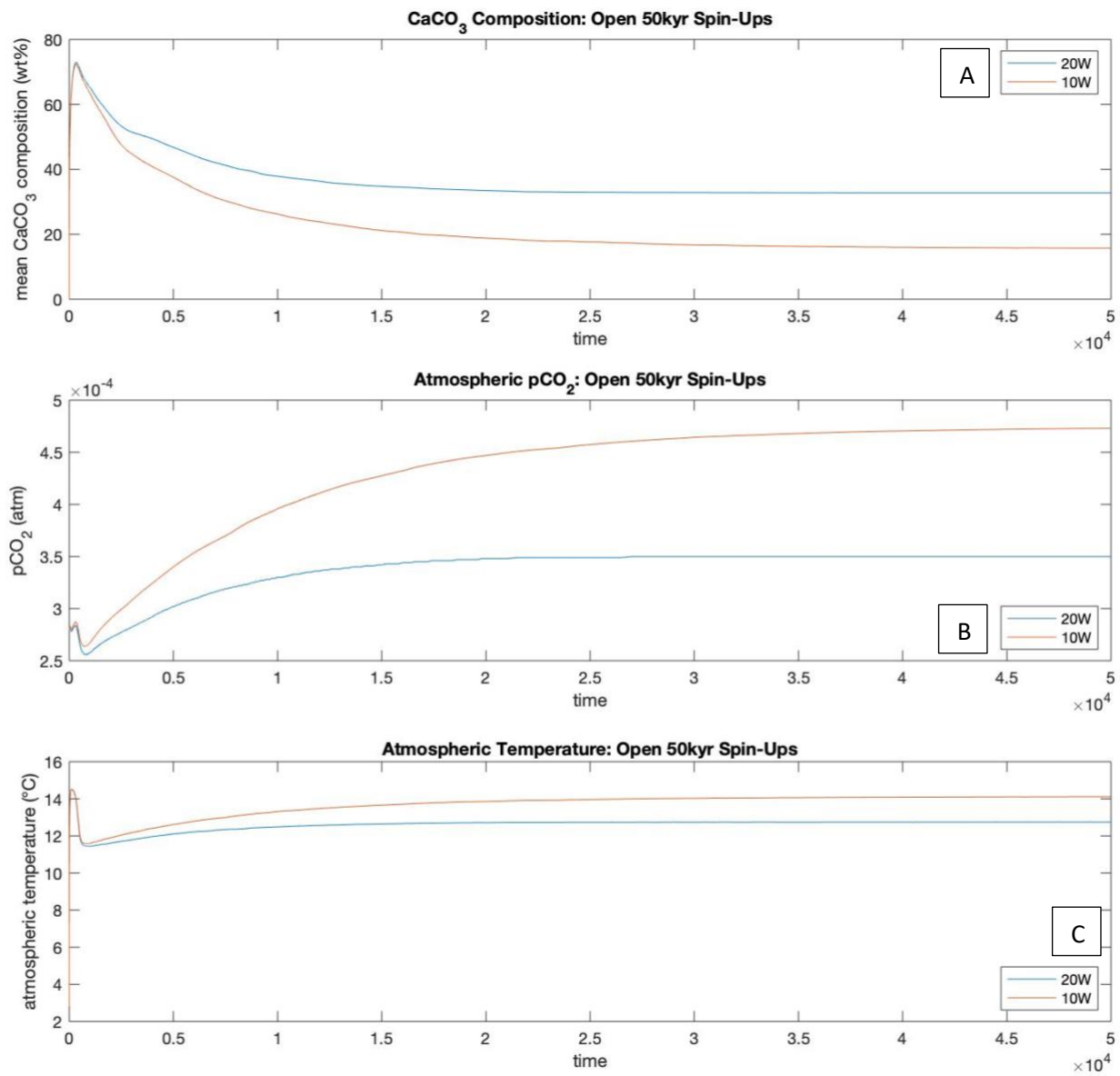


Figure 3.17; Weathering Spin-Up Comparison

Figure shows a comparison between open system spin-ups for initial weathering rates of 10W (red line) and 20W (blue line). (A) Sediment carbonate composition response (B) Atmospheric pCO<sub>2</sub> response (C) Atmospheric temperature response

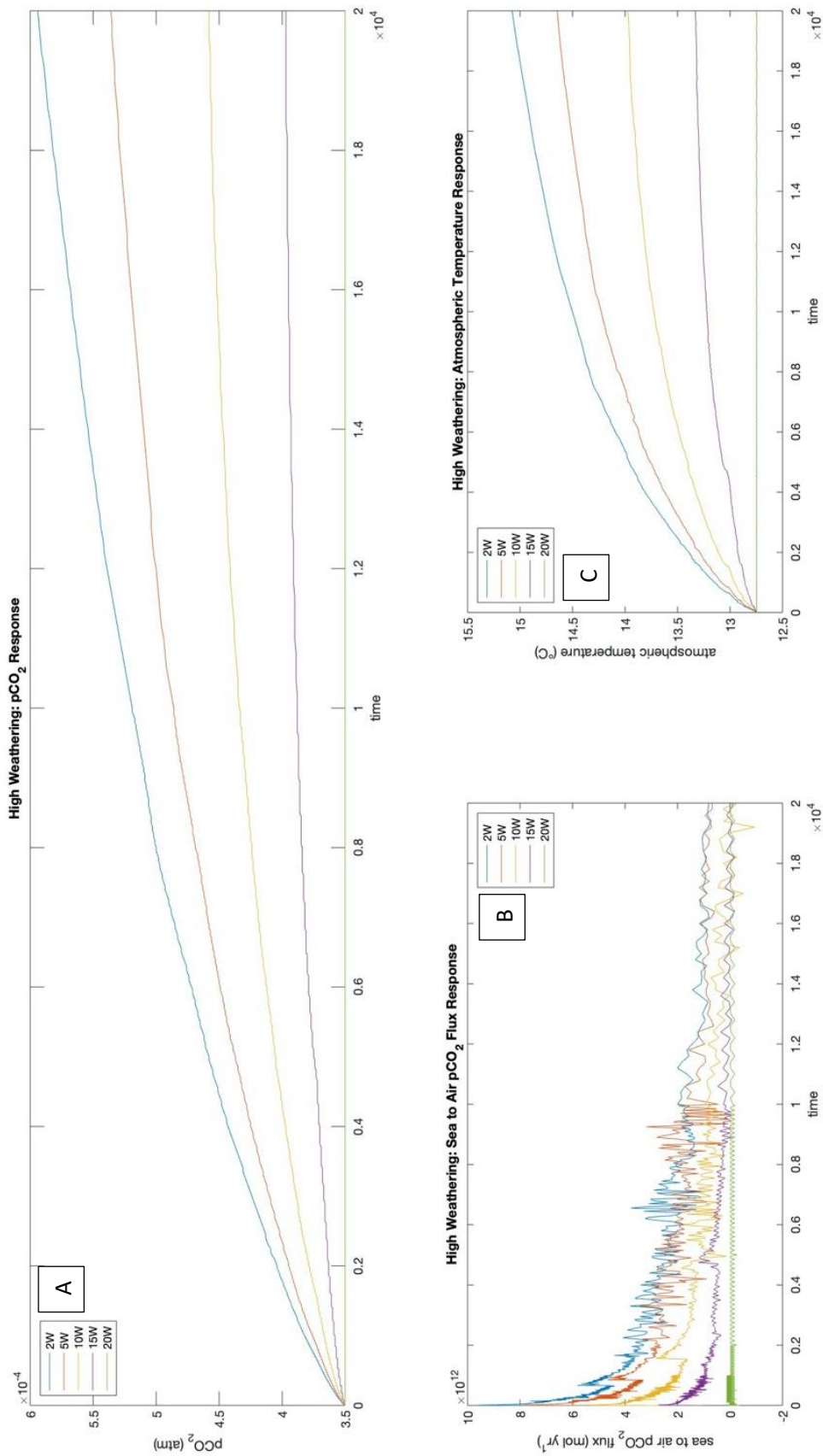


Figure 3.18; High Initial Weathering: Carbon and Climate Response

Figure shows  $p\text{CO}_2$  responses to different weathering rates applied to a spin-up using a higher initial weathering rate. (A)  $p\text{CO}_2$  response (B) Sea to air  $p\text{CO}_2$  flux response (C) Atmospheric temperature response.

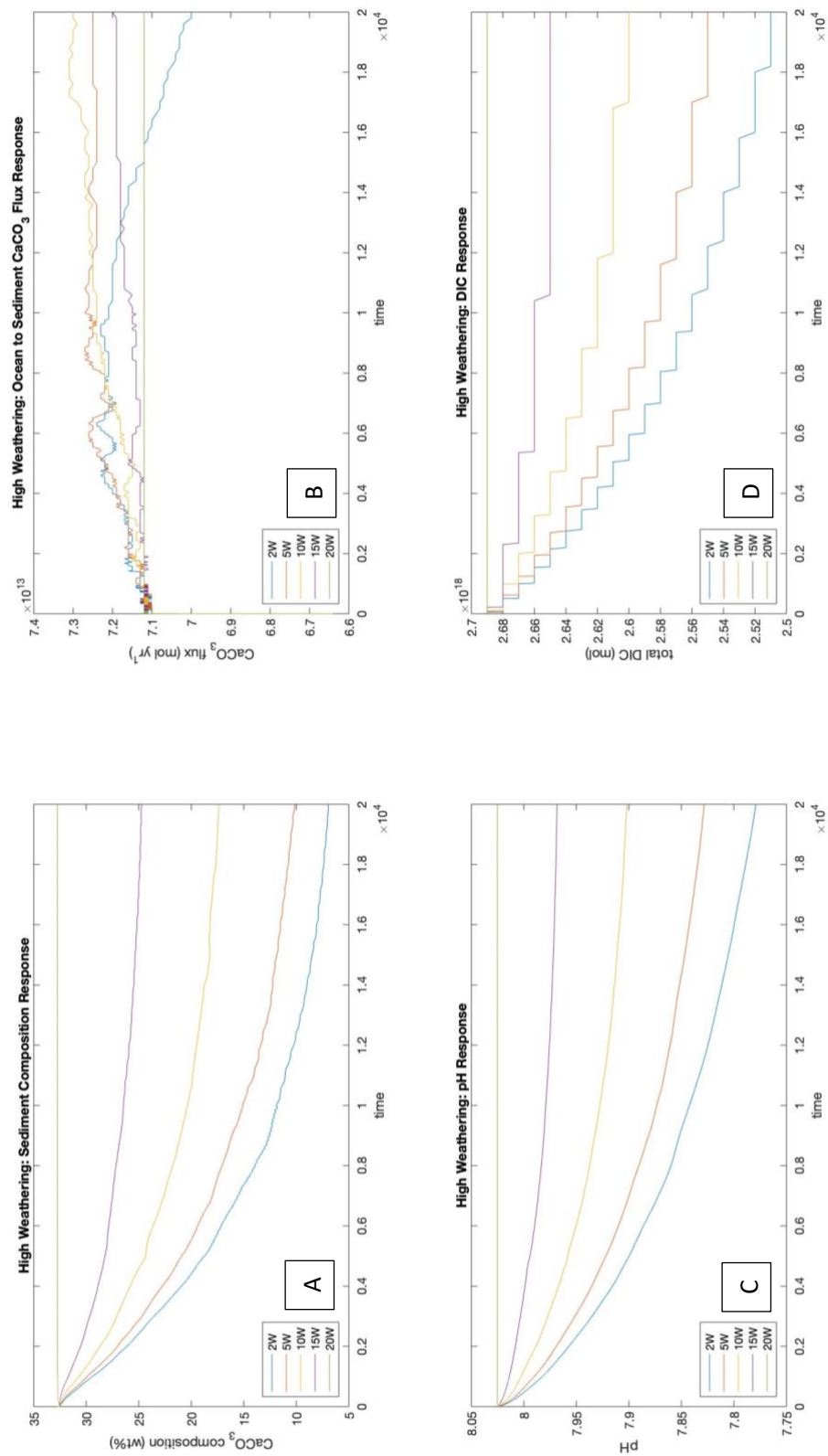


Figure 3.19; High Initial Weathering: Carbonate Chemistry Response

(A) Shows the sediment carbonate composition response to a higher initial weathering spin-up under different weathering rates (B) Ocean to sediment  $\text{CaCO}_3$  flux (C) pH response and (D) DIC response.

## 4. Discussion

This chapter will discuss the results from the model analysis in the context of current discussions in the literature.

### 4.1 Relative Strength of CaCO<sub>3</sub> Weathering

CaCO<sub>3</sub> weathering is commonly demoted as an unimportant control in the earth system carbon regulatory cycle and has not had significant influence at buffering ocean chemistry (Andersson, Mackenzie and Ver, 2003). This modelling exercise has proved otherwise, that CaCO<sub>3</sub> weathering rates do carry strong influence over the carbon cycle and its biogeochemical signals. As demonstrated by (Figures 3.1-3.7) weathering rates create a range of chemical controls and influences.

#### 4.1.1 Controls on Climate

CaCO<sub>3</sub> weathering is frequently argued to not be a significant control on climate and CO<sub>2</sub> changes on geological timescales, as it is compensated by precipitation and therefore in equilibrium on these timescales (Berner and Berner, 2012). It is also claimed such weathering operates on long timescales of 0.5-1myr to create influence within an observation window, only acting as geologic-scale “weathering thermostats” (Gaillardet et al., 2019; Poge von Strandmann et al., 2017). Others state the kinetics are too rapid and any signals are diluted (Morse et al., 2006). But growing interest and increasing observations have found similar trends to those modelled for this project, hence exemplifying an influence is very much visible on shorter timescales, to an extent whereby disequilibrium is possible to expose the signal (Brenner et al., 2016; Gaillardet et al., 2019; Martin, 2017; McGarth et al., 2015).

As this analysis demonstrates, different weathering rates affect the carbon and climate systems. (Figure 3.1) show  $p\text{CO}_2$  and temperature by range averages of  $1.6 \times 10^{-4}$  (atm) and  $2.4^\circ\text{C}$ , in a stable open system, respectively. A high weathering rate (20W) is able to reduce  $p\text{CO}_2$  by 20.6%, which consequently has resulting in a  $0.9^\circ\text{C}$  drop in atmospheric temperature. This weathering rate is therefore able to draw down  $p\text{CO}_2$  enough to cool the temperature by nearly a degree. Evidence of  $\text{CaCO}_3$  induced  $\text{CO}_2$  drawdown has been observed from the Mackenzie River Basin in Canada, showing an increase in  $\text{CaCO}_3$  weathering responsible for 70% of  $\text{CO}_2$  consumption (Beaulieu et al., 2012). A study of the worlds 60 largest rivers also found similar results, showing  $\text{CaCO}_3$  weathering has a  $\text{CO}_2$  uptake of  $0.29\text{PgC} - 0.15\text{PgC}$  (Martin, 2017), enabling buffering and  $\text{CO}_2$  sink abilities especially when flowing across  $\text{CaCO}_3$  geologies (Sabine and Mackenzie, 1995). This is similar to the consumption of  $\text{CO}_2$  by 20W across the 20kyr, achieving a reduction of 20.6%. These simulations therefore support a growing recognition of the  $\text{CO}_2$  sink and climate control of  $\text{CaCO}_3$  weathering, on recordable timescales (Brenner et al., 2016).

#### 4.1.2 Controls on Chemistry

Higher weathering is also able to alter ocean chemistry. (Figure 3.4) shows 20W is able to increase pH over the 20kyrs by 1.2%, while 2W decrease by 1.86%. An increase in pH for a high weathering rate demonstrates an alkalising buffer capacity that not even 10W can provide, also showing a slight pH decrease. This is also displayed by an increasing DIC for higher weathering rates (15W and 20W) showing

a resistance to the increasing CO<sub>2</sub>, which as shown by the Revelle factor (Equation 5), hence an increased buffer factor.

Revelle factor =  $(\Delta[\text{CO}_2] / [\text{CO}_2]) / (\Delta[\text{DIC}] / [\text{DIC}])$  (Equation 5)

These trends are distinguishable in observations around CaCO<sub>3</sub> weathering hotspots. Sabine et al (1995) note an 'alkalinity halo' around the Hawaiian Islands, caused by intense dissolution and transport of shallow carbonates, resulting in an export of 49  $\mu\text{mol C kg}^{-1}$  of DIC supplied from carbonate particle dissolution. DIC sensitivity is also observable from carbonate river catchments. The Wujiang River produced DIC concentrations 3 times higher than the global average, with a range of 2303-2783  $\mu\text{mol/L}$ , as well as a maximum basin pH of 8.9 (Zhong et al., 2017). This closely matches trends observed in figure 3.4 and gives justification to the role of carbonate weathering causing such trends.

The same can also be said for the impact of low weathering rates, which show similar carbonate deficient/low weathering flux location observations (Gislason Arnorsson and Ármannsson, 1996). Such locations tend to have less of a biological influence due to less nutrient supply, thus fluxes can be attributed to the physical biogeochemistry. (Figure 3.4) shows a strong effect of the weathering rate to create similar environments; the lowest weathering rate (2W) greatly reduces pH and DIC relative to higher weathering rates. Such an environment demonstrates key instabilities, which are exacerbated by a positive feedback. As the weakened weathering feedback is unable to counter the increased ocean CO<sub>2</sub> intake, pH



continues to decrease at increasing rate, as well as DIC. This type of imbalance is conducive to an ocean acting as a source of CO<sub>2</sub>, further contributing to the positive feedback (Sabine and Feely, 2007). It could also be argued that the modelled results may be an underestimation for a low CaCO<sub>3</sub> content location, due to a dissolution response to more acidic and CO<sub>2</sub> saturated waters (Krumins et al., 2013), hence some of the pH and DIC decreases are offset by a buffering dissolution flux in absence of weathering input. However, it has been observed that OM decomposition has a significant influence on dissolution, by increasing corrosivity of the pore water and biologically enhancing mixing of TA, contributing to rapid dissolution (Anderson, Bates and Mackenzie, 2007). However, the strength of this buffer as a meaningful contribution is disputed (Andersson Mackenzie and Ver, 2003; Andersson, Mackenzie and Lerman, 2005).

Overall, weathering is influential over the biogeochemistry behaviour of the ocean and its CO<sub>2</sub> sink capacity, supported by observations from environments of high and low CaCO<sub>3</sub> weathering.

#### 4.1.3 Sedimentary Controls

(Figure 3.3) also exemplifies these trends and how they influence the sediments. Higher weathering rates allow for more Ca<sup>2+</sup> to influx the oceans, hence the larger composition of CaCO<sub>3</sub> in sediments. However, this is also influenced by the changes to ocean chemistry which also help increased burial and preservation of carbonate sediments. Higher pH, reduced pCO<sub>2</sub> and a strong ocean sink allow for the balance of dissolution and burial to accommodate accumulation.

Gazeau et al (2014) find that a drop in pH by 1 unit has significant enhancements on  $\text{CaCO}_3$  dissolution which is in agreement with (Figure 3.3), demonstrating a chemical stabilising response of sediments. Also supported by Cyronak, Santos and Eyre (2013) who show that elevated  $\text{pCO}_2$  can shift sediments from net precipitation to dissolution. These trends are also commonly attributed to biological processes. Opdyke and Wilkinson (1990) argue  $\text{CaCO}_3$  sediment accumulation is ecosystem limited, restricted to paleolatitudes of tropical seas and shallow continental shelves. Bias to the biological dominant process is exemplified by Cardenas et al (2018), who find sub-Antarctic zones that are high (>45%) in carbonate compositions of sediments around the Drake Passage, Antarctica. This is attributed to the biological assemblages that spatially correlated to sediment composition. However, not acknowledged by this analysis is the large continental shelf and mountainous reservoir of weatherable  $\text{CaCO}_3$  rock, which could also influence the sedimentary signals.

External factors are also said to limit  $\text{CaCO}_3$  accumulation, not accounted for in the model. Mackenzie and Morse (1992) recognise a tectonic control through the Phanerozoic, suggesting  $\text{CaCO}_3$  accumulation is cyclic with SL changes independent of feedback controls such as weathering. Influence from sea level is feasible due to 86% of sediment mass lies within the continental shelf (Mackenzie and Morse, 1992). On the other hand, it could be interpreted that such sea level influence is only of significance after large weathering episodes, that there is not a *total* recycling if there is sufficient supply, thus amounting to a net increase overall in

accumulation while also able to provide a dissolution/recycling flux. Other variables such as pore water advection (Cyronak, Santos and Eyre, 2013), ocean currents (Sulpis et al., 2018) and OM decomposition (Andersson, 2015) are also able to influence dissolution.

Furthermore, a large accumulation of  $\text{CaCO}_3$  sediments allows for a second weathering reserve of resilience (Hay, 2008; Ridgwell, 2005). Episodes of high accumulation in the past have created large carbonate masses, such as those created in the Cretaceous which have provided a shallow-sea dissolution reservoir (Dameron et al., 2017). However, in the context of Cretaceous carbonate sedimentation, due to the very specific conditions of formation this availability of carbonate weathering reservoir replenishment and exposure may not be cyclic (Stanley, Ries and Hardie, 2002). It may also be the case that since the Cretaceous, an injection of such a volume of carbonate into the carbon cycle in both biological and physical realms will allow for continued recycling and a new routine of cyclicity. (Figure 3.3) implies such a mechanism by the observable pulse of dissolution able to reach new steady states for high weathering rates. However, as (Figure 3.3) exposes, a high consistent weathering rate is important to not deplete  $\text{CaCO}_3$  sediments before burial by dissolution.

This becomes especially important for shallow shelf environments, which account for half of global  $\text{CaCO}_3$  accumulation, and their  $\text{CO}_2$  sink role (O'Mara and Dunne, 2019; Brenner et al., 2016; Gazeau et al., 2014). Continental shelf/coastal sediments have achieved more attention due to their relatively fast dissolution and weathering

rates, because of the “biogeochemically active” properties that encourage high erodibility mechanically and chemically (Romero-Mujalli et al., 2019; Thompson et al., 2017). Therefore, a higher weathering rate may be a more accurate representation of what resilience may be provided at a carbonate coast.

#### 4.1.4 Bioturbation Influence

(Figures 3.14-3.16) reveal the relative importance of bioturbation in the context of changing weathering rates. As shown, the role of this process is insignificant ( $p > 0.05$ ) and varies most in responses for lower weathering rates. Other analyses considering bioturbation show that although the role is minor, it still holds some importance at creating a flux that can be greater than molecular porewater diffusion (Emersona and Hedges, 2006), which has been given importance in other studies (Martin, 2017; Andersson, Mackenzie and Lerman, 2006). Therefore, it can be fair to exclude both these processes as serious influences, and isolate changes to changes in carbonate weathering.

Panchuk, Ridgwell and Kump (2008) have also found that reducing bioturbation can also reduce the dissolution observed from modelled carbonate chemistry. This is especially important to accurately capture the dissolution intervals that respond to carbon perturbations and not to overestimate with a bioturbation flux that may have reduced in response anyway, inhibited by acidification effects (Wood, Widdicombe and Spicer, 2009; Donohue et al., 2012). Hence, analysis of event/scenario simulations will hold more accuracy with the absence of bioturbation.

## 4.2 CaCO<sub>3</sub> Weathering Response to CO<sub>2</sub> Forcing

### 4.2.1 PETM

#### **PETM Onset**

Climate and carbon responses vary substantially across weathering rates, representative of different degrees of resilience to the CO<sub>2</sub> forcing, even visible during the peak of the pulse whereby pCO<sub>2</sub> varies by  $3.69 \times 10^{-4}$  atm across weathering rates (Figure 3.12). Differences also exist in between other PETM studies, variant by their origins of forcing, event and recovery durations and weathering strengths (Honisch et al., 2012; Panchuk, Ridgwell and Kump, 2008; Zeebe and Zachos, 2013; McInerney and Wing, 2011; Panchuk et al., 2008; Kump, 2018). Dispute about the total PgC release ranges mostly between 2000PgC to 10000PgC, depending on the carbon source (Figure 4.1) (Honisch et al., 2012; Panchuk et al., 2008; Zeebe, Zachos and Dickens, 2008; Gutjahr et al., 2017). After a pulse of 4500PgC over 10kyrs for this analysis, peak pCO<sub>2</sub> ranges from  $1.2 \times 10^{-3}$  atm (2W) to  $4.54 \times 10^{-4}$  atm (20W) (Figure 3.12), demonstrating a high PETM climate sensitivity for a higher weathering rate, as also supported by (Penman and Zachos, 2018).

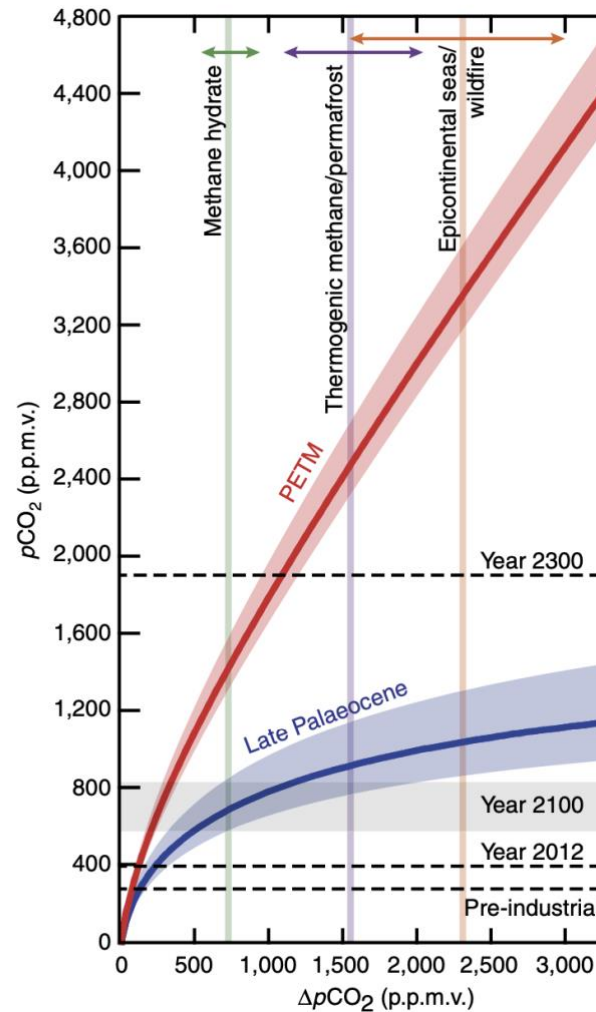


Figure 4.1; PETM  $p\text{CO}_2$  Change

Possible  $p\text{CO}_2$  increases for the PETM (red line) relative to initial Late Palaeocene levels (blue line). Adapted from (Schubert and Jahren, 2013).

Estimates of PETM  $p\text{CO}_2$  onset also range depending on the proxy and measurement methods used. Bering and Royer (2011) find background  $p\text{CO}_2$  ranges between 100-1,900 ppm, while Gehler, Gingerich and Pack (2016) show correlating to sedimentary strata using a triple oxygen isotope estimates at ~670ppm. Aside from tools of analysis, while Schubert and Jahren (2013) find that the CIE amplitude is larger in terrestrial records than marine, producing a combined (marine and terrestrial) background  $p\text{CO}_2$  of 674-1034 ppmv, and peak CIE  $p\text{CO}_2$  1384-3342 ppmv. This analysis projects  $p\text{CO}_2$  to be in the lower range of estimates for PETM

onset and CIE peak. As shown in (Figure 3.13), weathering rate has a control on this, showing that for pCO<sub>2</sub> increase from initial to peak, 2W increases 58.8% more than 20W. This supports the observations of marine resilience, due to a weathering response able to counter impacts of perturbation. For a doubling of weathering rate (10W vs 20W), *during* perturbation, pCO<sub>2</sub> is lowered by 29.5%.

Temperatures increase within the range of 4-9°C across the event (Dunkley Jones et al., 2013; Zeebe and Zachos, 2013; Gehler, Gingerich and Pack, 2016; Kump, 2018). This analysis produces a range of 4.97-6.56°C between weathering rates 2W-20W (Figure 3.12). 20W is therefore able to reduce event temperature to the lower estimate bounds, support that a negative feedback of carbonate weathering CO<sub>2</sub> drawdown may have been active given a sufficient weathering response.

Temperature is a key variable in reproducing the PETM, due to feedback influence which controls resilience during the event. Chemical weathering and run-off enhancement from an intensified hydrological cycle as a result of temperature increases has been indicated from increased terrestrial export and changes to coastal marine eutrophic dinoflagellate populations (Kelly et al., 2005; Crouch et al., 2001; 2003). This shows weathering response was reactive to the PETM onset and that any resilience provided would have increased in strength with time. This is supported by a lag in the pCO<sub>2</sub> increase relative to the temperature rise (Gehler, Gingerich and Pack, 2016), suggestive of a weathering process responding to temperature and influencing pCO<sub>2</sub> in doing so. Depending on the pre-event

weathering rate, a temperature increase may have transitioned a PETM profile to a higher weathering rate as shown by 20W (Figure 3.12).

Attempts have been made to parametrise a weathering response to a temperature enhanced hydrological cycle, but commonly at the expense of underestimating carbonate weathering by assumption of same rates and ratio of silicate weathering (Penman and Zachos, 2018; Komar, Zeebe and Dickens, 2013). This is applied, even though observations have been made throughout the PETM of increased terrestrial carbonate weathering and marine dissolution (Kelly et al., 2005). These processes respond to temperature differently, hence weather faster and to greater volumes than silicate weathering (Zeng, Liu and Kaufmann, 2019). Furthermore, it has been shown the increased precipitation was episodic with increased storms, which has greater erosive potential than a temperature increased rate of reaction (McInerney and Wing, 2011). Therefore, temperature and pCO<sub>2</sub> lags and leads demonstrated by high weathering rates (15W-20W) provide useful insight into the resilience that was responding to the PETM onset.

The pH decline for the PETM onset underpins the oceanic ecological response and recovery efficiency. Predictions of pH decline range from ~0.36-0.7 (Gutjahr et al., 2017; Zeebe and Zachos, 2013). Variations are argued to be due to the difference in event duration and carbon release applied. Sensitivity to perturbation thresholds can inhibit pH resilience (Vervoot et al., 2019; Gutjahr et al., 2017). It is then important to consider weathering rate and response to the event, and thus its influence over pH. Absence of a strong weathering influence creates acidic conditions of magnitude and



limit the resilience of the carbonate budget, causing ecological loss (Kawahata et al., 2019). Higher weathering rates (20W) applied in this analysis are able to offset pH decrease by 47% relative to a low weathering environment (2W) (Figure 3.13). A weathering induced dampened pH response can then complicate inferences taken from pH change, such as perturbation size (Gutjahr et al., 2017).

The impacts of PETM acidification are disproportionately felt in the deep-sea, causing dramatic benthic losses and reduced bioturbation (Panchuk, Ridgwell and Kump, 2008; Ridgwell, 2007). Although partly due to immediate dissolution beneath the CCD, above this zone arguments suggest this could be due to circulation breakdown (Zeebe and Zachos, 2007), deoxygenation from a weakened organic burial feedback (Armstrong McKay and Lenton, 2018; Zeebe and Zachos, 2013) or enhanced sediment pore-water acidification (Emerson and Hedges 2006; Andersson, 2015).

There is a different response in shallow waters, documenting only assemblage and ecosystem shifts (Honisch et al., 2012). This suggests a carbonate weathering refuge for shallow dwellers, which would be direct beneficiary of terrestrial carbonate influx (Penman and Zachos, 2018; McInerney and Wing, 2011; Zeebe and Zachos, 2013). This is an importance artefact of a high weathering environment, which even under perturbation would still likely show evidence of continued  $\text{CaCO}_3$  sediment composition, as shown for 20W in (Figure 3.13). This compares to other observations that show tried continuation of some  $\text{CaCO}_3$  wt% supply (Figure 4.2).

Therefore, even if only regionally, this potentially shows the resilience of carbonate weathering supply able to contribute under perturbed conditions.

## PETM Recovery

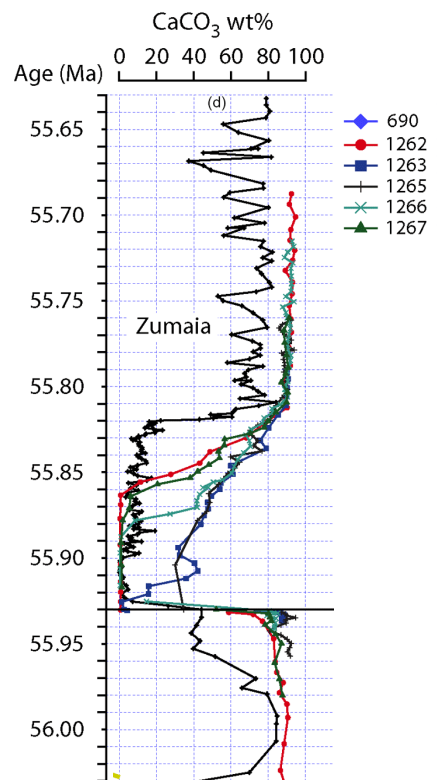


Figure 4.2; CaCO<sub>3</sub> Observations at PETM Onset Figure shows CaCO<sub>3</sub> records from range of deep ocean drill sites and Zumaia shallow shelf carbonate complex. Adapted from (Dunkley Jones et al., 2018).

The role of weathering has also been evidenced PETM-Recovery sediment records (Kennett and Stott, 1991). Carbon and Oxygen isotope excursions for the PETM have since been refined at additional ODPs, revealing periods of dissolution and burial (Panchuk, Ridgwell and Kump, 2008; Mackenzie and Anderson, 2013; Penman and Zachos, 2018; Turner, 2018). Erba et al (2010) find the dissolution occurs as pulses, existing with a long-term alkalinity recovery over 35krys. This behaviour could be inferred from the ocean-sediment flux remaining high through

this period and an inability to return to initial pH and to instead stabilise at a new state (Figures 3.12 and 3.13). This is also evident as transient pulses in accumulation are observed in the recovery phases (Zeebe and Zachos, 2013). Although results are deficient in clear oscillations, (Figure 3.13) depicts a similar environment of competing dissolution and accumulation, as burial trends lag behind the rapid responses of ocean-sediment  $\text{CaCO}_3$  fluxes, suggesting a suppressed burial through dissolution loss. This is impacted by weathering rate, as duration of burial inhibition increases with decreasing weathering rate, implying a new quasi-stable state takes longer to reach with inefficient weathering.

Rapid burial increase is another notable impact of the PETM recovery, commonly attribute to an enhanced terrestrial weathering pulse in response to an accelerated hydrological cycle and thermodynamically enhanced chemical weathering (Jenkyns, 2018; Penman and Zachos, 2018; McInerney and Wing, 2001; Kelly et al., 2005; Dunkley Jones et al., 2018). However, Armstrong McKay and Lenton (2018) suggest terrestrial weathering actually weakened as a resilience mechanism exhausted by breaching a tipping point preceding the event, and carbon-cycle destabilisation was the key push to climate instability during the PETM (Littler et al., 2014; Barnett et al., 2019). A reduction of continental weathering is also said to have caused a 40% decrease in Si weathering from 3Myrs after the PETM (Caves et al., 2016; Van der Plog et al., 2018). This suggests other processes could be directing the recovery, such as seawater reacting with fresh Igneous Province basalt (Kender et al., 2012; Jenkyns, 2018), or a strengthened biological pump (Bains et al., 2000; Stoll and Bains, 2003).

However, an increase in  $\text{CaCO}_3$  and Kaolinite deposits, representative of an increased terrestrial carbonate and silicate weathering, support a weathering resilience response (Kelly et al., 2005). These deposits have global coverage, clustered around shallows which further supports a terrestrial-weathered source (Akaegbobi, Ogungbesan and Ogala, 2011; Knox, 1998; Kelly et al., 2005; Erba et al., 2010; Dunkley Jones et al., 2018). Jones et al (2019) also find weathering and accumulation flux to increase 4-fold during recovery. An observed loss of calcifiers and reduced bioturbation during this event likely discounts a biology-driven recovery (Ridgwell, 2007), supporting sedimentation patterns out of sync with biological response, maintaining this was a geophysical process.

High weathering rates applied in this study produce recovery period wt% carbonate sediments 45.2% and 3.5% higher than initial (for 20W and 15W respectively) (Figure 3.14). This not only signifies increased burial but also increased preservation, potentially aided by a 'CCD overshoot' (Penman and Zachos, 2018). This is significant not only for immediate  $\text{CO}_2$  drawdown, but creates a renewed, larger  $\text{CaCO}_3$  sediment reserve, able to be exploited for future OAE's (Mackenzie and Anderson, 2013). The amplitude of recovery of wt%  $\text{CaCO}_3$  is similar to sedimentary observations (Figure 4.3).

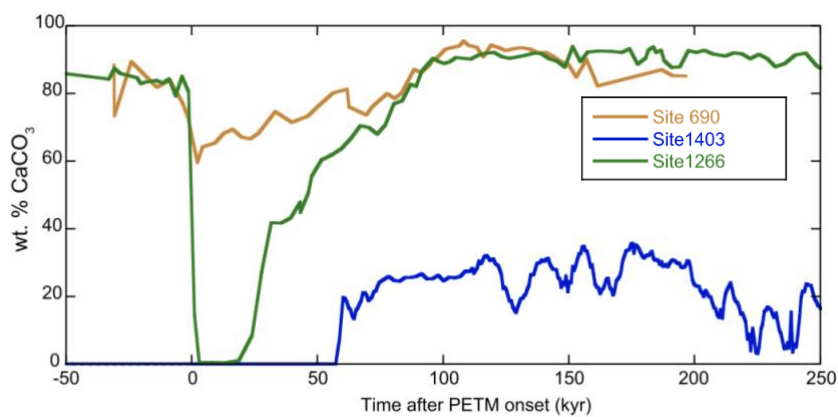


Figure 4.3; PETM  $\text{CaCO}_3$  Sediment Content Records

PETM records of  $\text{CaCO}_3$  wt% over event duration at sites U1403, 1266 and 690. Age models from correlating fine-fraction/bulk  $\delta^{13}\text{C}$  to (Rohlf et al., 2007). Figure adapted from (Penman and Zachos, 2018).

The rate of sedimentation is also comparable. For 20W, a rapid period of recovery occurs for 20kyrs after event, taking 15krs to return to initial wt%, followed by a gradual recovery period over ~50kyrs. While 15W rapidly recovers over ~30kyrs, and gradually thereafter. This aligns to other estimates for a rapid phase of recovery, also said to occur ~30kyrs after event (Kelly et al., 2005; McInerney and Wing, 2011; Erba et al., 2010). Ocean-sediment  $\text{CaCO}_3$  flux on the other and recovers quicker, rapidly so for 8kyr followed by a 30kyr gradual phase. Therefore, similar to Murphy, Farley and Zachos (2010), this could expose a 3-part recovery phase, whereby the first 8kyr is a competing recovery between dissolution and increased terrestrial weathering. As this does not significantly dampen the accumulation rate, it suggests terrestrial weathering was strong enough to override dissolution impacts and maintain burial. Although, a lag in accumulation visible for 15W and remaining rates, demonstrates this drop in weathering input is sufficient to allow a dissolution-dampening impact of accumulation. These rates are too fast to be explained by silicate weathering alone (Bowen and Zachos, 2010), thus exemplifies a process

capable to remove carbon through burial, indicative of carbonate weathering (Penman and Zachos, 2018).

On the other hand, pH takes longer to recover and does not restore original state despite high weathering and stable burial (Figure 3.13). pH for 20W increases for ~30kyr after event but stabilises at a pH 0.8% less than initial. This potentially explains the lag of ecological recovery, also noted by Penman and Zachos (2018) who identify sustained acidification of 0.3 pH units for 70kyrs. Delayed recovery could also be due to the weakened organic matter burial feedback (Hülse, Arndt and Ridgwell, 2019; Armstrong McKay and Lenton, 2018). This could be limiting the acidification recovery due to an inability to efficiently reduce  $p\text{CO}_2$ , which, as shown by (Figure 3.14), has a similar timing and magnitude of recovery to pH. This suggests although carbonate weathering is strong enough to onset substantial carbon cycle responses, a full recovery relies on additional feedbacks “catching up” to work in tandem with weathering and restore initial conditions.

As discussed, “catching up” could be a spatial resilience inconsistency, limited by interaction with a terrestrial weathering interface. ODP Site 690 (Figure 4.3) exposes this, containing consistently high carbonate content and ecological persistence (Kelly et al., 2005; Kelly, 2002). This is argued to be permissible from enhanced chemical weathering and run-off from continents, shown by increased radiogenic osmium seawater composition (Kelly et al., 2005; Robert and Kennett, 1994). This could be a signature from an orogenic period of the Andes, which by the PETM had aerial exposure and Molasse deposits (Olivero and Martinioni, 2001). This sets up a

situation of enhanced erosion and direct supply to shallow seas and transport via the CDW to proximity of Site 690 (Figure 4.4), especially given partial carbonate Andes geology, neighbouring ODP 690 (Laya and Tucker, 2012).

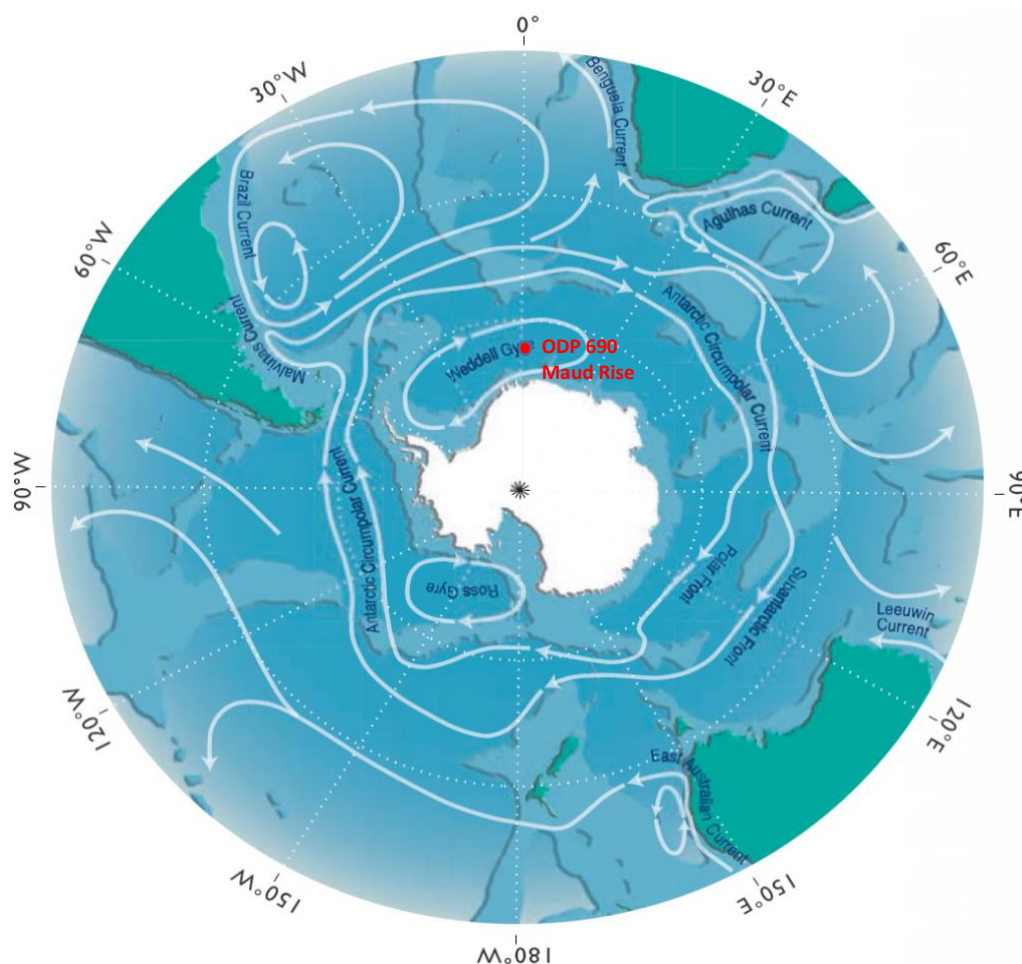


Figure 4.4; Southern Ocean Currents

Figure showing the interaction of currents around ODP 690 (red circle label). Adapted from (DAWE, 2002).

Therefore, given the results of this analysis and comparisons to other observations, there may have been regional resilience active during the PETM, consequent of a high carbonate weathering environment able to exert a strong enough negative feedback on the carbon and climate response and recovery.

## 4.2.2 Insights Through Time

### **Past Events: Lack of Resilience**

In addition to the PETM, other events have perturbed the carbon cycle through time, amounting to a diverse geologic history of responses and recoveries.

Weaker perturbation event resilience has been evident in the past with evident by longer recovery periods and more severe extinctions (Harnick et al., 2012). One example is the P-Tr; which due to an event of 13000-43000PgC over 20-40kyrs, caused widespread extinction in all ocean realms (Jin et al., 2000). A lack of resilience is said to be due to a combination of the length and scale of carbon perturbation, and insufficient species diversity and adaptability (Vervoort et al., 2019; Foster et al., 2017). However, central to any recovery, it is also argued the negative weathering feedback was also weaker (Kump, 2018).

Some carbonate weathering resilience is noted by shelf dissolution (Honisch et al., 2012; Kump, 2018) and a fall in sea-level exposing carbonates to weather, granting an initial stable pH phase (Clarkson et al., 2015). However, it is said that weathering resilience was soon exhausted, unable to keep up with persistent Siberian Traps emission and exacerbated by reduced uplift and high continentality (Kump, 2018). A similar scenario is exemplified by (Figure 3.19) showing an inability of resilience to maintain initial pH, decreasing by 3.1% for a weathering rate reduced by a factor of 10.



Events during the Cretaceous also resemble high CO<sub>2</sub> scenarios of the PETM, producing Ocean Anoxic Events (OAEs) 1a and 2. Consequence of volcanic degassing resulted in acidification and pCO<sub>2</sub> similar to the PETM (Kuhnt et al., 2017). Although these events were longer lasting at 150kyr (excluding recovery) (Honisch et al., 2012), recovery was characterised by lags and pulses in response, from a deep-water acidification delay after a 25-30kyr of dissolution, to acidification paused by alkalinity recoveries over 35kyr (Erba et al., 2010). This suggests a weaker weathering negative feedback to drive recovery.

Yet, environmental conditions for these Cretaceous events were encouraging for high weathering (high sea-level, accelerated hydrological cycle and large area of semi-arid continent) (Mackenzie and Morse, 1992; Jenkyns, 2018). Therefore, this could mean weathering resilience influence is event-duration limited, whereby after a long duration a tipping point is breached whereby weathering resilience is inefficient, similar to that suggested for the PETM (Littler et al., 2014; Barnet et al., 2019). Alternatively, this could point to a weaker foundation of carbonate weatherable reservoirs, compromising recycling of weathering influx enhanced by significant calcifier loss from deoxygenation (De Le Rocha et al., 1998). Although the Cretaceous as a period was prolific for high CaCO<sub>3</sub> deposition, lack of weathering accessibility to this reserve may have stunted recovery (Gale and Lovell, 2018).

### **Past Events: Carbonate Weathering Resilience**

Recovery and extinction resilience to events has generally increased through Earth's history, notably since the PETM (Figure 4.5) (Harnick et al., 2012). It is controversial

whether this solely represents increasing resilience, as this trend is influenced by the better preservation which can capture more of the recovery than for deeper time. Further, the scale of carbon perturbation has not matched preceding events; aside from current anthropogenic perturbation (Schobben, van de Schootbrugge and Wignall., 2019). Nonetheless, this does not discount the potential for increased carbonate weathering driven resilience playing a part in this trend. Such resilience is highlighted by an increase in carbonate burial through time from the late Eocene, indicative of a transition to a weathering-enhanced system (van der Ploeg et al., 2019).

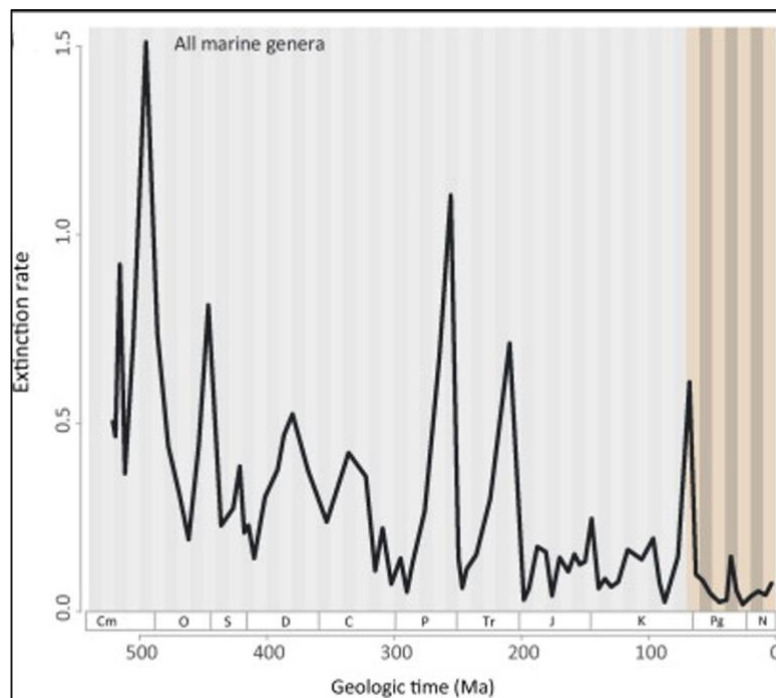


Figure 4.5; Mass Extinctions Through Time

Extinction rate of all marine genera in Phanerozoic. Adapted from (Harnick et al., 2012)

Dynamism of tectonics, sea level rise, hydrological cycle acceleration, glaciation, deforestation and exposure of carbonate massifs have all enhanced weathering resilience (Mackenzie and Morse, 1992). Continental shift from the continued break

up of Laurasia and Gondwana has triggered exhumation of weatherable strata. Formation of the Himalayas has been a result of this, which is argued to be a cause of long-term cooling and Antarctic ice sheet growth in the Miocene, due to enhanced carbonate weathering (Kawahata et al., 2019; Kender, Yu and Peck, 2014). Furthermore, this mountain range self-amplified weathering further with the prominence of the ITCZ and Indian monsoon system. Persistent and high-volume influx of carbonate weathering therefore overrides any short-term process such as ocean-circulation or ecology, especially given strong climate-chemistry feedbacks at this time (Unger and Yue, 2014).

This was not the only active weathering enhancement post-PETM, as glaciations resulting from Himalayan-influenced cooling also enhanced weathering (Vance, Teagle and Foster, 2009). High weathering fluxes at glacier terminus are identifiable in sediment and ecological responses, capable to create a CO<sub>2</sub> net reduction (Flores et al., 2012). Weathered material has physical characteristics complementary to these impacts, producing fine grains with high surface areas that intensify already fast kinetics of mineral weathering (Martin, 2017). However, studies tend to apply bias by assuming weathering and sedimentation rates from observations from rivers, which are temporally variable and magnitudes less than the fluxes from glaciation, demonstrated by the LGM experiencing weathering rates 2-3 times the average (Vance, Teagle and Foster, 2009).

Greater weathering response occurs during interglacials, which is said to be due to sea level rise able to influence rate of weathered supply (Riding, Liang and Braga,

2014) and communication between surface waters and deep-sea, which has shown to influence dissolution as a secondary supply of weathering resilience which occurs at the transition from interglacial to glacial (Mackenzie and Morse, 1992; Beaufort et al., 2011; Hodell, Charles and Sierro, 2001). This exposed a cyclic dynamic of carbonate behaviour than can be environmentally influenced, but also demonstrates importance of exposed sediments for weathering, then elucidating to the role of lithology. This signature responds to climate and C-cycle changes as demonstrated to a paralleled change to  $\delta_{18}\text{O}$  (Hodell, Charles and Sierro, 2001) but also responds to the glaciation changes they trigger.

In tandem to increased prevalence of weathering catalysts, a frequently unacknowledged active weathering enhancement is the role of the newly uplift Cretaceous chalk massifs (Mackenzie and Andersson, 2013). As reviewed in Chapter 1, 25m uplift is estimated to have been active in the early Eocene, induced by an Icelandic mantle plume providing a “Palaeocene Thermal swell” (Gale and Lovell, 2018; Nadin, Kuszniir and Toth, 1995), then further exposed by SLR from the Alpine orogeny (late Oligocene-mid Miocene) (Gibbard, 1995). This timing coincides with the observed increasing trend of alkalinity and other carbonate trends driven by weathering (Figure 4.6), most aligned with the most active phases of uplift (Dezes, Schmid and Ziegler, 2004).

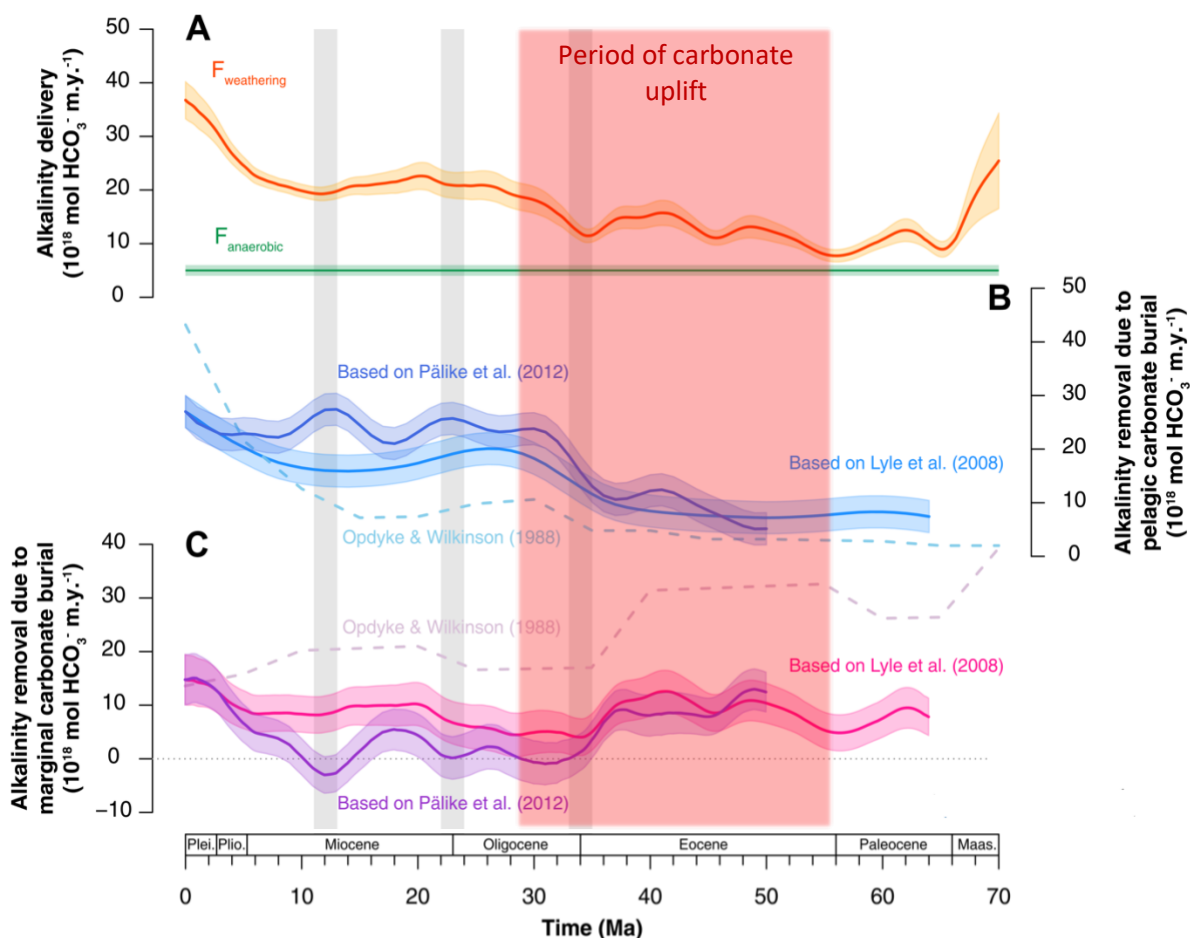


Figure 4.6; Cenozoic Alkalinity Changes

Modelled alkalinity delivery and removal throughout the Cenozoic. (A) continental weathering alkalinity (red line) with orange shading showing range of estimates, green line shows anaerobic delivery on continental margins. (B) removal by pelagic burial using range of maximum and minimum estimates (sources cited). (C) removal by marginal burial, calculated by the difference of  $F_{\text{weathering}}$ ,  $F_{\text{anaerobic}}$ , and  $F_{\text{pelagic}}$ . Red transparent box represents active period of carbonate uplift. Figure adapted from (van der Ploeg et al., 2019).

Therefore, using a system that has equilibrated to a high carbonate weathering rate as shown in this analysis, exposure and erosion of carbonate masses can be accounted for. Resilience is made evident by dampened  $\text{pCO}_2$  and temperature by 26% and 12% respectively for higher weathering state (Figure 3.17). This then amounts to a 54% greater reservoir of  $\text{CaCO}_3$  sediment accumulation, a foundation to resilience accessibility.

Applying different weathering rates on this state is then able to capture the episodic nature of weathering perturbations discussed. Although these results demonstrate larger ranges of responses relative to the same weathering rates applied to a fixed CO<sub>2</sub> stabilised state on 10W, this still does not discount the resilience brought to the system set-up by an 'open' higher weathering state, which as shown by (Figure 3.17) is more resilient. Nonetheless, as (Figures 3.18 and 3.19) show, a higher initial weathering rate encourages resiliency. Reducing weathering rate by 50% (20W to 10W) results in 30.86% and 9.57% increases in pCO<sub>2</sub> and temperature respectively, while decreasing by 42.02% and 1.56% for CaCO<sub>3</sub> sediment composition and pH respectively. But due to the initial stable conditions representative of a resilient state, the 20kyr-end climate and carbon system still remains in habitable bounds of temperature and pH (13.97°C and 7.9 respectively) (Krissansen-Totton, Arney and Catling, 2018). This is also evident with observed ecological responses to carbonate lithology, as pulses of diversification and geographic expansion of calcifiers has shown to match the timings of chalk uplift (Foster et al., 2020). Hence, high initial and continued weathering can potentially provide refuge and resilience to carbonate-sensitive species. Therefore, this may support the indication the trend of increasing ecological resilience shown by (Figure 4.5) was potentially driven by increasing system resilience by carbonate weathering.

Yet, it could be argued that instead of an importance of accessible carbonate weathering reserve, post-PETM resilience was influenced more so by climate and carbon controls on weathering processes (Zachos, Dickens and Zeebe, 2008). However, even with enforced high weathering of glaciers and chemical weathering, influence is reliant on lithology, as demonstrated by a lack of buffering from Icelandic

basalt weathering (Gislason et al., 1996). Chalk weathering rates are high due to porous and permeable characteristics and reactive composition to chemical weathering (Lawrence et al., 2013). Weathering rates in chalk aquifers are estimated to be  $3 \times 10^{-6} \text{ yr}^{-1}$  –  $10^{-5} \text{ yr}^{-1}$  (Bourdon et al., 2009), while surface weathering rates are not as constrained due to episodic erosive nature (Bowen and Take, 2014).

Therefore the existence of such a weatherable reservoir would likely have notable climate and carbon control, strongly coupled to an ability to be a self-regulating system (Mackenzie and Andersson, 2013) and potentially in the form of high productivity and surface acidification in northern latitude regions where these masses predominantly cover (McKay et al., 2012; Beaufort et al., 2011).

These results are therefore useful to demonstrate stability of a system with consistent high weathering and continued resilience with variable weathering rate changes representative of Earth system weathering perturbations. Thus, supporting the importance of *weatherability* in a system to enhance resilience, as Caves et al (2016) suggests was a determinant of Cenozoic cooling, as the strength of the weathering feedback also increased. A reserve of carbonate lithology strengthens the carbonate weathering negative feedback and the controls it exerts. Therefore, the continued influence must be assessed for future Earth system response and resilience.

### 4.2.3 Looking to the Future

#### Current RCP Predictions

Studies to recreate perturbation events through time to understand process responses can be useful but can never be a *perfect* analogue for the future (Honisch et al., 2012). Assumptions are applied to future predictions based on what has been observed in the past. This results in bias to only apply known process behaviour. Consequently, potential exists to ignore important which may have differing scales of influence under future conditions (Lunt et al., 2013).

Predictions partitioned into RCPs for the 2014 IPCC report, forecast the changes summarised in Table 4 for the mid- and late-21<sup>st</sup> century, relative to 1986-2005. Such changes are likely to have significant effects on the ocean carbon cycle and the biological contributors, especially for RCPs capable of >1.5°C warming, described as *more likely* in the most recent IPCC analysis (IPCC, 2019). (Figures 3.8 and 3.9) show carbon and climate responses under different weathering rates for a RCP6 scenario. Given that observed pH decrease from the pre-industrial is ~0.1 (IPCC 2014), during perturbation decreases show a similar decrease of ~0.25 by reference year 2100, in Table 4. Higher weathering (20W) minimises pH reduction by an average of 0.02 across 1000-year perturbation (relative to 10W). However, the 19,000 years following the event, 20W recovers pH to a state 0.06 higher than initial, 1.3 higher than 10W. This could therefore mean that an immediate higher-weathering pH resilience may not be globally significant but will play an important role for the longer recovery and eventual reduction in CO<sub>2</sub>.



Similarly, 20W has an important role on the longer-term recovery. During perturbation temperature ranges by  $\sim 0.5$  °C between lowest and highest weathering rates for RCP6 and RCP8.5. Relative to Table 4, this suggests scale of weathering could be meaningful for the increase magnitude for RCP6, but less so for RCP8.5 given temperature increases are roughly twice as high. Whereas for the longer-term 19000-year recovery, 20W greatly reduces temperature after perturbation to a cooler state than initial for RCP6, and a  $\sim 3$  °C warmer state than initial for RCP8.5. These predictions are therefore very sensitive to the regulatory feedbacks assumed in their estimations, and thus likely will produce impacts that are spatially and temporally varied depending on the weathering response and create new recovered systems.

*Table 4; RCP Responses Table showing various carbon and climate responses to different RCP's. Data from (IPCC, 2014).*

<b>Change relative to reference period (1986-2005)</b>	<b>RCP2.6</b>	<b>RCP4.5</b>	<b>RCP6.0</b>	<b>RCP8.5</b>
<i>Mean temperature increase mid-century (2046-2065) (°C)</i>	1.0	1.4	1.3	2.0
<i>Mean temperature increase end-century (2081-2100) (°C)</i>	1.0	1.8	2.2	3.7
<i>Global mean sea level rise (2046-2065) (m)</i>	0.24	0.26	0.25	0.30
<i>Global mean sea level rise (2081-2100) (m)</i>	0.40	0.47	0.48	0.63
<i>Global mean pH decreases by (to 2100)</i>	0.065	0.145	0.205	0.31

<i>Mean cumulative CO<sub>2</sub> emissions 2012-2100 (GtC)</i>	270	780	1060	1685
---	-----	-----	------	------

One of those impacts is on ecology, already observed in already high CO<sub>2</sub> and acidifying environments, which will likely extrapolate as a global trend with the continued increase. Extinctions are predicted to be on similar scales as the Permian-Triassic (Zeebe and Zachos, 2013). Calcification physiological responses to anthropogenic CO<sub>2</sub> are also likely to exacerbate current observation trends of Forams thinning (de Moel et al., 2008), muscle wastage in expense of calcification (Wood, Spice and Widdicombe, 2008) and inhibition of limb regeneration due to energy deficits (Wood et al., 2009). Given current IPCC pH predictions (Table 4) and those from this analysis with 10W (Figure 3.10 and 3.12), physical health would seriously be inhibited for vulnerable calcifying organisms. This is supported by a study by (Gattuso et al., 2015), predicting a cross-organism and ecosystem increase in risk from moderate to very high risk of impact from RCP2.6 to RCP8.5, due to the expected ocean changes (Figure 4.7).

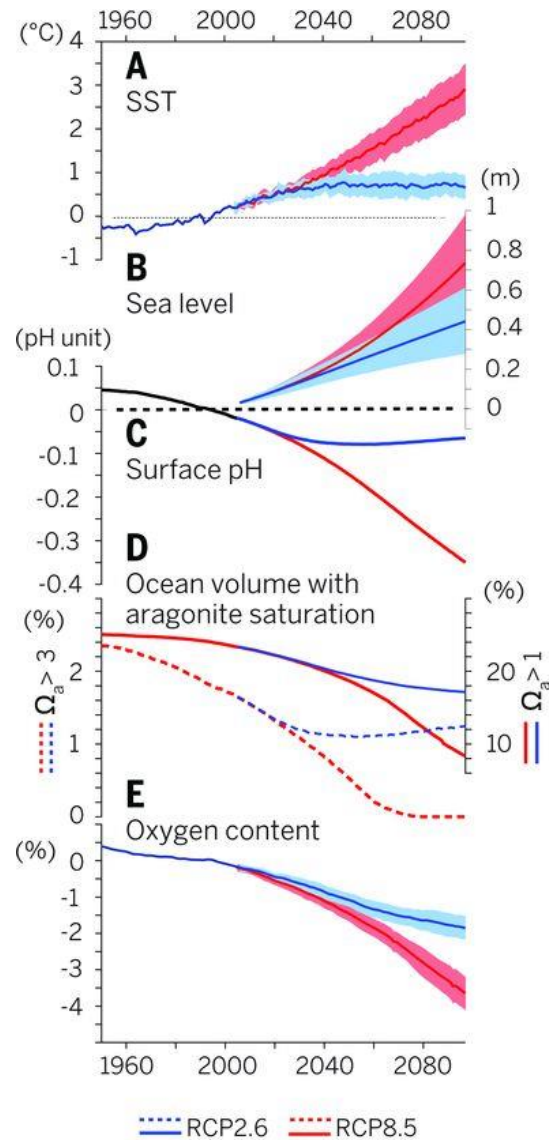


Figure 4.7; RCP Ocean Changes

Changes in global averages for RCP 8.5 (red line) and RCP 2.6 (blue line). (A) SST, (B) Sea Level, (C) Surface pH, (D) % total ocean with aragonitic  $\text{CaCO}_3$  saturation state above 1 and 3, (E) Dissolved Oxygen. Figure adapted from (Gattuso et al., 2015)

Impacts on ecological functionality also have financial consequences. The bounds on fisheries would be very sensitive to the amount of  $\text{CO}_2$  and OA over the next decades and thus could limit the exploitive wealth and livelihood permissible through fishing (Falkowski, Barber and Smetacek, 1998). This has potential impact in intertidal rocky-shore habitats, which although not as expansive as the deep ocean,

caters for 50% of marine life and supports global services worth US \$5-10 trillion a year (Hawkins et al., 2016). This will affect not only food security but also coastal tourism (e.g. reef dives and snorkelling) which is predicted to overall decline and regionally shift in response to species migration (Weatherdon et al., 2016).

### **Role of Coastal Carbonate Weathering**

However, given the composite nature of IPCC outputs, multi-model approaches apply a range of assumptions of how feedbacks will respond (Eyring et al., 2019). A negative feedback of dissolution will enhance in response to ocean acidification, but alone will be an insufficient buffer to anthropogenic CO<sub>2</sub> emissions (Andersson, Mackenzie and Ver, 2003) but the influence of increased erosion and weathering in response to climate change, has been poorly constrained (Legge et al., 2020).

Coastal environments are predicted to experience more erosion due to increasing sea levels and wave energy as a consequence of changing climates (Allan and Koman, 2006). Sea level predictions (Table 4) as a result of thermo-expansion of the ocean and ice melt has already caused coastal loss (Domingues et al., 2008; Beaulieu et al., 2012; Autret et al., 2017). Increased sea levels will mean more of the coast, and more importantly the cliffs, will be exposed to more submersion and erosion, meaning increased weathering of rock surface and acidic corrosion and salt crystallisation and removed protection of beach morphology (Autret et al., 2017; Lawrence et al., 2013; Earlie, Masselink and Russell, 2018).

In addition to increased erosion at the sea-interface, increased storm intensity and frequency is also predicted as temperatures increase (Prein et al., 2017; Seneviratne

et al., 2012). This not only exacerbates the increased water levels and precipitation but brings more destructive energy to the system catalysing future coastal erosion and aerial vulnerability (Earlie, Masselin and Russell, 2018; Ireson et al., 2009). This is significant for chalk and rocky cliffs, which cover over 80% of global coastlines and are 55% weaker than equivalents further inland (Price et al., 1993; Ireson et al., 2009).

Chalk cliffs are especially vulnerable due to the porosity, joint and fracture physicalities (Dodge-Wan and Nagarajan, 2019; Duperret et al., 2004). As discussed, these are geologically recent features thus the role and response to perturbations through time has yet to be quantified. Spatially expansive uplift has covered ice-free continental areas with ~15% exposed carbonate rock (Ford and Williams, 2013). Hence, this creates capacity for not yet accounted for controls of resilience through carbonate weathering; greater in volume, erodibility and coverage than previously parametrised carbonate weathering (Romero-Mujalli, Hartmann and Börker, 2019; Colbourn, Ridgwell and Lenton, 2015).

Given that the severity of a 1 in a 100-year event has now become a 1 in a 30 year event (Marsooli et al., 2019), the event-rate of coastal erosion will likely follow this increase in frequency and thus will create a new average rate of weathering/erosion for this environment that will need acknowledgement in models. A call for increased regional weathering consideration is commonly concluded from future scenario research (Ranasinghe, 2020; Baldry, Mountford and Greenwood, 2017). But, the scale of rate, volume and coverage from chalk erosion is quantifiable on a global

scale due to widespread coverage and active transfer through currents distributing to coasts deficient of carbonate coasts.

Envisioning what this will look like for the carbon cycle in the future may follow the resilience and recovery trends presented for 20W (Figures 3.8 and 3.10). This would suggest the influence of high  $\text{CaCO}_3$  weathering is able to bring immediate and continued event system resilience to perturbation, maintaining resilience to a level that almost resists any change. However, a 15% difference between the two RCPs suggests that this influence can be weakened, or more countered, by a higher increase in emission forcing. As discussed, this may allude to the 'exhaustion' of this feedback if the forcing is too great (Littler et al., 2014; Barnet et al., 2019; Kump, 2018).

Given the sensitivity of ecology to ocean chemistry changes, this could have profound differences to the predicted ecosystem responses and survival. Although limited by numbers of observation, a system change may take place by migration to carbonate coasts for ocean acidification refuge (Wood et al., 2010). The same has been shown for acidic environments, whereby a decreasing pH gradient also reflects a decreasing trend in calcifying species, losing resilience to  $\text{pH} < 7.8$  (Foo et al., 2018).

Resilience from higher weathering is also evident in the climate responses. (Figures 3.8 and 3.10) show that  $\text{pCO}_2$  change from initial to end of simulation is 82% and 55% less for 20W than for 10W (RCP6 and RCP8.5 respectively). Furthermore,

event peaks of pCO<sub>2</sub> are 4.4% and 2.3% less for 20W than for 10W (RCP6 and RCP8.5 respectively). Also supported by more values for higher weathering sea-to-air pCO<sub>2</sub> flux, this demonstrates oceans under higher weathering rates are able to respond as sinks, while those with lower weathering become weaker sinks relatively fast. This also has impacts on the climate, as 20W final temperatures are 1.02°C and 1.98°C less than that for 10W (RCP6 and RCP8.5 respectively). Hence, carbonate weathering will likely have a strong influence over the capacity of future carbon and climate response and recovery. This will translate to added space before tipping points are breached, which are responsive to rate and magnitude of carbon and climate response (Lenton et al., 2019).

However, it could be argued that this erosion is not sufficient to represent a global weathering rate of  $20 \times 10^{12}$  mol Ca<sub>2+</sub> yr<sup>-1</sup> due to the weaker communication with the deep ocean and fast kinetics of dissolution (Martin, 2017; Peng et al., 2016; Morse Andersson and Mackenzie, 2006). However, climate change induced glacial recession has also created new highly erosive areas of suspended sediment, as shown in Norway and Iceland (Bogen, 2009; Hawley et al., 2017). Increased attention to glacial erosion has exposed poorly constrained weathering was from these basins and thus absent from weathering budgets, even though glacial weathering fluxes have increased by 30% in 4 decades (Meire et al., 2016; Beaulieu et al., 2012). Additionally, it has been found alpine environments experience preferential weathering in carbonate bedrock, creating a CO<sub>2</sub> sink (Scribner et al., 2015; Anderson et al., 1997).

Therefore, the discharge of weathered  $\text{CaCO}_3$  could be great, given the volume at which it is forcefully eroded and the coastal interface it is released to which is highly connected to deep-water currents and advected offshore (Wadham et al., 2013; Arrigo et al., 2017). Already likely impacts on key biological pump ecological networks and the  $\text{CO}_2$  sink potential, creates conceivable influence of these environments previously not granted due attention. This in combination with increased coastal weathering could support predictions under higher weathering rates (e.g. 15W and 20W).

Accounting this influence could translate to refined predictions of system responses and timescales of recovery. Current estimates scale recovery of oceans will take from 2300-2700 (Tyrell, 2007; Andersson, Mackenzie and Lerman, 2006). This recovery is said to be mostly driven by decreased calcification which by the year 3000, has capacity to decrease  $\text{CO}_2$  by 4-13% (Ridgwell et al., 2007). While (Figures 3.8-3.11) demonstrate recovery can be directed by rate of carbonate weathering. 20W shows a return to initial  $\text{pCO}_2$  by year 13200 for RCP6. While 10W is 58.75% slower in recovery and does not return to initial  $\text{pCO}_2$ . 20W also recovers pH by year 7750, whereas 10W lags behind by 16250 years, and does not return to initial. Therefore, although without consideration of other recovery factors such as temperature, ecosystem type, ocean circulation etc. weathering evidently is an important recovery driver.

Bioturbation is also argued to place an influential role in recovery, through importance of recycled  $\text{CaCO}_3$  for resilience (Broecker, 2003). However, as shown by (Figures 3.14-3.16) their influence is dwarfed by the control of carbonate



weathering. As supported by (Tyrell, 2007), showing carbonate weathering as a negative feedback with potential to increase rate of CCD recovery. This assumption is made from a temperature-led increased limestone weathering, thus appreciation of a weathering enhancement brought by responsive chalk coasts and ability to measurably enhance recovery duration and magnitude, is supported.

Overall, this analysis of the current future predictions has elevated the influence likely to come from high carbonate weathering. Not only by the ability to recover, but to also hold influence to offset immediate response and condense recovery period.

### 4.3 Limitations

#### **Weathering Sensitivity**

Although this project was able to successfully meet aims and objectives using cGENIE, limitations do exist with the model and assumptions applied for this study. For practicality, a choice of only 5 weathering rates were analysed, informed by other studies and observations. Yet rates are still generalised from the scarce observations available, thus comparative accuracy is limited. Weathering rates forced in these experiments are also fixed, therefore any weathering responses are muted. Although literature has supported the assumption of a generalised high rate due to the enhanced weathering processes active on the exposed carbonates in this project (Lawrence et al., 2013), it is likely weathering rates would still evolve in response to changes in temperature led rates (Kump, Brantley and Arthur, 2000).

Nonetheless, it was important to force weathering rates instead of, similar to other studies, allowing weathering to be a responsive product of temperature (Mills et al., 2018) or burial (Greene et al., 2019). By forcing, responses can be isolated to weathering rate, without a noise from other feedbacks at play. Function to do this in cGENIE allowed other models to be excluded e.g. LOSCAR (Zeebe, 2012), which has parametrised  $\text{CaCO}_3$  weathering as a function of  $\text{pCO}_2$ . Not only does this not allow flexibility to alter this without  $\text{pCO}_2$  changes, but also is unlikely to represent complex interactions  $\text{pCO}_2$  has with weathering, temperature and hydrology (Penman and Zachos, 2018). Alternatively, models that prioritised coastal interactions could have been used to assess the immediate impacts of terrestrial interactions. SOCM (Shallow-water Ocean Carbonate Model) (Andersson et al., 2003) does this, but has a representative “weathering” flux from riverine input and has a carbonate chemistry that is biased to reef environments. Therefore, to satisfy the aims of this project, weathering rate has been assessed as the independent variable.

### **Scenario Set-Up**

The assumptions made in this model to represent geological events using the same set up is compromised by the different paleogeographic configurations, ecological structures and environmental feedbacks would all be different depending on the time period assessed. Although paleogeographic set-ups were available with cGENIE (e.g. Cretaceous, PETM), a ‘fake world’ set up was still applied to maintain flexibility and try to isolate weathering response away from any influence of paleogeography. The assumption of global weathering homogeneity was also applied, due to the

resolution of the model. Although this was useful in reference to global events, carbonate coverage is still spatially limited, and its influence mostly restricted to the coastal zone. It is important to assess regionality, to refine predictions and relationships of ecological and carbon-cycle response (Ranasinghe, 2020; Barnard et al., 2019).

### **Time Constraints**

A constraint on this project was time. Training and introduction of the model was kindly provided by Andy Ridgwell in November 2019 but this meant analysis could not start until return from visit (from UC Riverside). Running the model was also time consuming; initial 50kyr spin up runs took ~3 days to complete, in addition to 20kyr runs taking ~1.5 days to complete. This especially depleted time when trialling and finally running an 80kyr duration for the PETM runs. With additional time, this project could have delved into greater accuracy with weathering rates, representative of the different processes discussed. Other weathering rates could have also been tested that were more accurate to the enhancement, e.g. land use change, sea level rise, and other climate change impacts (Zeng, Liu, Kaufmann, 2019). Nonetheless, the outputs of this project have been useful to gauge an influence and relative importance of carbonate weathering on a new configuration of cGENIE and provide evidence to support the novel idea of carbonate cliff resilience for recent and future considerations.

## 5. Conclusions

### 5.1 Summary

This project has provided a novel analysis of the role of carbonate weathering in context of ocean-systems resilience. The study has quantified the carbon and climate system sensitivities to rates of carbonate weathering and responses to past and future perturbations.

The responsivity to different weathering rates has shown to be wide-ranging across geochemical dynamics and climate. Higher weathering rates have consistently shown to provide resilience to a stable earth system state, through the addition of alkalinity and enhancement of an ocean carbon sink. Lower weathering rates have had a weakening effect, in some cases demonstrating runaway instability. The analysis has been valuable to show the significant sensitivities of weathering and how this employs great uncertainty for studies that apply bias and generalised weathering rates or apply as a dependent variable (Galliardet et al., 2018; Penman and Zachos, 2018).

The role of carbonate weathering has also been tested on past and future events. Application of a PETM perturbation has exposed a consistent resilience of higher weathering rates. These outputs in correlation to regional observations have aided the explanation behind regional discrepancies in response and recovery over the PETM (Dunkley Jones et al., 2018; Honisch et al., 2012) potentially due to hot spots of carbonate weathering. Assessment of other past events which have undergone weathering fluctuations, but under a system with higher initial carbonate weathering,

has also shown trends of high carbonate weathering resilience. This study has exposed the link between growing resilience with carbonate weathering, by the increased carbonate exposure (van der Ploeg et al., 2019; Harnick et al., 2012). Hence, evidencing the past role and resilience of this process.

Expanding on the omission of carbonate weathering resilience for geologic CO<sub>2</sub> perturbations, assessment of future perturbations has also evidenced the role of carbonate weathering, and how it will influence future resilience. Accounting for the previously underestimated role of coastal carbonate geologies and the enhancement of weathering they will experience has provided new insight of this influence. Not only has higher weathering rates shown to reduce the severity of event, but also increase rate and magnitude of recovery to a point whereby initial conditions can be met and surpassed. However, as shown by other studies, the ability of carbonate weathering to employ such resilience can be exhausted by the scale of perturbation (Littler et al., 2014).

Overall, this study has brought attention to the current underestimations and assumptions of carbonate weathering influence, that has embedded bias to past and future perturbation responses. Acknowledgement of exposure and responsive weathering processes has shown to provide resilience to oceanic carbon and climate systems, which will be crucial to temporally and spatially constrain future impacts.

## 5.2 Future Opportunities

With this new insight, additional questions and opportunity for research exists to improve the relatively weak scientific understanding of carbonate weathering resilience (Caves et al., 2016).

These findings necessitate the requirement for more observations that account for a geochemical influence of carbonate coastal geologies. This is crucial to inform the current responses of biogeochemical systems and how different exposures and erosive forces are altering weathering (Legge et al., 2020), but also contextualise geologic records and how they were influenced by carbonate geologies exposed at the time. This then removes the reliance for such bias assumptions of weathering rates in future estimations, which apply homogenous shallow-water geologies (Baldry, Mountford and Greenwood, 2017).

Observations improve the accuracy but also satisfy the continued call for increased spatial resolution in models, to capture coastal environments and hence the geochemical response to alternate geologies (Ranasinghe, 2020). This, alongside improvements to models to embed more adaptability to the spatial weathering variance, will enhance the accuracy of predictions and improve regional applicability by removing a global generalisation.

Ultimately, refining the scales of carbonate weathering will improve our understanding of resilience and its evolution. This is important for direction of carbon

sequestration efforts and current carbon potential storage capacity of a range of environments, including shallow seas and continental shelves (Legge et al., 2020; Gattuso et al., 2018; Smale et al., 2018). Additionally, the coastal interface of weathering influence and level of responsivity makes carbonate weathering an important consideration for species health and migration and resultantly the biology pump (Hofman and Schellnhuber, 2009).

Hence, this research informs potential avenues of geoengineering, to the benefit of carbon draw-down and ecological function. Locating, quantifying and modelling the influence scale of carbonate weathering provides opportunity to contribute to efforts that already seek to alkalise the oceans with carbonate weathering (Taylor et al., 2015), apply carbonate weathering locales as vulnerable species refuge migrations (Gazeau et al., 2007), and potentially utilise these buffered environments for aquaculture currently reliant on input of artificial  $\text{CaCO}_3$  (Ellis, Urbina and Wilson, 2016).

## 6. Appendices

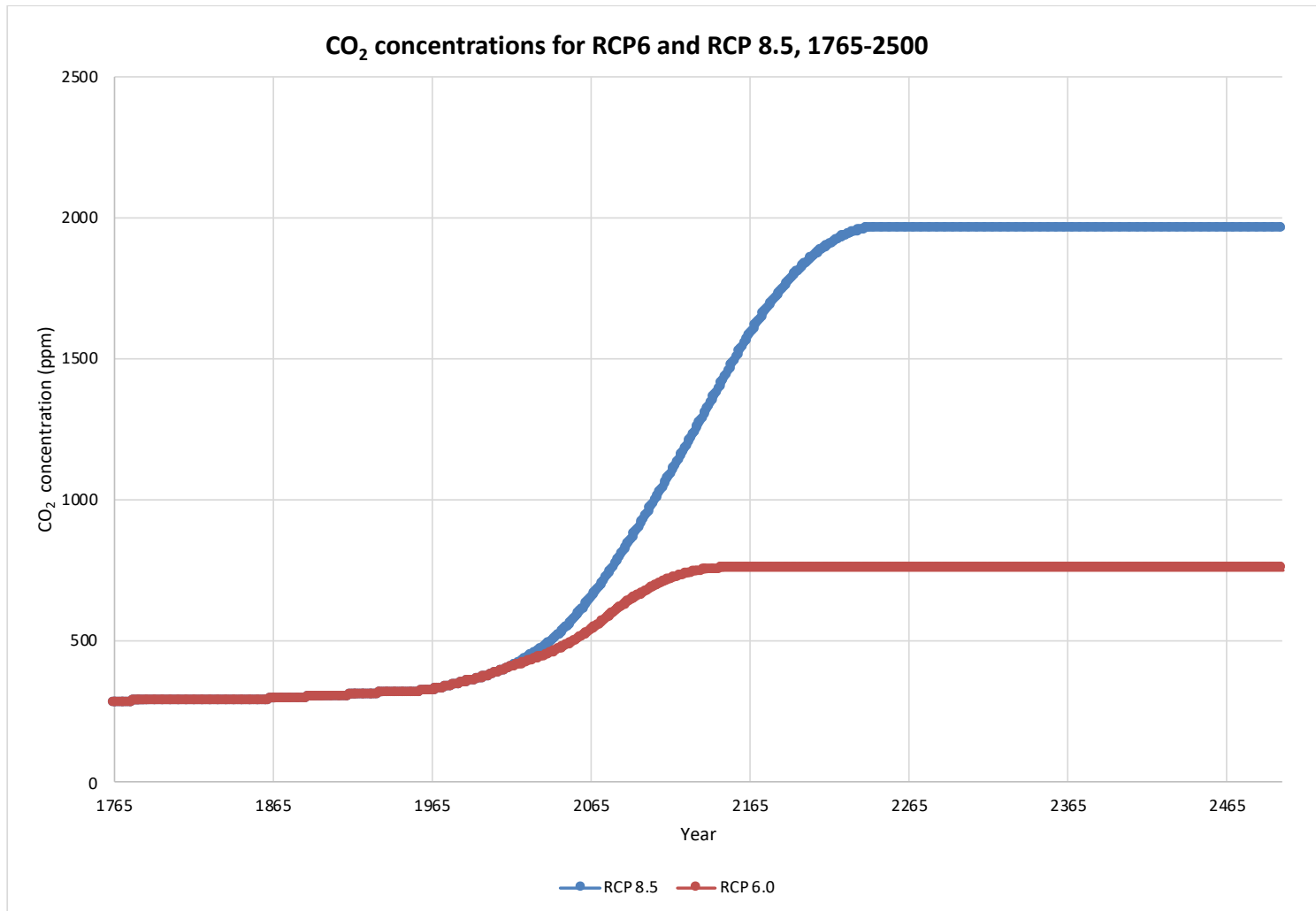


Figure 6.A; RCP CO<sub>2</sub> Concentrations

Figure shows the data used to input rate of CO<sub>2</sub> increase for RCP experiments. Data downloaded from RCP Database 2009 ([iiasa.ac.at](http://iiasa.ac.at))



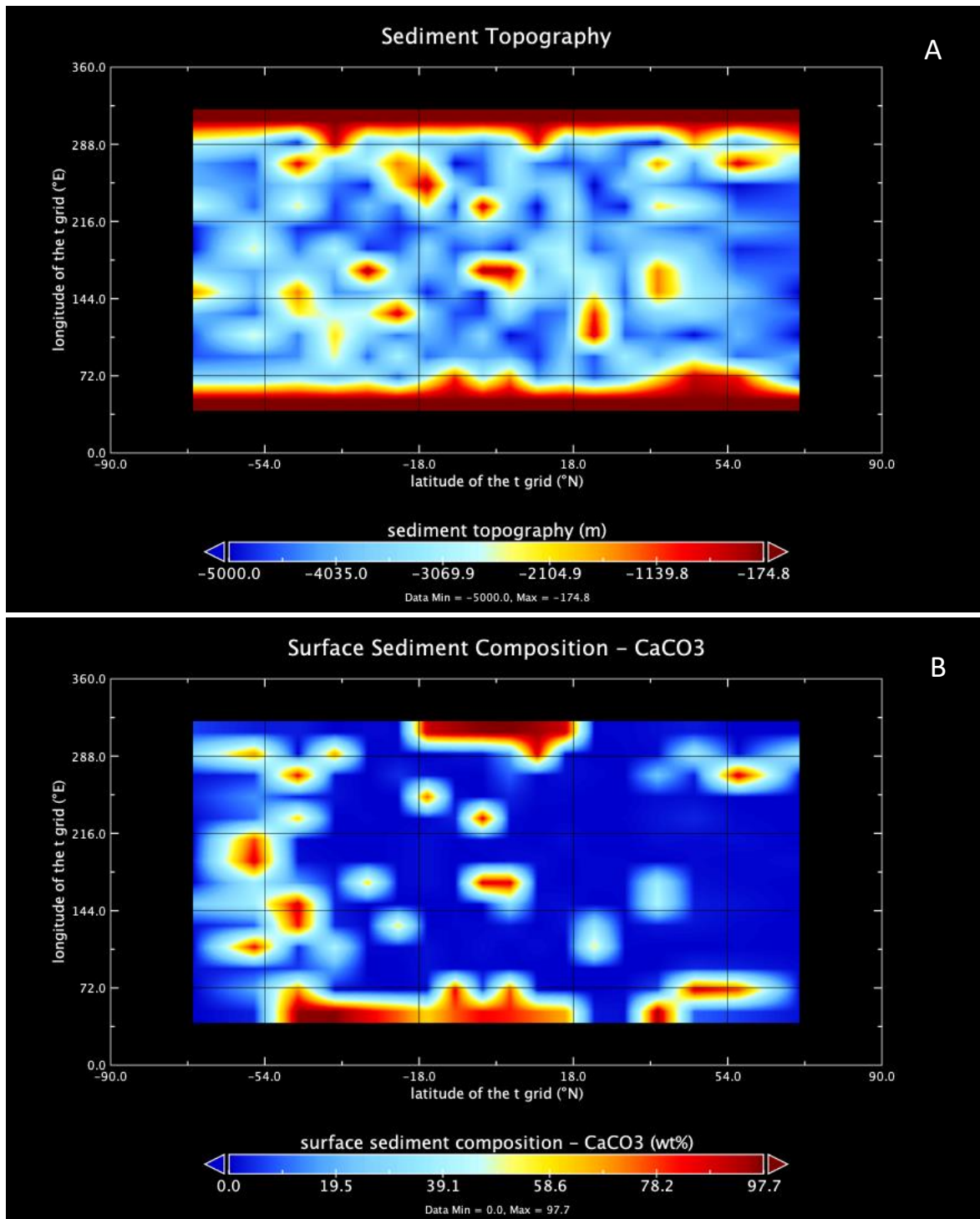


Figure 6.B Model Configuration Maps

Figure shows the sediment configuration used in FAKE WORLD configuration. (A) shows the topography of sediment while (B) shows the surface sediment  $\text{CaCO}_3$  composition after initial 50kyr equilibrium spin up.

## 7. Bibliography

Akaegbobi, I., Ogungbesan, G. and Ogala, J., 2011. Carbonate microfacies and major element content of the Paleocene – Eocene sections exposed at the Sagamu quarry, eastern Dahomey basin, Nigeria. *Global Journal of Geological Science*, 9(2), pp.241-251.

Aldiss, D., Farrant, A. and Hopson, P., 2012. Geological mapping of the Late Cretaceous Chalk Group of southern England: a specialised application of landform interpretation. *Proceedings of the Geologists' Association*, 123(5), pp.728-741.

Allan, J. and Komar, P., 2006. Climate Controls on US West Coast Erosion Processes. *Journal of Coastal Research*, 223, pp.511-529.

Amiotte Suchet, P., Probst, J. and Ludwig, W., 2003. Worldwide distribution of continental rock lithology: Implications for the atmospheric/soil CO<sub>2</sub> uptake by continental weathering and alkalinity river transport to the oceans. *Global Biogeochemical Cycles*, 17(2).

Andersson, A. J. (2003), Climate change and anthropogenic effects on shallow-water carbonate biogeochemistry, M.S. theses, Oceanography, University of Hawaii at Manoa, HI, USA

Andersson, A. J. (2006) Biogeochemical Consequences of Rising Atmospheric CO<sub>2</sub> and Ocean Acidification in the Global Coastal Ocean and Carbonate Ecosystems, PhD Theses, Oceanography, University of Hawaii at Manoa, HI, USA

Andersson, A. J., and F. T. Mackenzie (2004), The shallow-water ocean: A source or sink of atmospheric CO<sub>2</sub>?, *Frontiers Ecol. Environ.*, 2, 348– 353.

Andersson, A. J., F. T. Mackenzie, and A. Lerman (2005), Coastal ocean and carbonate systems in the high CO<sub>2</sub> world of the Anthropocene, *American Journal of Science*, 305, 875–918.

Andersson, A., 2015. A fundamental paradigm for coral reef carbonate sediment dissolution. *Frontiers in Marine Science*, 2.

Andersson, A., Bates, N. and Mackenzie, F. (2007). Dissolution of Carbonate Sediments Under Rising pCO<sub>2</sub> and Ocean Acidification: Observations from Devil's Hole, Bermuda. *Aquatic Geochemistry*, 13(3), pp.237-264.

Andersson, A., Mackenzie, F. and Lerman, A., 2006. Coastal ocean CO<sub>2</sub>-carbonic acid-carbonate sediment system of the Anthropocene. *Global Biogeochemical Cycles*, 20(1).

Andersson, A., Mackenzie, F. and Ver, L., 2003. Solution of shallow-water carbonates: An insignificant buffer against rising atmospheric CO<sub>2</sub>. *Geology*, 31(6), p.513.

Archer, D., 2003. Biological Fluxes in the Ocean and Atmospheric pCO<sub>2</sub>. *Treatise on Geochemistry*, pp.275-291.

Armstrong McKay, D. and Lenton, T., 2018. Reduced carbon cycle resilience across the Palaeocene–Eocene Thermal Maximum. *Climate of the Past*, 14(10), pp.1515-1527.

Armstrong, H. and Allen, M., 2010. Shifts in the Intertropical Convergence Zone, Himalayan exhumation, and late Cenozoic climate. *Geology*, 39(1), pp.11-14.

Arrigo, K., van Dijken, G., Castelao, R., Luo, H., Rennermalm, Å., Tedesco, M., Mote, T., Oliver, H. and Yager, P., 2017. Melting glaciers stimulate large summer phytoplankton blooms in southwest Greenland waters. *Geophysical Research Letters*, 44(12), pp.6278-6285.

Aurin, D. and Dierssen, H., 2012. Advantages and limitations of ocean color remote sensing in CDOM-dominated, mineral-rich coastal and estuarine waters. *Remote Sensing of Environment*, 125, pp.181-197.

Autret, R., Dodet, G., Suanez, S., Roudaut, G. and Fichaut, B., 2018. Long-term variability of supratidal coastal boulder activation in Brittany (France).

*Geomorphology*, 304, pp.184-200.

Bach, L., Gill, S., Rickaby, R., Gore, S. and Renforth, P., 2019. CO2 Removal With Enhanced Weathering and Ocean Alkalinity Enhancement: Potential Risks and Co-benefits for Marine Pelagic Ecosystems. *Frontiers in Climate*, 1.

Baldry, K., Hardman-Mountford, N. and Greenwood, J. (2017). Estimating total alkalinity for coastal ocean acidification monitoring at regional to continental scales in Australian coastal waters. *Biogeosciences Discussions*, pp.1-23.

Barnard, P., Erikson, L., Foxgrover, A., Hart, J., Limber, P., O'Neill, A., van Ormondt, M., Vitousek, S., Wood, N., Hayden, M. and Jones, J., 2019. Dynamic flood modeling essential to assess the coastal impacts of climate change. *Scientific Reports*, 9(1).

Barnet, J., Littler, K., Westerhold, T., Kroon, D., Leng, M., Bailey, I., Röhl, U. and Zachos, J., 2019. A High-Fidelity Benthic Stable Isotope Record of Late Cretaceous–Early Eocene Climate Change and Carbon-Cycling. *Paleoceanography and Paleoclimatology*, 34(4), pp.672-691.

Bauer, J.E., Cai, W.-J., Raymond, P.A., Bianchi, T.S., Hopkinson, C.S. and Regnier, P.A.G. (2013) The changing carbon cycle of the coastal ocean, *Nature*, 504(7478): 61–70

Baumann, K., Böckel, B., Donner, B., Gerhardt, S., Henrich, R., Vink, A., Volbers, A., Willems, H. and Zonneveld, K., 2003. Contribution of Calcareous Plankton Groups to the Carbonate Budget of South Atlantic Surface Sediments. *The South Atlantic in the Late Quaternary*, pp.81-99.

Beaufort, L., Probert, I., de Garidel-Thoron, T., Bendif, E., Ruiz-Pino, D., Metzl, N., Goyet, C., Buchet, N., Coupel, P., Grelaud, M., Rost, B., Rickaby, R. and de Vargas, C., 2011. Sensitivity of coccolithophores to carbonate chemistry and ocean acidification. *Nature*, 476(7358), pp.80-83.

Beaulieu, E., Godd ris, Y., Donnadieu, Y., Labat, D. and Roelandt, C., 2012. High sensitivity of the continental-weathering carbon dioxide sink to future climate change. *Nature Climate Change*, 2(5), pp.346-349.

Beerling, D. and Royer, D., 2011. Convergent Cenozoic CO<sub>2</sub> history. *Nature Geoscience*, 4(7), pp.418-420.

Berger, W., 1982. Increase of carbon dioxide in the atmosphere during deglaciation: the coral reef hypothesis. *Naturwissenschaften*, 69(2), pp.87-88.

Berner, E. and Berner, R., 2012. *Global Environment*. 2nd ed. Princeton, N.J.: Princeton University Press.

Berner, R., 1990. Atmospheric Carbon Dioxide Levels Over Phanerozoic Time. *Science*, 249(4975), pp.1382-1386.

Berner, R., 2003. The long-term carbon cycle, fossil fuels and atmospheric composition. *Nature*, 426(6964), pp.323-326.

Berner, R., Lasaga, A. and Garrels, R., 1983. The carbonate-silicate geochemical cycle and its effect on atmospheric carbon dioxide over the past 100 million years. *American Journal of Science*, 283(7), pp.641-683.

Blondeau-Patissier, D., Gower, J., Dekker, A., Phinn, S. and Brando, V., 2014. A review of ocean color remote sensing methods and statistical techniques for the detection, mapping and analysis of phytoplankton blooms in coastal and open oceans. *Progress in Oceanography*, 123, pp.123-144.

Bogen, J., 2009. The impact of environmental changes on the sediment loads of Norwegian rivers. *CATENA*, 79(3), pp.251-256.

Bourdon, B., Bureau, S., Andersen, M., Pili, E. and Hubert, A., 2009. Weathering rates from top to bottom in a carbonate environment. *Chemical Geology*, 258(3-4), pp.275-287.

Bowen, G. and Zachos, J., 2010. Rapid carbon sequestration at the termination of the Palaeocene–Eocene Thermal Maximum. *Nature Geoscience*, 3(12), pp.866-869.

Bowman, E. and Take, W., 2014. The runout of chalk cliff collapses in England and France—case studies and physical model experiments. *Landslides*, 12(2), pp.225-239.

Bralower, T., Meissner, K., Alexander, K. and Thomas, D., 2014. The dynamics of global change at the Paleocene-Eocene thermal maximum: A data-model comparison. *Geochemistry, Geophysics, Geosystems*, 15(10), pp.3830-3848.

Brenner, H., Braeckman, U., Le Guitton, M. and Meysman, F., 2016. The impact of sedimentary alkalinity release on the water column CO<sub>2</sub> system in the North Sea. *Biogeosciences*, 13(3), pp.841-863.

Broecker, W., 2003. The Oceanic CaCO<sub>3</sub> Cycle. *Treatise on Geochemistry*, pp.529-549.

Caldeira, K. and Wickett, M. (2003). Oceanography: Anthropogenic carbon and ocean pH. *Nature*, 425(6956), pp.365-365

Cape, M., Vernet, M., Pettit, E., Wellner, J., Truffer, M., Akie, G., Domack, E., Leventer, A., Smith, C. and Huber, B., 2019. Circumpolar Deep Water Impacts Glacial Meltwater Export and Coastal Biogeochemical Cycling Along the West Antarctic Peninsula. *Frontiers in Marine Science*, 6.

Cardell, C., Rivas, T., Mosquera, M., Birginie, J., Moropoulou, A., Prieto, B., Silva, B. and Van Grieken, R., 2003. Patterns of damage in igneous and sedimentary rocks under conditions simulating sea-salt weathering. *Earth Surface Processes and Landforms*, 28(1), pp.1-14.

Cárdenas, P., Lange, C., Vernet, M., Esper, O., Srain, B., Vorrath, M., Ehrhardt, S., Müller, J., Kuhn, G., Arz, H., Lembke-Jene, L. and Lamy, F., 2019. Biogeochemical proxies and diatoms in surface sediments across the Drake Passage reflect oceanic domains and frontal systems in the region. *Progress in Oceanography*, 174, pp.72-88.

Caves, J., Jost, A., Lau, K. and Maher, K., 2016. Cenozoic carbon cycle imbalances and a variable weathering feedback. *Earth and Planetary Science Letters*, 450, pp.152-163.

Chen, Y., Hedding, D., Li, X., Greyling, A. and Li, G., 2020. Weathering dynamics of Large Igneous Provinces (LIPs): A case study from the Lesotho Highlands. *Earth and Planetary Science Letters*, 530, p.115871.

Chen, Z., Ding, Z., Yang, S., Zhang, C. and Wang, X., 2016. Increased precipitation and weathering across the Paleocene-Eocene Thermal Maximum in central China. *Geochemistry, Geophysics, Geosystems*, 17(6), pp.2286-2297.

Clargo, N., Salt, L., Thomas, H. and de Baar, H. (2015). Rapid increase of observed DIC and pCO<sub>2</sub> in the surface waters of the North Sea in the 2001-2011 decade ascribed to climate change superimposed by biological processes. *Marine Chemistry*, 177, pp.566-581.

Clarkson, M., Kasemann, S., Wood, R., Lenton, T., Daines, S., Richoz, S., Ohnemüller, F., Meixner, A., Poulton, S. and Tipper, E. (2015). Ocean acidification and the Permo-Triassic mass extinction. *Science*, 348(6231), pp.229-232.

Colbourn, G., Ridgwell, A. and Lenton, T., 2015. The time scale of the silicate weathering negative feedback on atmospheric CO<sub>2</sub>. *Global Biogeochemical Cycles*, 29(5), pp.583-596.

Colbourn, G., Ridgwell, A., & Lenton, T. M. (2013). The Rock Geochemical Model (RokGeM) v0.9. *Geoscientific Model Development*, 6(5), 1543–1573.

Crouch, E., Heilmann-Clausen, C., Brinkhuis, H., Morgans, H., Rogers, K., Egger, H. and Schmitz, B., 2001. Global dinoflagellate event associated with the late Paleocene thermal maximum. *Geology*, 29(4), p.315.

Crowley, T., Hyde, W. and Short, D., 1989. Seasonal cycle variations on the supercontinent of Pangaea. *Geology*, 17(5), p.457.

Cummings, V., Hewitt, J., Van Rooyen, A., Currie, K., Beard, S., Thrush, S., Norkko, J., Barr, N., Heath, P., Halliday, N., Sedcole, R., Gomez, A., McGraw, C. and Metcalf, V., 2011. Ocean Acidification at High Latitudes: Potential Effects on Functioning of the Antarctic Bivalve *Laternula elliptica*. *PLoS ONE*, 6(1), p.e16069.

Cyronak, T., Santos, I. and Eyre, B., 2013. Permeable coral reef sediment dissolution driven by elevated pCO<sub>2</sub> and pore water advection. *Geophysical Research Letters*, 40(18), pp.4876-4881.

D'Antonio, M., Ibarra, D. and Boyce, C., 2019. Land plant evolution decreased, rather than increased, weathering rates. *Geology*, 48(1), pp.29-33.

Dameron, S., Leckie, R., Clark, K., MacLeod, K., Thomas, D. and Lees, J., 2017. Extinction, dissolution, and possible ocean acidification prior to the Cretaceous/Paleogene (K/Pg) boundary in the tropical Pacific. *Palaeogeography, Palaeoclimatology, Palaeoecology*, 485, pp.433-454.



Danise, S., Twitchett, R., Little, C. and Clémence, M., 2013. The Impact of Global Warming and Anoxia on Marine Benthic Community Dynamics: an Example from the Toarcian (Early Jurassic). *PLoS ONE*, 8(2), p.e56255.

De La Rocha, C., Brzezinski, M., DeNiro, M. and Shemesh, A., 1998. Silicon-isotope composition of diatoms as an indicator of past oceanic change. *Nature*, 395(6703), pp.680-683.

de Moel, H., Ganssen, G., Peeters, F., Jung, S., Kroon, D., Brummer, G. and Zeebe, R., 2009. Planktic foraminiferal shell thinning in the Arabian Sea due to anthropogenic ocean acidification?. *Biogeosciences*, 6(9), pp.1917-1925.

Department of Agriculture, Water and the Environment, 2002. *The Southern Ocean's Global Reach*. Australian Government.

Dessert, C., Dupré, B., Gaillardet, J., François, L. and Allègre, C., 2003. Basalt weathering laws and the impact of basalt weathering on the global carbon cycle. *Chemical Geology*, 202(3-4), pp.257-273.

Dèzes, P., Schmid, S. and Ziegler, P., 2004. Evolution of the European Cenozoic Rift System: interaction of the Alpine and Pyrenean orogens with their foreland lithosphere. *Tectonophysics*, 389(1-2), pp.1-33.

Dèzes, P., Schmid, S. and Ziegler, P., 2004. Evolution of the European Cenozoic Rift System: interaction of the Alpine and Pyrenean orogens with their foreland lithosphere. *Tectonophysics*, 389(1-2), pp.1-33.

Dodge-Wan, D. and Nagarajan, R., 2019. Boring of Intertidal Sandstones by Isopod *Sphaeroma triste* in NW Borneo (Sarawak, Malaysia). *Journal of Coastal Research*, 36(2), p.238.

Domingues, C., Church, J., White, N., Gleckler, P., Wijffels, S., Barker, P. and Dunn, J., 2008. Improved estimates of upper-ocean warming and multi-decadal sea-level rise. *Nature*, 453(7198), pp.1090-1093.

Donohue, P., Calosi, P., Bates, A., Laverock, B., Rastrick, S., Mark, F., Strobel, A. and Widdicombe, S., 2012. Impact of exposure to elevated pCO<sub>2</sub> on the physiology and behaviour of an important ecosystem engineer, the burrowing shrimp *Upogebia deltaura*. *Aquatic Biology*, 15(1), pp.73-86.

Duarte, C., Hendriks, I., Moore, T., Olsen, Y., Steckbauer, A., Ramajo, L., Carstensen, J., Trotter, J. and McCulloch, M. (2013). Is Ocean Acidification an Open-Ocean Syndrome? Understanding Anthropogenic Impacts on Seawater pH. *Estuaries and Coasts*, 36(2), pp.221-236

Dubiel, R., Parrish, J., Parrish, J. and Good, S., 1991. The Pangaeian Megamonsoon: Evidence from the Upper Triassic Chinle Formation, Colorado Plateau. *PALAIOS*, 6(4), p.347.

Dunkley Jones, T., Manners, H., Hoggett, M., Kirtland Turner, S., Westerhold, T., Leng, M., Pancost, R., Ridgwell, A., Alegret, L., Duller, R. and Grimes, S., 2018. Dynamics of sediment flux to a bathyal continental margin section through the Paleocene–Eocene Thermal Maximum. *Climate of the Past*, 14(7), pp.1035-1049.

Duperret, A., Genter, A., Martinez, A. and Mortimore, R., 2004. Coastal chalk cliff instability in NW France: role of lithology, fracture pattern and rainfall. Geological Society, London, Engineering Geology Special Publications, 20(1), pp.33-55.

Duperret, A., Taibi, S., Mortimore, R. and Daigneault, M. (2005). Effect of groundwater and sea weathering cycles on the strength of chalk rock from unstable coastal cliffs of NW France. *Engineering Geology*, 78(3-4), pp.321-343.

E.M. Crouch, H. Brinkhuis, H. Visscher, H. Adatte, M.–P. Bolle

Earlie, C., Masselink, G. and Russell, P., 2018. The role of beach morphology on coastal cliff erosion under extreme waves. *Earth Surface Processes and Landforms*, 43(6), pp.1213-1228.

Ellis, R., Urbina, M. and Wilson, R. (2016). Lessons from two high CO<sub>2</sub> worlds - future oceans and intensive aquaculture. *Global Change Biology*, 23(6), pp.2141-2148.

Elsworth, G., Galbraith, E., Halverson, G. and Yang, S., 2017. Enhanced weathering and CO<sub>2</sub> drawdown caused by latest Eocene strengthening of the Atlantic meridional overturning circulation. *Nature Geoscience*, 10(3), pp.213-216.

Emerson, S. and Hedges, J. (2006). Sediment Diagenesis and benthic flux. In: H. Elderfield, ed., *The Ocean and Marine Geochemistry*. London: Elsevier, pp.304-311.

Emerson, S. and Hedges, J., 2008. *Chemical Oceanography And The Marine Carbon Cycle*. Cambridge: Cambridge University Press.

Erba, E., Bottini, C., Weissert, H. and Keller, C., 2010. Calcareous Nannoplankton Response to Surface-Water Acidification Around Oceanic Anoxic Event 1a. *Science*, 329(5990), pp.428-432.

Ernst, R. and Youbi, N., 2017. How Large Igneous Provinces affect global climate, sometimes cause mass extinctions, and represent natural markers in the geological record. *Palaeogeography, Palaeoclimatology, Palaeoecology*, 478, pp.30-52.

Ernst, R.E., 2014. *Large Igneous Provinces*. Cambridge University Press (653 p.).

Eyring, V., Cox, P., Flato, G., Gleckler, P., Abramowitz, G., Caldwell, P., Collins, W., Gier, B., Hall, A., Hoffman, F., Hurtt, G., Jahn, A., Jones, C., Klein, S.,

Krasting, J., Kwiatkowski, L., Lorenz, R., Maloney, E., Meehl, G., Pendergrass, A., Pincus, R., Ruane, A., Russell, J., Sanderson, B., Santer, B., Sherwood, S., Simpson, I., Stouffer, R. and Williamson, M., 2019. Taking climate model evaluation to the next level. *Nature Climate Change*, 9(2), pp.102-110.

Fagherazzi, S., Howard, A. and Wiberg, P., 2004. Modeling fluvial erosion and deposition on continental shelves during sea level cycles. *Journal of Geophysical Research*, 109(F3).

Falkowski, P., Barber, R. and Smetacek, V., 1998. Biogeochemical Controls and Feedbacks on Ocean Primary Production. *Science*, 281(5374), pp.200-206.

Feng (冯玉铭), E., Keller, D., Koeve, W. and Oschlies, A. (2016). Could artificial ocean alkalization protect tropical coral ecosystems from ocean acidification?. *Environmental Research Letters*, 11(7), p.074008.

Fennel, K., Gehlen, M., Brasseur, P., Brown, C., Ciavatta, S., Cossarini, G., Crise, A., Edwards, C., Ford, D., Friedrichs, M., Gregoire, M., Jones, E., Kim, H., Lamouroux, J., Murtugudde, R. and Perruche, C., 2019. Advancing Marine Biogeochemical and Ecosystem Reanalyses and Forecasts as Tools for Monitoring and Managing Ecosystem Health. *Frontiers in Marine Science*, 6.

Flores, J., Filippelli, G., Sierro, F. and Latimer, J., 2012. The “White Ocean” Hypothesis: A Late Pleistocene Southern Ocean Governed by Coccolithophores and Driven by Phosphorus. *Frontiers in Microbiology*, 3.

Foo, S., Bryne, M., Ricevuto, E. and Gambi, M., 2020. The Carbon Dioxide Vents of Ischia, Italy, A Natural System to Assess Impacts of Ocean Acidification on Marine Ecosystems: An Overview of Research and Comparisons with Other Vent Systems. In: S. Hawkins, A. Evans, A. Dale, L. Firth and I. Smith, ed., *Oceanography and Marine Biology*, 1st ed. Boca Raton: CRC Press, pp.237-262.

Ford, D. and Williams, P., 2013. *Karst Hydrogeology And Geomorphology*. New York, NY: John Wiley & Sons.

Foster, W., Danise, S., Price, G. and Twitchett, R., 2017. Subsequent biotic crises delayed marine recovery following the late Permian mass extinction event in northern Italy. *PLOS ONE*, 12(3), p.e0172321.

Foster, W., Garvie, C., Weiss, A., Muscente, A., Aberhan, M., Counts, J. and Martindale, R., 2020. Resilience of marine invertebrate communities during the early Cenozoic hyperthermals. *Scientific Reports*, 10(1).

Gaillardet, J., Calmels, D., Romero-Mujalli, G., Zakharova, E. and Hartmann, J., 2019. Global climate control on carbonate weathering intensity. *Chemical Geology*, 527, p.118762.

Gale, A. and Lovell, B., 2018. The Cretaceous–Paleogene unconformity in England: Uplift and erosion related to the Iceland mantle plume. *Proceedings of the Geologists' Association*, 129(3), pp.421-435.

Gasson, E., DeConto, R., Pollard, D. and Levy, R., 2016. Dynamic Antarctic ice sheet during the early to mid-Miocene. *Proceedings of the National Academy of Sciences*, 113(13), pp.3459-3464.

Gattuso, J., Magnan, A., Billé, R., Cheung, W., Howes, E., Joos, F., Allemand, D., Bopp, L., Cooley, S., Eakin, C., Hoegh-Guldberg, O., Kelly, R., Pörtner, H., Rogers, A., Baxter, J., Laffoley, D., Osborn, D., Rankovic, A., Rochette, J., Sumaila, U., Treyer, S. and Turley, C., 2015. Contrasting futures for ocean and society from different anthropogenic CO<sub>2</sub> emissions scenarios. *Science*, 349(6243), p.aac4722.

Gazeau, F., Alliouane, S., Bock, C., Bramanti, L., Lopez Correa, M., Gentile, M., Hirse, T., Portner, H. and Ziveri, P., 2014. Impact of ocean acidification and

warming on the Mediterranean mussel (*Mytilus galloprovincialis*). *Frontiers in Marine Science*, 1.

Gazeau, F., Quiblier, C., Jansen, J., Gattuso, J., Middelburg, J. and Heip, C. (2007). Impact of elevated CO<sub>2</sub> on shellfish calcification. *Geophysical Research Letters*, 34(7).

Gehler, A., Gingerich, P. and Pack, A., 2016. Temperature and atmospheric CO<sub>2</sub> concentration estimates through the PETM using triple oxygen isotope analysis of mammalian bioapatite. *Proceedings of the National Academy of Sciences*, 113(28), pp.7739-7744.

Gibbard, P.L., 1995. Formation of the Strait of Dover. In: Preece, R.C. (Ed.), *Island Britain—A Quaternary Perspective*, 15–26, Geological Society Special Publication, 96.

Gillieson, D., 2005. Karst in Southeast Asia. In: A. Gupta, ed., *The physical geography of Southeast Asia*. Oxford: Oxford University Press, pp.157-176.

Gislason, S., Arnorsson, S. and Armannsson, H., 1996. Chemical weathering of basalt in Southwest Iceland; effects of runoff, age of rocks and vegetative/glacial cover. *American Journal of Science*, 296(8), pp.837-907.

Goddéris, Y., Donnadieu, Y., Lefebvre, V., Le Hir, G. and Nardin, E., 2012. Tectonic control of continental weathering, atmospheric CO<sub>2</sub>, and climate over Phanerozoic times. *Comptes Rendus Geoscience*, 344(11-12), pp.652-662

Greene, S., Ridgwell, A., Kirtland Turner, S., Schmidt, D., Pälike, H., Thomas, E., Greene, L. and Hoogakker, B., 2019. Early Cenozoic Decoupling of Climate and Carbonate Compensation Depth Trends. *Paleoceanography and Paleoclimatology*, 34(6), pp.930-945.

Gruber, N., Gloor, M., Mikaloff Fletcher, S., Doney, S., Dutkiewicz, S., Follows, M., Gerber, M., Jacobson, A., Joos, F., Lindsay, K., Menemenlis, D., Mouchet, A., Müller, S., Sarmiento, J. and Takahashi, T., 2009. Oceanic sources, sinks, and transport of atmospheric CO<sub>2</sub>. *Global Biogeochemical Cycles*, 23(1).

Gustafsson, E., Omstedt, A. and Gustafsson, B., 2015. The air-water CO<sub>2</sub> exchange of a coastal sea - A sensitivity study on factors that influence the absorption and outgassing of CO<sub>2</sub> in the Baltic Sea. *Journal of Geophysical Research: Oceans*, 120(8), pp.5342-5357.

Gutjahr, M., Ridgwell, A., Sexton, P., Anagnostou, E., Pearson, P., Pälike, H., Norris, R., Thomas, E. and Foster, G., 2017. Very large release of mostly volcanic carbon during the Palaeocene–Eocene Thermal Maximum. *Nature*, 548(7669), pp.573-577.

Hain, M., Sigman, D. and Haug, G., 2014. The Biological Pump in the Past. *Treatise on Geochemistry*, pp.485-517.

Harnik, P., Lotze, H., Anderson, S., Finkel, Z., Finnegan, S., Lindberg, D., Liow, L., Lockwood, R., McClain, C., McGuire, J., O'Dea, A., Pandolfi, J., Simpson, C. and Tittensor, D., 2012. Extinctions in ancient and modern seas. *Trends in Ecology & Evolution*, 27(11), pp.608-617.

Hautmann, M., Benton, M. and Tomašových, A., 2008. Catastrophic ocean acidification at the Triassic-Jurassic boundary. *Neues Jahrbuch für Geologie und Paläontologie - Abhandlungen*, 249(1), pp.119-127.

Hawkings, J., Hatton, J., Hendry, K., de Souza, G., Wadham, J., Ivanovic, R., Kohler, T., Stibal, M., Beaton, A., Lamarche-Gagnon, G., Tedstone, A., Hain, M., Bagshaw, E., Pike, J. and Tranter, M., 2018. The silicon cycle impacted by past ice sheets. *Nature Communications*, 9(1).

Hawkins, S.J., Evans, A.J., Firth, L.B., Genner, M.J., Herbert, R.J.H., Adams, L.C., Moore, P.J., Mieszkowska, N., Thompson, R.C., Burrows, M.T. and Fenberg, P.B. (2016) Impacts and effects of ocean warming on intertidal rocky habitats In, Laffoley, D. and Baxter, J.M. (eds.) Explaining ocean warming: Causes, scale, effects and consequences. Full report. Gland, CH, IUCN pp. 147-176.

Hawley, S., Pogge von Strandmann, P., Burton, K., Williams, H. and Gíslason, S., 2017. Continental weathering and terrestrial (oxyhydr)oxide export: Comparing glacial and non-glacial catchments in Iceland. *Chemical Geology*, 462, pp.55-66.

Hay, W., 2008. Evolving ideas about the Cretaceous climate and ocean circulation. *Cretaceous Research*, 29(5-6), pp.725-753.

Hayhoe, K., J. Edmonds, R.E. Kopp, A.N. LeGrande, B.M. Sanderson, M.F. Wehner, and D.J. Wuebbles, 2017: Climate models, scenarios, and projections. In: *Climate Science Special Report: Fourth National Climate Assessment, Volume I* [Wuebbles, D.J., D.W. Fahey, K.A. Hibbard, D.J. Dokken, B.C. Stewart, and T.K. Maycock (eds.)]. U.S. Global Change Research Program, Washington, DC, USA, pp. 133-160

Heggheim, T., Madland, M., Risnes, R. and Austad, T. (2005). A chemical induced enhanced weakening of chalk by seawater. *Journal of Petroleum Science and Engineering*, 46(3), pp.171-184.

Hills, R., 1991. Chalk porosity and Tertiary uplift, Western Approaches Trough, SW UK and NW French continental shelves. *Journal of the Geological Society*, 148(4), pp.669-679.

Hodell, D., Charles, C. and Sierro, F., 2001. Late Pleistocene evolution of the ocean's carbonate system. *Earth and Planetary Science Letters*, 192(2), pp.109-124.



Hofmann, M. and Schellnhuber, H., 2009. Oceanic acidification affects marine carbon pump and triggers extended marine oxygen holes. *Proceedings of the National Academy of Sciences*, 106(9), pp.3017-3022.

Honisch, B., Ridgwell, A., Schmidt, D., Thomas, E., Gibbs, S., Sluijs, A., Zeebe, R., Kump, L., Martindale, R., Greene, S., Kiessling, W., Ries, J., Zachos, J., Royer, D., Barker, S., Marchitto, T., Moyer, R., Pelejero, C., Ziveri, P., Foster, G. and Williams, B., 2012. The Geological Record of Ocean Acidification. *Science*, 335(6072), pp.1058-1063.

Honjo, S., Eglinton, T., Taylor, C., Ulmer, K., Sievert, S., Bracher, A., German, C., Edgcomb, V., Francois, R., Iglesias-Rodriguez, M., Van Mooy, B. and Rapeta, D., 2014. Understanding the Role of the Biological Pump in the Global Carbon Cycle: An Imperative for Ocean Science. *Oceanography*, 27(3), pp.10-16.

Hülse, D., Arndt, S. and Ridgwell, A., 2019. Mitigation of Extreme Ocean Anoxic Event Conditions by Organic Matter Sulfurization. *Paleoceanography and Paleoclimatology*, 34(4), pp.476-489.

Ikeda, M., Tada, R. and Ozaki, K., 2017. Astronomical pacing of the global silica cycle recorded in Mesozoic bedded cherts. *Nature Communications*, 8(1).

IPCC, 2014: *Climate Change 2014: Synthesis Report. Contribution of Working Groups I, II and III to the Fifth Assessment Report of the Intergovernmental Panel on Climate Change* [Core Writing Team, R.K. Pachauri and L.A. Meyer (eds.)]. IPCC, Geneva, Switzerland, 151 pp.

IPCC, 2019: *Summary for Policymakers. In: IPCC Special Report on the Ocean and Cryosphere in a Changing Climate* [H.-O. Pörtner, D.C. Roberts, V. Masson-Delmotte, P. Zhai, M. Tignor, E. Poloczanska, K. Mintenbeck, A. Alegría, M. Nicolai, A. Okem, J. Petzold, B. Rama, N.M. Weyer (eds.)]. In press.

Ireson, A., Mathias, S., Wheeler, H., Butler, A. and Finch, J. (2009). A model for flow in the chalk unsaturated zone incorporating progressive weathering. *Journal of Hydrology*, 365(3-4), pp.244-260.

Ivory, S., McGlue, M., Ellis, G., Lézine, A., Cohen, A. and Vincens, A., 2014. Vegetation Controls on Weathering Intensity during the Last Deglacial Transition in Southeast Africa. *PLoS ONE*, 9(11), p.e112855.

Jenkyns, H., 2018. Transient cooling episodes during Cretaceous Oceanic Anoxic Events with special reference to OAE 1a (Early Aptian). *Philosophical Transactions of the Royal Society A: Mathematical, Physical and Engineering Sciences*, 376(2130), p.20170073.

Jin, Y., 2000., Y. Wang., W. Wang., Q. H. Shang., C. Q. Cao., D. H. Erwin. Pattern of Marine Mass Extinction Near the Permian-Triassic Boundary in South China. *Science*, 289(5478), pp.432-436.

Jones, M., Percival, L., Stokke, E., Frieling, J., Mather, T., Riber, L., Schubert, B., Schultz, B., Tegner, C., Planke, S. and Svensen, H., 2019. Mercury anomalies across the Palaeocene–Eocene Thermal Maximum. *Climate of the Past*, 15(1), pp.217-236.

Kapsenberg, L., Alliouane, S., Gazeau, F., Mousseau, L. and Gattuso, J. (2017). Coastal ocean acidification and increasing total alkalinity in the northwestern Mediterranean Sea. *Ocean Science*, 13(3), pp.411-426.

Kawahata, H., Fujita, K., Iguchi, A., Inoue, M., Iwasaki, S., Kuroyanagi, A., Maeda, A., Manaka, T., Moriya, K., Takagi, H., Toyofuku, T., Yoshimura, T. and Suzuki, A., 2019. Perspective on the response of marine calcifiers to global warming and ocean acidification—Behavior of corals and foraminifera in a high CO<sub>2</sub> world “hot house”. *Progress in Earth and Planetary Science*, 6(1).

Kelly, D., 2002. Response of Antarctic (ODP Site 690) planktonic foraminifera to the Paleocene-Eocene thermal maximum: Faunal evidence for ocean/climate change. *Paleoceanography*, 17(4), pp.23-1-23-13.

Kelly, D., Zachos, J., Bralower, T. and Schellenberg, S., 2005. Enhanced terrestrial weathering/runoff and surface ocean carbonate production during the recovery stages of the Paleocene-Eocene thermal maximum. *Paleoceanography*, 20(4).

Kender, S., Aturamu, A., Zalasiewicz, J., Kaminski, M. and Williams, M., 2019. Benthic foraminifera indicate Glacial North Pacific Intermediate Water and reduced primary productivity over Bowers Ridge, Bering Sea, since the Mid-Brunhes Transition. *Journal of Micropalaeontology*, 38(2), pp.177-187.

Kender, S., Stephenson, M., Riding, J., Leng, M., Knox, R., Peck, V., Kendrick, C., Ellis, M., Vane, C. and Jamieson, R., 2012. Marine and terrestrial environmental changes in NW Europe preceding carbon release at the Paleocene–Eocene transition. *Earth and Planetary Science Letters*, 353-354, pp.108-120.

Kender, S., Yu, J. and Peck, V., 2014. Deep ocean carbonate ion increase during mid Miocene CO<sub>2</sub> decline. *Scientific Reports*, 4(1).

Kennedy, D., Stephenson, W. and Naylor, L., 2014. Chapter 1 Introduction to the rock coasts of the world. Geological Society, London, *Memoirs*, 40(1), pp.1-5.

Kiessling, W. and Simpson, C., 2010. On the potential for ocean acidification to be a general cause of ancient reef crises. *Global Change Biology*, 17(1), pp.56-67.

Kitidis, V., Hardman-Mountford, N., Litt, E., Brown, I., Cummings, D., Hartman, S., Hydes, D., Fishwick, J., Harris, C., Martinez-Vicente, V., Woodward, E. and Smyth, T. (2012). Seasonal dynamics of the carbonate system in the Western English Channel. *Continental Shelf Research*, 42, pp.30-40.

Kline, D., Teneva, L., Hauri, C., Schneider, K., Miard, T., Chai, A., Marker, M., Dunbar, R., Caldeira, K., Lazar, B., Rivlin, T., Mitchell, B., Dove, S. and Hoegh-Guldberg, O. (2015). Six Month In Situ High-Resolution Carbonate Chemistry and Temperature Study on a Coral Reef Flat Reveals Asynchronous pH and Temperature Anomalies. *PLOS ONE*, 10(6), p.e0127648

Knox, R., 1996. Tectonic controls on sequence development in the Palaeocene and earliest Eocene of southeast England: implications for North Sea stratigraphy. Geological Society, London, Special Publications, 103(1), pp.209-230.

Komar, N. and Zeebe, R., 2011. Oceanic calcium changes from enhanced weathering during the Paleocene-Eocene thermal maximum: No effect on calcium-based proxies. *Paleoceanography*, 26(3),

Komar, N., Zeebe, R. and Dickens, G., 2013. Understanding long-term carbon cycle trends: The late Paleocene through the early Eocene. *Paleoceanography*, 28(4), pp.650-662.

Krissansen-Totton, J., Arney, G. and Catling, D., 2018. Constraining the climate and ocean pH of the early Earth with a geological carbon cycle model. *Proceedings of the National Academy of Sciences*, 115(16), pp.4105-4110.

Krumins, V., Gehlen, M., Arndt, S., van Cappellen, P. and Regnier, P. (2013). Dissolved inorganic carbon and alkalinity fluxes from coastal marine sediments: model estimates for different shelf environments and sensitivity to global change. *Biogeosciences Discussions*, 9(7), pp.8475-8539.

Kuhnt, W., Holbourn, A., Beil, S., Aquit, M., Krawczyk, T., Flögel, S., Chellai, E. and Jabour, H., 2017. Unraveling the onset of Cretaceous Oceanic Anoxic Event 2 in an extended sediment archive from the Tarfaya-Laayoune Basin, Morocco. *Paleoceanography*, 32(8), pp.923-946.

Kump, L., 2018. Prolonged Late Permian–Early Triassic hyperthermal: failure of climate regulation?. *Philosophical Transactions of the Royal Society A: Mathematical, Physical and Engineering Sciences*, 376(2130), p.20170078.

Kump, L., Brantley, S. and Arthur, M., 2000. Chemical Weathering, Atmospheric CO<sub>2</sub>, and Climate. *Annual Review of Earth and Planetary Sciences*, 28(1), pp.611-667.

Kwiatkowski, L., Gaylord, B., Hill, T., Hosfelt, J., Kroeker, K., Nebuchina, Y., Ninokawa, A., Russell, A., Rivest, E., Sesboüé, M. and Caldeira, K. (2016). Nighttime dissolution in a temperate coastal ocean ecosystem increases under acidification. *Scientific Reports*, 6, p.22984.

Late Palaeocene–early Eocene dinoflagellate cyst records from the Tethys; further observations on the global distribution of *Apectodinium* (2003). In: S. Wing, P.D. Gingerich, B. Schmitz, E. Thomas (Eds.), *Causes and Consequences of Globally Warm Climates in the Early Paleogene*: Geol. Soc. Am. Spec. Pap, vol. 369, Geological Society of America Inc, Boulder, Colorado (2003), pp. 113-131

Lawrence, J., Mortimore, R., Stone, K. and Busby, J. (2013). Sea saltwater weakening of chalk and the impact on cliff instability. *Geomorphology*, 191, pp.14-22

Laya, J. and Tucker, M., 2012. Facies analysis and depositional environments of Permian carbonates of the Venezuelan Andes: Palaeogeographic implications for Northern Gondwana. *Palaeogeography, Palaeoclimatology, Palaeoecology*, 331-332, pp.1-26.

Le Cozannet, G., Bulteau, T., Castelle, B., Ranasinghe, R., Wöppelmann, G., Rohmer, J., Bernon, N., Idier, D., Louisor, J. and Salas-y-Mélia, D., 2019. Quantifying uncertainties of sandy shoreline change projections as sea level rises. *Scientific Reports*, 9(1).

Legge, O., Johnson, M., Hicks, N., Jickells, T., Diesing, M., Aldridge, J., Andrews, J., Artioli, Y., Bakker, D., Burrows, M., Carr, N., Cripps, G., Felgate, S., Fernand, L., Greenwood, N., Hartman, S., Kröger, S., Lessin, G., Mahaffey, C., Mayor, D., Parker, R., Queirós, A., Shutler, J., Silva, T., Stahl, H., Tinker, J., Underwood, G., Van Der Molen, J., Wakelin, S., Weston, K. and Williamson, P., 2020. Carbon on the Northwest European Shelf: Contemporary Budget and Future Influences. *Frontiers in Marine Science*, 7.

Lenton, T. and Britton, C., 2006. Enhanced carbonate and silicate weathering accelerates recovery from fossil fuel CO<sub>2</sub> perturbations. *Global Biogeochemical Cycles*, 20(3).

Lenton, T. and Vaughan, N. (2009). The radiative forcing potential of different climate geoengineering options. *Atmospheric Chemistry and Physics Discussions*, 9(1), pp.2559-2608.

Lenton, T. and Watson, A., 2004. Biotic enhancement of weathering, atmospheric oxygen and carbon dioxide in the Neoproterozoic. *Geophysical Research Letters*, 31(5).

Lenton, T. and Watson, A., 2011. *Revolutions That Made The Earth*. Oxford: Oxford University Press.

Lenton, T., 2019. *Biosphere Resilience From Precambrian To Present Day*.

Lenton, T., Rockström, J., Gaffney, O., Rahmstorf, S., Richardson, K., Steffen, W. and Schellnhuber, H., 2019. Climate tipping points — too risky to bet against. *Nature*, 575(7784), pp.592-595.

Letortu, P., Costa, S., Maquaire, O. and Davidson, R., 2019. Marine and subaerial controls of coastal chalk cliff erosion in Normandy (France) based on a 7-year laser scanner monitoring. *Geomorphology*, 335, pp.76-91.

Littler, K., Röhl, U., Westerhold, T. and Zachos, J., 2014. A high-resolution benthic stable-isotope record for the South Atlantic: Implications for orbital-scale changes in Late Paleocene–Early Eocene climate and carbon cycling. *Earth and Planetary Science Letters*, 401, pp.18-30.

Lovelock, J. and Margulis, L., 1974. Atmospheric homeostasis by and for the biosphere: the gaia hypothesis. *Tellus*, 26(1-2), pp.2-10.

Lunt, D., Elderfield, H., Pancost, R., Ridgwell, A., Foster, G., Haywood, A., Kiehl, J., Sagoo, N., Shields, C., Stone, E. and Valdes, P., 2013. Warm climates of the past—a lesson for the future?. *Philosophical Transactions of the Royal Society A: Mathematical, Physical and Engineering Sciences*, 371(2001), p.20130146.

Mackenzie, F. and Andersson, A., 2013. The Marine Carbon System and Ocean Acidification during Phanerozoic Time. *Geochemical Perspectives*, pp.1-227.

Mackenzie, F. and Morse, J., 1992. Sedimentary carbonates through Phanerozoic time. *Geochimica et Cosmochimica Acta*, 56(8), pp.3281-3295.

Mackenzie, F., Ver, L. and Lerman, A., 2000. Coastal-Zone Biogeochemical Dynamics under Global Warming. *International Geology Review*, 42(3), pp.193-206.

Maher, K., DePaolo, D. and Lin, J., 2004. Rates of silicate dissolution in deep-sea sediment: In situ measurement using  $^{234}\text{U}/^{238}\text{U}$  of pore fluids. *Geochimica et Cosmochimica Acta*, 68(22), pp.4629-4648.

Marsooli, R., Lin, N., Emanuel, K. and Feng, K., 2019. Climate change exacerbates hurricane flood hazards along US Atlantic and Gulf Coasts in spatially varying patterns. *Nature Communications*, 10(1).

Martin, J. (2017). Carbonate minerals in the global carbon cycle. *Chemical Geology*, 449, pp.58-72.

McGrath, T., McGovern, E., Cave, R. and Kivimäe, C., 2016. The Inorganic Carbon Chemistry in Coastal and Shelf Waters Around Ireland. *Estuaries and Coasts*, 39(1), pp.27-39.

McInerney, F. and Wing, S., 2011. The Paleocene-Eocene Thermal Maximum: A Perturbation of Carbon Cycle, Climate, and Biosphere with Implications for the Future. *Annual Review of Earth and Planetary Sciences*, 39(1), pp.489-516.

McKay, R., Naish, T., Carter, L., Riesselman, C., Dunbar, R., Sjunneskog, C., Winter, D., Sangiorgi, F., Warren, C., Pagani, M., Schouten, S., Willmott, V., Levy, R., DeConto, R. and Powell, R., 2012. Antarctic and Southern Ocean influences on Late Pliocene global cooling. *Proceedings of the National Academy of Sciences*, 109(17), pp.6423-6428.

Meinshausen, M., Smith, S., Calvin, K., Daniel, J., Kainuma, M., Lamarque, J., Matsumoto, K., Montzka, S., Raper, S., Riahi, K., Thomson, A., Velders, G. and van Vuuren, D., 2011. The RCP greenhouse gas concentrations and their extensions from 1765 to 2300. *Climatic Change*, 109(1-2), pp.213-241.

Meire, L., Meire, P., Struyf, E., Krawczyk, D., Arendt, K., Yde, J., Juul Pedersen, T., Hopwood, M., Rysgaard, S. and Meysman, F., 2016. High export of dissolved silica from the Greenland Ice Sheet. *Geophysical Research Letters*, 43(17), pp.9173-9182.

Meissner, K., McNeil, B., Eby, M. and Wiebe, E., 2012. The importance of the terrestrial weathering feedback for multimillennial coral reef habitat recovery. *Global Biogeochemical Cycles*, 26(3).

Meybeck, M., 1986. Composition chimique des ruisseaux non pollués en France. Chemical composition of headwater streams in France. *Sciences Géologiques. Bulletin*, 39(1), pp.3-77.



Midtkandal, I., Svensen, H., Planke, S., Corfu, F., Polteau, S., Torsvik, T., Faleide, J., Grundvåg, S., Selnes, H., Kürschner, W. and Olaussen, S., 2016. The Aptian (Early Cretaceous) oceanic anoxic event (OAE1a) in Svalbard, Barents Sea, and the absolute age of the Barremian-Aptian boundary. *Palaeogeography, Palaeoclimatology, Palaeoecology*, 463, pp.126-135.

Montserrat, F., Renforth, P., Hartmann, J., Leermakers, M., Knops, P. and Meysman, F. (2017). Olivine Dissolution in Seawater: Implications for CO<sub>2</sub> Sequestration through Enhanced Weathering in Coastal Environments. *Environmental Science & Technology*, 51(7), pp.3960-3972.

Moore, C. and Shedd, W., 1977. In: D. Taylor, ed., *Proceedings of Third International Coral Reef Symposium Vol. 2: Geology*. Miami, Florida: Rosenstiel School of Marine and Atmospheric Science, pp.499- 505.

Morse, J. and Mackenzie, F. (1990). *Geochemistry of sedimentary carbonates*. Amsterdam: Elsevier.

Morse, J., Andersson, A. and Mackenzie, F., 2006. Initial responses of carbonate-rich shelf sediments to rising atmospheric pCO<sub>2</sub> and “ocean acidification”: Role of high Mg-calcites. *Geochimica et Cosmochimica Acta*, 70(23), pp.5814-5830.

Moses, C. and Robinson, D., 2011. Chalk coast dynamics: Implications for understanding rock coast evolution. *Earth-Science Reviews*, 109(3-4), pp.63-73.

Mulec, J. and Prelovšek, M., 2015. Freshwater biodissolution rates of limestone in the temperate climate of the Dinaric karst in Slovenia. *Geomorphology*, 228, pp.787-795.

Mumallah, N. (1998). Reaction rates of hydrochloric acid with chalks. *Journal of Petroleum Science and Engineering*, 21(3-4), pp.165-177.

Nadin, P., Kuszniir, N. and Toth, J., 1995. Transient regional uplift in the Early Tertiary of the northern North Sea and the development of the Iceland Plume. *Journal of the Geological Society*, 152(6), pp.953-958.

Naylor, L. and Viles, H., 2002. A new technique for evaluating short-term rates of coastal bioerosion and bioprotection. *Geomorphology*, 47(1), pp.31-44.

O'Mara, N. and Dunne, J., 2019. Hot Spots of Carbon and Alkalinity Cycling in the Coastal Oceans. *Scientific Reports*, 9(1).

Oeser, R. and von Blanckenburg, F., 2020. Decoupling silicate weathering from primary productivity – how ecosystems regulate nutrient uptake along a climate and vegetation gradient. *Biogeosciences*, European Geosciences Union,.

Olivero, E. and Martinioni, D., 2001. A review of the geology of the Argentinian Fuegian Andes. *Journal of South American Earth Sciences*, 14(2), pp.175-188.

Opdyke, B. and Wilkinson, B., 1988. Surface area control of shallow cratonic to deep marine carbonate accumulation. *Paleoceanography*, 3(6), pp.685-703.

Opdyke, B. and Wilkinson, B., 1990. Paleolatitude distribution of Phanerozoic marine ooids and cements. *Palaeogeography, Palaeoclimatology, Palaeoecology*, 78(1-2), pp.135-148.

Panchuk, K., Ridgwell, A. and Kump, L., 2008. Sedimentary response to Paleocene-Eocene Thermal Maximum carbon release: A model-data comparison. *Geology*, 36(4), p.315.

Paquay, F. and Zeebe, R. (2013). Assessing possible consequences of ocean liming on ocean pH, atmospheric CO<sub>2</sub> concentration and associated costs. *International Journal of Greenhouse Gas Control*, 17, pp.183-188.

Payne, J., Turchyn, A., Paytan, A., DePaolo, D., Lehrmann, D., Yu, M. and Wei, J., 2010. Calcium isotope constraints on the end-Permian mass extinction. *Proceedings of the National Academy of Sciences*, 107(19), pp.8543-8548.

Peng, C., Anabaraonye, B., Crawshaw, J., Maitland, G. and Trusler, J., 2016. Kinetics of carbonate mineral dissolution in CO<sub>2</sub>-acidified brines at storage reservoir conditions. *Faraday Discussions*, 192, pp.545-560.

Penman, D. and Zachos, J., 2018. New constraints on massive carbon release and recovery processes during the Paleocene-Eocene Thermal Maximum. *Environmental Research Letters*, 13(10), p.105008.

Perry, C., Murphy, G., Kench, P., Edinger, E., Smithers, S., Steneck, R. and Mumby, P., 2014. Changing dynamics of Caribbean reef carbonate budgets: emergence of reef bioeroders as critical controls on present and future reef growth potential. *Proceedings of the Royal Society B: Biological Sciences*, 281(1796), p.20142018.

Prein, A., Liu, C., Ikeda, K., Trier, S., Rasmussen, R., Holland, G. and Clark, M., 2017. Increased rainfall volume from future convective storms in the US. *Nature Climate Change*, 7(12), pp.880-884.

Prentice, IC, Farquhar, GD, Fasham, MJR, Goulden, ML, Heimann, M, Jaramillo, VJ, Kheshgi, HS, Le Quéré, C, Scholes, RJ & Wallace, DWR 2001, The carbon cycle and atmospheric carbon dioxide. in JT Houghton, Y Ding, DJ Griggs, M Noguer, PJVD Linden, X Dai, K Maskell & CA Johnson (eds), *Climate Change 2001: The Scientific Basis*. Cambridge University Press, pp. 183 - 237.

Price, M., Downing, R. A., Edmunds, W. M., 1993. The Chalk as an aquifer. In: Downing, R. A., Price, M., Jones, G. P. (Eds.), *The Hydrogeology of the Chalk of North-West Europe*. Clarendon Press, Oxford

Price, N., Martz, T., Brainard, R. and Smith, J. (2012). Diel Variability in Seawater pH Relates to Calcification and Benthic Community Structure on Coral Reefs. *PLoS ONE*, 7(8), p.e43843.

Ranasinghe, R., 2020. On the need for a new generation of coastal change models for the 21st century. *Scientific Reports*, 10(1).

Renforth, P. and Henderson, G., 2017. Assessing ocean alkalinity for carbon sequestration. *Reviews of Geophysics*, 55(3), pp.636-674.

*Research*, 19(15-16), pp.2019-2040.

Ridgwell, A. and Schmidt, D., 2010. Past constraints on the vulnerability of marine calcifiers to massive carbon dioxide release. *Nature Geoscience*, 3(3), pp.196-200.

Ridgwell, A. and Zeebe, R., 2005. The role of the global carbonate cycle in the regulation and evolution of the Earth system. *Earth and Planetary Science Letters*, 234(3-4), pp.299-315.

Ridgwell, A., 2005. A Mid Mesozoic Revolution in the regulation of ocean chemistry. *Marine Geology*, 217(3-4), pp.339-357.

Ridgwell, A., 2007. Interpreting transient carbonate compensation depth changes by marine sediment core modeling. *Paleoceanography*, 22(4).

Ridgwell, A., and Hargreaves, J. C. 2007. Regulation of atmospheric CO<sub>2</sub> by deep-sea sediments in an Earth system model. *Global Biogeochemical Cycles*, 21.

Ridgwell, A., Hargreaves, J. C., Edwards, N. R., Annan, J. D., Lenton, T. M., Marsh, R., Yool, A., and Watson, A. (2007). Marine geochemical data assimilation in an efficient Earth System Model of global biogeochemical cycling. *Biogeosciences*, 4(1), 87–104.

Ridgwell, A., Zondervan, I., Hargreaves, J. C., Bijma, J., & Lenton, T. M. (2007). Assessing the potential long-term increase of oceanic fossil fuel CO<sub>2</sub> uptake due to CO<sub>2</sub> calcification feedback. *Biogeosciences*, 4(4), 481–492.

Riding, R., Liang, L. and Braga, J., 2014. Millennial-scale ocean acidification and late Quaternary decline of cryptic bacterial crusts in tropical reefs. *Geobiology*, 12(5), pp.387-405.

Robert, C. and Kennett, J., 1994. Antarctic subtropical humid episode at the Paleocene-Eocene boundary: Clay-mineral evidence. *Geology*, 22(3), p.211.

Robinson, D. and Jerwood, L. (1987). Sub-aerial weathering of chalk shore platforms during harsh winters in southeast England. *Marine Geology*, 77(1-2), pp.1-14.

Rodríguez-Tovar, F., Uchman, A., Alegret, L. and Molina, E., 2011. Impact of the Paleocene–Eocene Thermal Maximum on the macrobenthic community: Ichnological record from the Zumaia section, northern Spain. *Marine Geology*, 282(3-4), pp.178-187.

Romero-Mujalli, G., Hartmann, J., Börker, J., Gaillardet, J. and Calmels, D., 2019. Ecosystem controlled soil-rock pCO<sub>2</sub> and carbonate weathering – Constraints by temperature and soil water content. *Chemical Geology*, 527, p.118634.

Röthlisberger, R., Crosta, X., Abram, N., Armand, L. and Wolff, E., 2010. Potential and limitations of marine and ice core sea ice proxies: an example from the Indian Ocean sector. *Quaternary Science Reviews*, 29(1-2), pp.296-302.

Royer, D., 2016. Climate Sensitivity in the Geologic Past. *Annual Review of Earth and Planetary Sciences*, 44(1), pp.277-293.

Rushby, A., Johnson, M., Mills, B., Watson, A. and Claire, M., 2018. Long-Term Planetary Habitability and the Carbonate-Silicate Cycle. *Astrobiology*, 18(5), pp.469-480.

S.A. Foo, M. Byrne, E. Ricevuto, M.C. Gambi., 2018. The carbon dioxide vents of Ischia, Italy, a natural system to assess impacts of ocean acidification on marine ecosystems: an overview of research and comparisons with other vent systems. *In* S.J. Hawkins, A.J. Evans, A.C. Dale, L.B. Flirth, I.P. Smith (Eds.), *Oceanography and Marine Biology: an Annual Review*, vol. 56 (2018), pp. 237-310

Sabine CL, Feely RA (2007) The oceanic sink for carbon dioxide. *In*: Reay D, Hewitt CN, Smith K, Grace J (eds) *Greenhouse gas sinks*. CAB International, Oxfordshire, pp 31–46

Sabine, C. and Mackenzie, F., 1995. Bank-derived carbonate sediment transport and dissolution in the Hawaiian Archipelago. *Aquatic Geochemistry*, 1(2), pp.189-230.

Sabine, C., Mackenzie, F., Winn, C. and Karl, D., 1995. Geochemistry of carbon dioxide in seawater at the Hawaii Ocean Time Series Station, ALOHA. *Global Biogeochemical Cycles*, 9(4), pp.637-651.

Saltzman, M., 2017. Silicate weathering, volcanic degassing, and the climate tug of war. *Geology*, 45(8), pp.763-764.

Sarmiento, J., Hughes, T., Stouffer, R. and Manabe, S., 1998. Simulated response of the ocean carbon cycle to anthropogenic climate warming. *Nature*, 393(6682), pp.245-249.

Schmitz, B., Pujalte, V. and Núñez-Betelu, K., 2001. Climate and sea-level perturbations during the Incipient Eocene Thermal Maximum: evidence from

siliciclastic units in the Basque Basin (Ermua, Zumaia and Trabakua Pass), northern Spain. *Palaeogeography, Palaeoclimatology, Palaeoecology*, 165(3-4), pp.299-320.

Schobben, M., van de Schootbrugge, B. and Wignall, P., 2019. Interpreting the Carbon Isotope Record of Mass Extinctions. *Elements*, 15(5), pp.331-337.

Schubert, B. and Hope Jahren, A., 2013. Reconciliation of marine and terrestrial carbon isotope excursions based on changing atmospheric CO<sub>2</sub> levels. *Nature Communications*, 4(1).

Scribner, C., Martin, E., Martin, J., Deuerling, K., Collazo, D. and Marshall, A., 2015. Exposure age and climate controls on weathering in deglaciated watersheds of western Greenland. *Geochimica et Cosmochimica Acta*, 170, pp.157-172.

Seneviratne, S.I., Nicholls, D. Easterling, C.M. Goodess, S. Kanae, J. Kossin, Y. Luo, J. Marengo, K. McInnes, M. Rahimi, M. Reichstein, A. Sorteberg, C. Vera, and X. Zhang, 2012: Changes in climate extremes and their impacts on the natural physical environment. In: *Managing the Risks of Extreme Events and Disasters to Advance Climate Change Adaptation* [Field, C.B., V. Barros, T.F. Stocker, D. Qin, D.J. Dokken, K.L. Ebi, M.D. Mastrandrea, K.J. Mach, G.-K. Plattner, S.K. Allen, M. Tignor, and P.M. Midgley (eds.)]. A Special Report of Working Groups I and II of the Intergovernmental Panel on Climate Change (IPCC). Cambridge University Press, Cambridge, UK, and New York, NY, USA, pp. 109-230.

Sexton, P., Norris, R., Wilson, P., Pälike, H., Westerhold, T., Röhl, U., Bolton, C. and Gibbs, S., 2011. Eocene global warming events driven by ventilation of oceanic dissolved organic carbon. *Nature*, 471(7338), pp.349-352.

Shen, S., Crowley, J., Wang, Y., Bowring, S., Erwin, D., Sadler, P., Cao, C., Rothman, D., Henderson, C., Ramezani, J., Zhang, H., Shen, Y., Wang, X., Wang,

W., Mu, L., Li, W., Tang, Y., Liu, X., Liu, L., Zeng, Y., Jiang, Y. and Jin, Y., 2011. Calibrating the End-Permian Mass Extinction. *Science*, 334(6061), pp.1367-1372.

Shields, G. and Mills, B., 2017. Tectonic controls on the long-term carbon isotope mass balance. *Proceedings of the National Academy of Sciences*, 114(17), pp.4318-4323.

Shutler, J., Wanninkhof, R., Nightingale, P., Woolf, D., Bakker, D., Watson, A., Ashton, I., Holding, T., Chapron, B., Quilfen, Y., Fairall, C., Schuster, U., Nakajima, M. and Donlon, C., 2019. Satellites will address critical science priorities for quantifying ocean carbon. *Frontiers in Ecology and the Environment*, 18(1), pp.27-35.

Sigman, D. M. & Hain, M. P. (2012) The Biological Productivity of the Ocean. *Nature Education Knowledge* 3(6):5

Simmons, C., Mysak, L. and Matthews, H., 2016. An investigation of carbon cycle dynamics since the Last Glacial Maximum: Complex interactions between the terrestrial biosphere, weathering, ocean alkalinity, and CO<sub>2</sub> radiative warming in an Earth system model of intermediate complexity. *Climate of the Past Discussions*, pp.1-54.

Smith, S. and Hollibaugh, J. (1993). Coastal metabolism and the oceanic organic carbon balance. *Reviews of Geophysics*, 31(1), pp.75-89.

Sobolev, S., Sobolev, A., Kuzmin, D., Krivolutskaya, N., Petrunin, A., Arndt, N., Radko, V. and Vasiliev, Y., 2011. Linking mantle plumes, large igneous provinces and environmental catastrophes. *Nature*, 477(7364), pp.312-316.

St. Pierre, K., St. Louis, V., Schiff, S., Lehnherr, I., Dainard, P., Gardner, A., Aukes, P. and Sharp, M., 2019. Proglacial freshwaters are significant and previously



unrecognized sinks of atmospheric CO<sub>2</sub>. Proceedings of the National Academy of Sciences, 116(36), pp.17690-17695.

Stanley, S., 2009. Evidence from ammonoids and conodonts for multiple Early Triassic mass extinctions. Proceedings of the National Academy of Sciences, 106(36), pp.15264-15267.

Stanley, S., Ries, J. and Hardie, L., 2002. Nonlinear partial differential equations and applications: From the Cover: Low-magnesium calcite produced by coralline algae in seawater of Late Cretaceous composition. Proceedings of the National Academy of Sciences, 99(24), pp.15323-15326.

Stanley, S., Ries, J. and Hardie, L., 2005. Seawater chemistry, coccolithophore population growth, and the origin of Cretaceous chalk. Geology, 33(7), p.593.

Stuijs, A. and Brinkhuis, H., 2008. Rapid carbon injection and transient global warming during the Paleocene-Eocene thermal maximum. Netherlands Journal of Geosciences - Geologie en Mijnbouw, 87(3), pp.201-206.

Sulpis, O., Boudreau, B., Mucci, A., Jenkins, C., Trossman, D., Arbic, B. and Key, R., 2018. Current CaCO<sub>3</sub> dissolution at the seafloor caused by anthropogenic CO<sub>2</sub>. Proceedings of the National Academy of Sciences, 115(46), pp.11700-11705.

Taylor, L., Quirk, J., Thorley, R., Kharecha, P., Hansen, J., Ridgwell, A., Lomas, M., Banwart, S. and Beerling, D. (2015). Enhanced weathering strategies for stabilizing climate and averting ocean acidification. Nature Climate Change, 6(4), pp.402-406.

Thompson, C., Silburn, B., Williams, M., Hull, T., Sivyer, D., Amoudry, L., Widdicombe, S., Ingels, J., Carnovale, G., McNeill, C., Hale, R., Marchais, C., Hicks, N., Smith, H., Klar, J., Hiddink, J., Kowalik, J., Kitidis, V., Reynolds, S., Woodward,

E., Tait, K., Homoky, W., Kröger, S., Bolam, S., Godbold, J., Aldridge, J., Mayor, D., Benoist, N., Bett, B., Morris, K., Parker, E., Ruhl, H., Statham, P. and Solan, M., 2017. An approach for the identification of exemplar sites for scaling up targeted field observations of benthic biogeochemistry in heterogeneous environments. *Biogeochemistry*, 135(1-2), pp.1-34.

Townsend, A., Vitousek, P. and Holland, E., 1992. Tropical soils could dominate the short-term carbon cycle feedbacks to increased global temperatures. *Climatic Change*, 22(4), pp.293-303.

Turner, S., 2018. Constraints on the onset duration of the Paleocene–Eocene Thermal Maximum. *Philosophical Transactions of the Royal Society A: Mathematical, Physical and Engineering Sciences*, 376(2130), p.20170082.

Tyrrell, T., 2007. Calcium carbonate cycling in future oceans and its influence on future climates. *Journal of Plankton Research*, 30(2), pp.141-156.

Unger, N. and Yue, X., 2014. Strong chemistry-climate feedbacks in the Pliocene. *Geophysical Research Letters*, 41(2), pp.527-533.

van Buchem, F., Smit, F., Buijs, G., Trudgill, B. and Larsen, P., 2017. Tectonostratigraphic framework and depositional history of the Cretaceous–Danian succession of the Danish Central Graben (North Sea) – new light on a mature area. *Geological Society, London, Petroleum Geology Conference series*, 8(1), pp.9-46.

van der Ploeg, R., Boudreau, B., Middelburg, J. and Sluijs, A., 2019. Cenozoic carbonate burial along continental margins. *Geology*, 47(11), pp.1025-1028.

Vance, D., Teagle, D. and Foster, G., 2009. Variable Quaternary chemical weathering fluxes and imbalances in marine geochemical budgets. *Nature*, 458(7237), pp.493-496.

Vervoort, P., Adloff, M., Greene, S. and Kirtland Turner, S., 2019. Negative carbon isotope excursions: an interpretive framework. *Environmental Research Letters*, 14(8), p.085014.

Wadham, J., Hawkings, J., Tarasov, L., Gregoire, L., Spencer, R., Gutjahr, M., Ridgwell, A. and Kohfeld, K., 2013. Ice sheets matter for the global carbon cycle. *Nature Communications*, 10(1).

Walker, J., Hays, P. and Kasting, J., 1981. A negative feedback mechanism for the long-term stabilization of Earth's surface temperature. *Journal of Geophysical Research*, 86(C10), p.9776.

Walker, L., Wilkinson, B. and Ivany, L., 2002. Continental Drift and Phanerozoic Carbonate Accumulation in Shallow-Shelf and Deep-Marine Settings. *The Journal of Geology*, 110(1), pp.75-87.

Weatherdon, L., Magnan, A., Rogers, A., Sumaila, U. and Cheung, W., 2016. Observed and Projected Impacts of Climate Change on Marine Fisheries, Aquaculture, Coastal Tourism, and Human Health: An Update. *Frontiers in Marine Science*, 3.

Wizemann, A., Nandini, S., Stuhldreier, I., Sánchez-Noguera, C., Wisshak, M., Westphal, H., Rixen, T., Wild, C. and Reymond, C., 2018. Rapid bioerosion in a tropical upwelling coral reef. *PLOS ONE*, 13(9), p.e0202887.

Wood, H., Spicer, J. and Widdicombe, S., 2008. Ocean acidification may increase calcification rates, but at a cost. *Proceedings of the Royal Society B: Biological Sciences*, 275(1644), pp.1767-1773.

Wood, H., Spicer, J., Lowe, D. and Widdicombe, S. (2010). Interaction of ocean acidification and temperature; the high cost of survival in the brittlestar *Ophiura ophiura*. *Marine Biology*, 157(9), pp.2001-2013

Wood, H., Widdicombe, S. and Spicer, J., 2009. The influence of hypercapnia and the infaunal brittlestar *Amphiura filiformis* on sediment nutrient flux – will ocean acidification affect nutrient exchange?. *Biogeosciences*, 6(10), pp.2015-2024.

Yates, K., Dufore, C., Smiley, N., Jackson, C. and Halley, R. (2007). Diurnal variation of oxygen and carbonate system parameters in Tampa Bay and Florida Bay. *Marine Chemistry*, 104(1-2), pp.110-124.

Zachos, J., Dickens, G. and Zeebe, R., 2008. An early Cenozoic perspective on greenhouse warming and carbon-cycle dynamics. *Nature*, 451(7176), pp.279-283.

Zachos, J., Opdyke, B., Quinn, T., Jones, C. and Halliday, A., 1999. Early cenozoic glaciation, antarctic weathering, and seawater  $87\text{Sr}/86\text{Sr}$ : is there a link?. *Chemical Geology*, 161(1-3), pp.165-180.

Zachos, J., Röhl, U., Schellenberg, S., Sluijs, A., Hodell, D., Kelly, D., Thomas, E., Nicolo, M., Raffi, I., Lourens, L., McCarren, H. and Kroon, D., 2005. Rapid Acidification of the Ocean During the Paleocene-Eocene Thermal Maximum. *Science*, 308(5728), pp.1611-1615.

Zeebe, R., 2012. LOSCAR: Long-term Ocean-atmosphere-Sediment CARbon cycle Reservoir Model v2.0.4. *Geoscientific Model Development*, 5(1), pp.149-166.

Zeng, S., Liu, Z. and Kaufmann, G., 2019. Sensitivity of the global carbonate weathering carbon-sink flux to climate and land-use changes. *Nature Communications*, 10(1).

Zhong, J., Li, S., Tao, F., Yue, F. and Liu, C., 2017. Sensitivity of chemical weathering and dissolved carbon dynamics to hydrological conditions in a typical karst river. *Scientific Reports*, 7(1).